universität wien

# MASTERARBEIT | MASTER'S THESIS

Titel | Title

Developing organic colours through rational mixing of molecular electrochromic hues

verfasst von | submitted by

Vincent Simon Königstein B.Sc.

angestrebter akademischer Grad | in partial fulfilment of the requirements for the degree of

Master of Science (MSc)

Wien | Vienna, 2025

| | |
|---|---|
| Studienkennzahl lt. Studienblatt \| Degree programme code as it appears on the student record sheet: | UA 066 862 |
| Studienrichtung lt. Studienblatt \| Degree programme as it appears on the student record sheet: | Masterstudium Chemie |
| Betreut von \| Supervisor: | Univ.-Prof. Davide Bonifazi PhD |

## Acknowledgement

I would like to thank Professor Davide Bonifazi for giving me the opportunity to join his research group and for guiding me through the thesis. He continuously inspired me throughout my studies at the University of Vienna and helped me excel in my work.

For her unwavering support during my thesis, I would like to thank my supervisor, Dr. Teodora Moiseanu. She stood by me with selfless dedication, and I am deeply grateful for the knowledge and guidance she shared. Working alongside her was a true pleasure, and her kindness and encouragement will stay with me in the future.

For his extended help with the spectroscopic analysis of the monomers and polymers, I want to thank El Czar Galleposo. I learned a lot from him and his work ethic inspired me throughout my thesis. In the lab, I want to thank Moritz Riegler for being such an amazing and inspiring lab partner and Dr. Davide Zanetti and Nils Pellinger for the several scientific discussions we had, which impact on my work can't be overlooked.

I would like to thank Alma Krpuljevic-Hanic for her administrative work and for always being so calm and kind.

To Igor Echevarria Poza and Edrin Sulejmani, I want to say thank you and I truly appreciate their work behind the scenes in making sure that everything runs smoothly in the labs.

I want to thank the rest of the Bonifazi team, who I am happy to be able to call many of you friends after these six months. The time in and outside the lab would not have been the same!

At last, I want to thank my family and my partner Lisa for supporting me throughout all of my studies and never stopping to believe in me.

## Abstract

The aim of this thesis was to synthesise a series of electrochromic monomers derived from phenothiazine (**1**), to rationally mix them based on their spectroelectrochemical (SEC) properties to create new hues (Scheme 1).

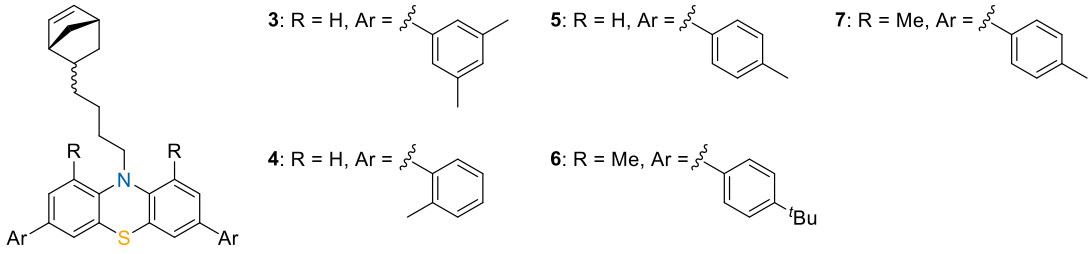


*Scheme 1: The substrate scope of the synthesized phenothiazine-based monomers.*

Towards this goal five monomers were successfully synthesised by aryl-substitution *para* to the nitrogen atom of commercially available **1** and from 1,9-dimethyl-10*H*-phenothiazine (**2**), which was prepared separately. Further, the synthetic pathway of the monomers was optimised to adjust for an efficient production in larger scales and the method's adaptability demonstrated. All monomers were spectroelectrochemically (SEC) characterised and in total a purple, cyan and green colour were obtained and these objectively quantified in the Comission internationale de l'éclairage (CIE) colour space. Through the installation of methyl groups *ortho* to the nitrogen atom of phenothiazine photophysical and electronic properties were manipulated demonstrating the potential for fine-tuning of phenothiazines. For monomers **4** and **7** a reversible switch from a bleached to a coloured state upon oxidation was observed. Further, the SEC results were used to rationally mix different coloured monomers by ring-opening metathesis polymerisation (ROMP) in a highly controlled manner (Scheme 2). The copolymers were obtained within a polydispersity index (PDI) of 1.05 and further characterised by SEC measurements.

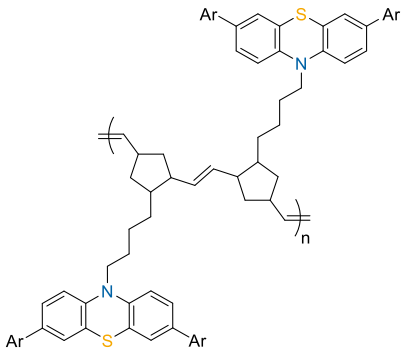


Scheme 2: General strucutre of the phenothiazine-based polymers.

## Kurzfassung

Das Ziel dieser Arbeit war es eine Serie von Monomeren welche aus Phenothiazin (**1**) Einheiten bestehen mit elektrochromen Eigenschaften zu synthetisieren um auf Grundlage der spektroelektrochemischen (SEC) Eigenschaften diese rational zu mischen um neue Farbtöne zu erhalten (Abbildung 1).

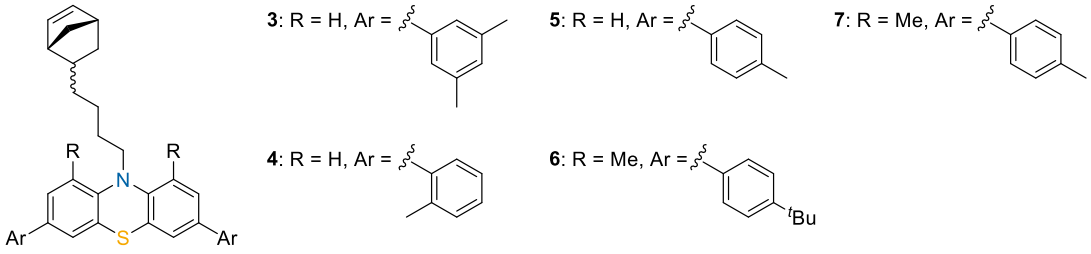


*Abbildung 1: Substratumfang der synthetisierten auf Phenothiazin basierenden Monomere.*

Um dieses Ziel zu erreichen, wurden fünf mit Aryl-Gruppen in *para* Posititon substituierte Monomere auf der Basis von Phenothiazin und 1,9-dimethyl-10*H*-phenothiazine (**2**) synthetisiert (Abbildung 1). Weiterführend, wurde der Syntheseweg für eine effiziente Produktion in großem Maßstab optimiert und die Adaptivität dieser demonstriert. Alle Monomere wurden spektroeletrochemisch (SEC) charakterisiert und insgesamt eine violette, eine turquoise und eine grüne Farbe erhalten, welche objektiv anhand des CIE-Normvalenzsystem (CIE-Comission internationale de l'éclairage) bestimmt wurden. Für die Monomere auf der Basis von **2** konnte das Oxidationspotential und die UV-Vis Absorption der Monomere durch Einführen der Methyl Gruppen nach wünschen angepasst werden. Für die Monomere **4** und **6** konnte ein reversibler Wechsel von einem farblosen zu einem farbigen Zustand beobachtet werden. Außerdem wurden die Ergebnisse der SEC-Messungen genutzt um verschieden farbige Monomere rational durch ringöffnende co-Polymerisierung (ROMP) zu mischen. Die Copolymere wurden mit einer Polydispersität von 1.05 erhalten und spektroelektrochemisch charakterisiert.

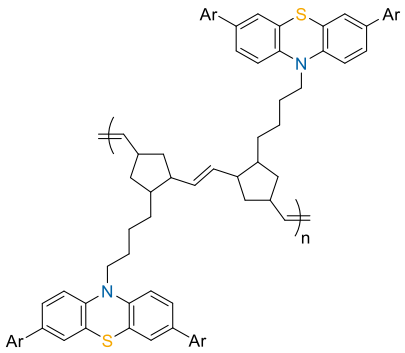


*Abbildung 2: Die generelle Struktur der auf Phenothiazin basierenden Polymere.*

**Contents**

# 1. Introduction

## 1.1 Electrochromism

Electrochromic materials undergo a reversible change of colour following an oxidation or reduction.[1] The switching between colours stems from the change in absorption upon an electrochemical stimulus, and usually ranges from the UV-visible to the near-infrared region, but can even extend to the microwave region.[2] Most electrochromic materials switch from a colourless state to a coloured state, whereas the colourless state is referred to as bleached.[3] First observed in tungsten oxide ($WO_3$) by Deb, electrochromism has been studied from inorganic to organic materials.[2,4] Materials that have more than two different colours by switching between multiple redox states are referred to as polyelectrochromic.[1] An example are the organic molecule group of Viologens that possess three distinct redox states, each having a distinct colour or being colourless. Electrochromic devices do not emit light, like displays with light-emitting diodes (LEDs), OLEDs or liquid-crystal displays (LCDs), and so excel with a lower energy consumption, owing to their optical memory effect. They further outperform with wide viewing and illumination angle, as well as angle-independent contrast.[5] Applications of electrochromic materials can range from smart windows, utilizing the ability to switch from a bleached to a coloured phase, to next-generation displays, that excel in outdoor readability and are less straining on the eyes. Their low energy consumption makes them suitable for energy-saving displays with low refreshment rates, such as billboards, electronic paper or information storage.[3] Electrochromic devices can be cheaply produced through printing or coating. For large areas spray or spin coating is advantageous, allowing a simple processing of electrochromic solutions onto a wide range of substrates. Inkjet printing ss a simple, highly adaptive processing technique, having the advantage of direct patterning. The need for fine patterning is indispensable for modern applications such as segmented displays. Electrochromic materials can be deposited on a wide variety of substrates, from glass, plastics to gels, to obtain devices with a high bending radius and excellent mechanical durability. Preferably, substrates that are transparent in the visible region of the electromagnetic spectrum are suitable, such as borosilicate glass, polyesters (PET) or acrylate polymers.[6] The substrate can be made compatible with electrochromic material by coating them with a layer of an electrically conductive material. These should fulfil desirable characteristics such as transparency, sufficient electric conductance and corrosion resistance. Common materials are indium/tin oxide (ITO) or poly(3,4-ethlenedioxythiophene):poly(styrene sulfonate) (PEDOT:PSS) (Figure 2). Classically an ion transport layer (ITL) is included to enhance the transfer of ions and an ion storage layer to ensure electrochemical stability, improving the device's lifespan (Figure 1). The electrochromic layer is placed

between one of the electrodes and the ITL, for which today electrochromic conjugated polymers are the most established. They excel as alternatives to inorganic electrochromic devices with their flexibility, ease of processing, low processing cost and colour-tuning properties. Furthermore, colours can be simply mixed through copolymerization.

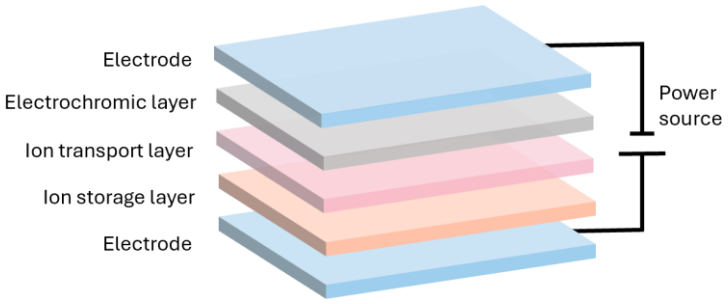


*Figure 1: Scheme of the classic design of a layered electrochromic device.*

Controlling the colour in electrochromic devices is a key element, with the goal being control and tuneability over the full spectrum. Over the years, a wide range of conjugated electrochromic polymers have been developed, covering a broad range colour palette. Ranging from the deep blue colour of PEDOT, over green copolymers, to red open-chain dioxothiophene polymers.[7–9] In 2024, Chen et al. achieved a black electronic material covering the whole visible region of the electromagnetic spectrum by copolymerization of 3,4-propylenedioxythiophene with a benzothiadiazole unit. This marked a great milestone, as a broadly absorbing and homogeneous coverage of the full spectrum is challenging and previous black electrochromic materials lacked sufficient intensity or left gaps in the absorption. These results were only achieved through meticulous optimization of the synthesis conditions and a careful choice of monomers. This highlights the problems that remain with conjugated polymers for electrochromic materials, as the precise control over polymerization remains a challenge and a lack of adaptability, limiting the colour options.[10] Considering its endlessness, to cover the full colour palette, designing and tuning for every colour an electrochromic material individual would be a task close to impossible. Alternative approaches to copolymerization have shown the possibility of a tunable colour palette, by stacking different coloured electrochromic polymer films. With the three conducting polymers: polythiophene (red), polyaniline (green) and PEDOT (blue) a total of thirteen colours could be achieved (Figure 2).[11]

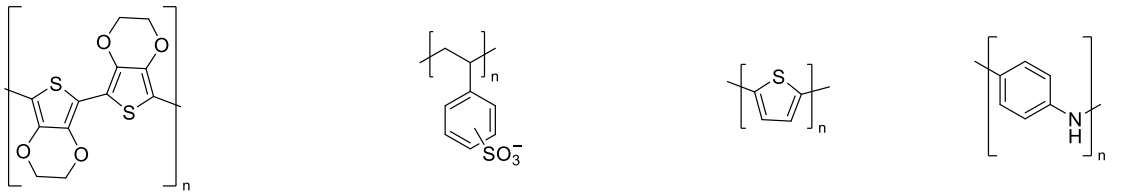


*Figure 2: The structure of poly(3,4-ethylenedioxythiophene) (PEDOT),polystyrene sulfonate (PSS), polythiophene (PT) and polyaniline (PANI).*

Different ratios of the polymer layers were explored to achieve different hues, a single layer of polythiphene was observed as pink while three layers gave a red colour. While the broad color palette from only three colours is remarkable an elegant approach for the controlled mixing of the colours is missing.[11] To understand how colours can be tuned and mixed the underlying principles are crucial.

### 1.2 Colour

The human perception of colour arises from the visual recognition of the electromagnetic spectrum. A single wavelength or a combination of wavelengths determines the perception of one distinct colour. Within the narrow visible range, the longest wavelengths are perceived by the human eye as red and the shortest as violet, while electromagnetic radiation extends into the infrared and on the opposite into the ultraviolet range, which are invisible to the human eye.[12] To grasp the broad colour spectrum, colour theories have been developed to describe, quantify and predict the perception of colour. Young developed the principle of primary colours, the idea that all colours could be matched by mixing three distinct colours, laying the basis for the trichromatic theory. Later revised by Helmholz, this came known as the Young-Helmholtz theory of colour perception, in which they defined the visible spectrum as a combination of blue, green and red. These concepts are the basis for manipulation and expansion of the colour palette through mixing. While the effect of mixing colours has been observed since ancient times, colours and their manipulation is generally described by contemporary colour theory using the principles of additive and subtractive mixing.[13]

Additive mixing is based on the red–green–blue (RGB) model and subtractive mixing on the red-yellow-blue (RYB) model. As described in the trichromatic theory these primary colours can be used to produce a multitude of hues, following the principles of their respective models. In the RGB model, colours can be mixed from the direct additive mixing of emissive light sources, with white being the full sum of red, green and blue (Figure 3, left).[14,15] Accordingly this method is employed light-emitting displays, headlights or in general in light emitting diodes (LEDs). In contrast, the subtractive colour model describes the perceived

colour following the subtraction of absorbed light from the rest which is reflected back to the light source. The subtractive model is used in the application of material with light absorbing properties such as pigments or electrochromic materials. For pigments and inks used in printing, the cyan, magenta, yellow and black (CMYK) model is used.[15] When these colours are mixed, the act as filters subtracting from a white light source or surface, with the full sum of cyan, magenta and yellow resulting in black (Figure 3, right).[14]

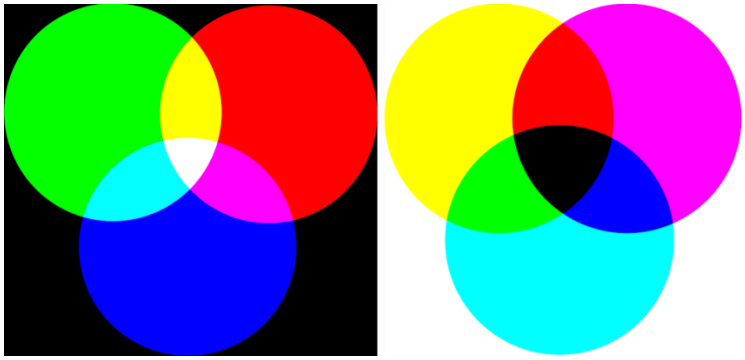

*Figure 3: On the left, additive colour mixing of red, green and blue and on the right subtractive colour mixing of yellow, magenta and cyan.*

The understanding of these concepts can be credited to the work of Newton, who first demonstrated color dispersion with a triangular prism. With the prism he was able to break apart a beam of light into different colours, which he named the spectrum. Based on these findings, Newton devised the first colour diagram in the form of a circle. Also called the colour wheel, it consists of all pure spectral colours drawn around the outer rim and white at the centre, with the complimentary colours being placed opposite to each other (Figure 4, A).[12] Following this first concept for a chromacity diagram, based on the trichromatic theory, experimental work to develop a colour-matching theory led to the development of the tristimulus values: hue, saturation and luminance. The light field colour can be described with these values, whereas all colours with the same hue and saturation are represented along a straight line, where the position along the line is determine by the luminance.[12] Through this relationship only the hue and saturation are needed to represent any color and can be used as coordinates. By projecting these so-called chromacity coordinates on a plane with the gamut of all colours lying inside the plane and the spectral colours on the border, any colour independent of its luminance can be displayed.[12] Such a representation is the CIE chromticity diagram, with the tristimulus values xyz or xyY (Figure 4, B). The x,y coordinates describe the hue and saturation, while Y is proportional to the luminance. In the diagram all the chromaticity's visible to the human eye are represented, with the white-point lying in the middle at x,y=0.333. Every point on the outer curve is the chromatic value of a spectral colour, which is the colour evoked by monochromatic light.

Through the combination of these spectral colours the non-spectral colours can be obtained, which are represented inside the boundaries of the curve, through additive mixing. This makes the CIE colour space an essential tool for the development of modern digital systems with emissive colours.[12] To describe the colour of pigments, the CIE L*a*b space was invented (Figure 5).

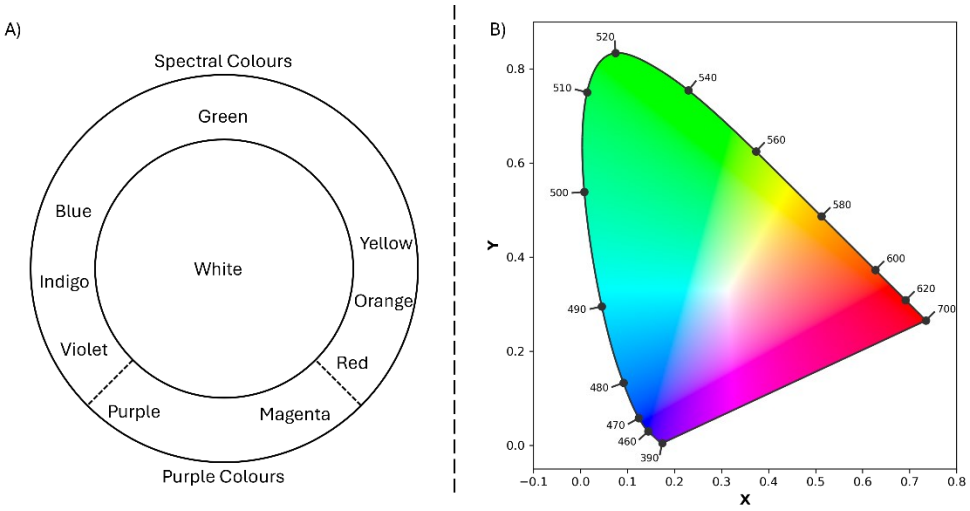


*Figure 4: A) Newton's circle, the first color diagram. B) The CIExyz colour space created in python using the "colour-science" package*

The values can be obtained through transformation from the CIE xyY system. In the plot, a* represents the amount of red and green, while b* represents the amount of yellow and blue. The luminance is represented along the z axis, ranging from zero for black to 100 for white.

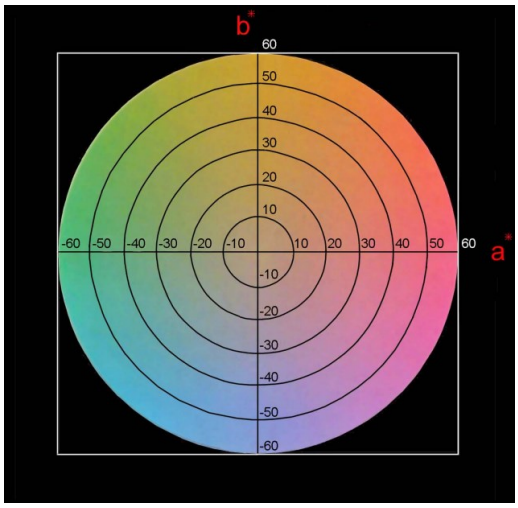


*Figure 5: The CIELAB colour space, as copied from the book "Color Vision and Colorimetry Theory and Applications".*[12]

### 1.3 Phenothiazine

Phenothiazine (**1**) is a heterocyclic compound and is the parent compound of the large class of its derivatives, that were synthesized in the early days of organic dye chemistry.[16] Its structure and that of its oxidized species, the radical cation ($\mathbf{1}^{\cdot+}$) have been well studied, and especially its geometry highlighted. The neutral species of **1** has a bend geometry, that is referred to as a butterfly-like structure. In the neutral species **1** has an angel of 158.5° between the benzene rings.[17] Upon oxidation and the formation of the radical cation $\mathbf{1}^{\cdot+}$, the geometry relaxes to almost planarity with an angle of 172.2° between the benzene rings (Figure 6).[18]

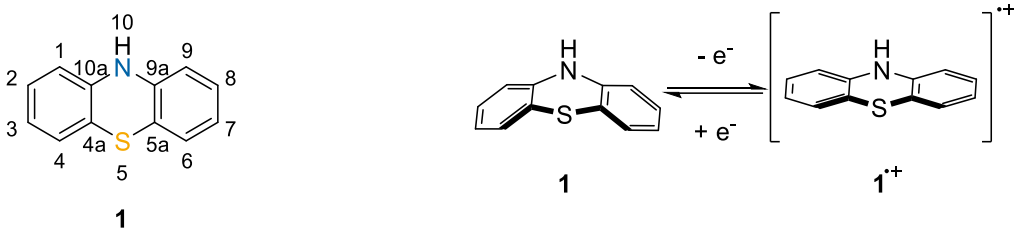


*Figure 6: Numbering of 10H-phenothiazine, also its butterfly geometry in the neutral state and the planar geometry of the radical cation.*

Molecule **1** was first synthesized by the German chemist August Bernthsen in 1883 from diphenylamine (**8**) by heating it with sulfur in high boiling solvents and catalytic amounts of iodine (Figure 7).[16,19] It was studied with its derivatives as part of new synthetic dyes, and the remarkable colour difference in contrast to their strong structural resemblance sparked interest. Phenothiazine was determined to be the parent compound and the effect of substitution of the proton in position 10 and of the 3,7 positions investigated. One compound that intrigued the researcher early on is methylthionium chloride (**9**), a salt known for its vibrant blue colour and so also known under its common name methylene blue **9** (Figure 7). As a solid it is a dark green powder in its neutral form, but upon dissolving in water it oxidizes and the rich blue colour is formed.[20] The change of colour upon oxidation in the molecules part of the phenothiazine class has been related to the change in geometry, with the planarity leading to a better overlap of the π-orbitals of the carbon- and nitrogen-atom and the carbon- and sulfur-atom.[21]

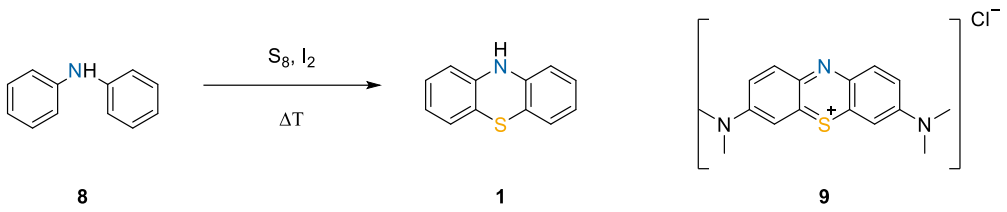


*Figure 7: The reaction scheme for the classic Bernthsen synthesis of phenothiazine and the phenothiazine derivative methylene blue.*

Over the years, the substituent effects on phenothiazine related to the geometry have been studied at the 10*H*, 1 and 9 or the 3 and 7 positions. These findings give insight into how the photophysical and electronic properties of phenothiazine can be tuned. In 1988, Wagner et al studied the substituent effect on the absorption spectra of the phenothiazine radical, by substituting phenothiazine with alkyl and aryl groups at the amine. They found, that none of the parent phenothiazines had an absorption in the visible region of the UV-Vis spectrum in the neutral state, but that their radical cation possesses absorption bands in the 350-850 nm range. With the onset of the lowest energy absorption of the radical cation exhibiting a bathochromic shift of up to 115 nm, through the substitution of the amine with a methyl group.[22]

For a detailed look into the insight, the work of S. Odom and C. Risko must be highlighted, as they did extensive studies of substituent effects on **1** and its oxidised species $\mathbf{1}^{\cdot+}$. In 2015 they showed that bulkier alkyl substituents of the amine lead to a higher oxidation potential, due to an increasingly constrained geometry of the radical cation. While the parent species **1** can change to an almost planar geometry upon oxidation, bulkier substituent lead to a bend geometry of the radical cation. In correlation to the size of the substituent, an increase in the half wave oxidation potential $E^{ox}_{1/2}$ of up to 0.36 V was observed.[23] In following studies, they found that methyl substituents acting as electron donating groups in the 3, 7 positions decrease the oxidation potential by 0.14 V, while methyl groups in 1, 9 positions can increase the oxidation potential by 0.26 V. The effect of the placement, in the 1, 9 position is related to the hindered planarization of the radical cation due to the steric effect of the methyl groups.[24] On the other hand, the methyl groups have the largest donating effect in the 3, 7 positions, as these are the most electropositive, leading to a strong decrease in the oxidation potential by 0.14 V.[25] Further, a bathochromic shift in the UV-Vis spectra was observed for the methyl groups in the 1,9 position than those in the 3,7 positions. As density functional theory (DFT) calculations revealed, the positioning of the methyl groups affects the electronic gap between the highest-occupied-molecular-orbital (HOMO) and the HOMO-1, which influences the UV-Vis absorption of the radical cation. [26] By tuning this transition the colour of the radical cation can be controlled.

## 1.4 Phenothiazine in electrochromic materials

With the combination of its tunable electronic and spectroscopic properties, **1** has sparked interest in its use in OLEDs, batteries and electrochromic materials. The Müller working group has done extensive research since 2000 on these properties, from studies of single molecules to conjugated oligophenothiazines polymers.[27] To study substituent effect, they synthesized a collection of 3-aryl 10*H*-phenothiazine from 3-bromo-10*H*-phenothizine utilizing a simple Suzuki coupling (Figure 8). They found that the substituents in the 3 position lead to a high bathochromic shift for the electron donating aryl groups and an increasing hypsochromic shift for electron withdrawing aryl substituent, due to pronounced charge transfer characteristics. In their studies the did not investigate how the photophysical properties of the radical cation are affected and if all of the molecules exhibit e reversible oxidation process.[28] These results hint at the possibilities of how aryl substituted phenothiazine derivatives could be utilized for electrochromic materials.

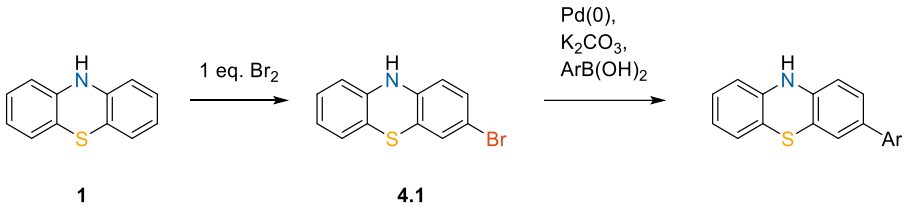


*Figure 8: Synthesis of 3-aryl 10H-phenothiazines by the Mueller group.*

Previously, Tu et al. developed a series of *N*-substituted phenothiazine derivatives as novel electrochromic materials, observing a color change from colorless to red or green at potentials of above 2.4 V (Figure 9). The reversibility of this oxidation process was not determined in the publication. For the radical cation of **1** (**1**$^{\cdot+}$) the colour green was, while all other *N*-substituted phenothiazines exhibited a red colour. In this study, no further effort was made in the characterisation of the photophysical properties of the radical cation. By dissolving the derivatives of **1** in an electrolyte solution, they could be incorporated into electrochromic devices These simple devices showed stability in over 100 redox cycles and switching times of less than 250 ms.[29]

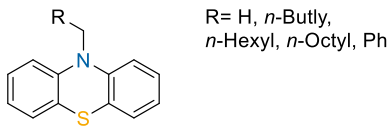


*Figure 9: N-Substituted phenothiazine for electrochromic materials.*

These previous findings have demonstrated the possible extent of phenothiazines in electrochromic materials, but their full potential remains unexplored. While green and red colours have been investigated, other potential hues arising from the disclosed radical cations remain to be studied. The ability to tune the photophysical and electronic properties of the native phenothiazine core through aryl substitution is well described, yet their applications as electrochromic materials remain largely unexamined. Beyond extending the colour palette of electrochromic phenothiazines, an alternative strategy is required to capture the full range of possible hues. Hence, a method for the rational mixing of electrochromic colours is needed.

# 2. Methods

## 2.1 Palladium Catalyzed cross-couplings

### 2.1.1 Suzuki-Miyaura cross-coupling

For the coupling of aryl substituents to an unsaturated halide, the Suzuki-Miyaura coupling has proven to be the most reliable option.[30] In essence, a C-C bond is formed between an aryl or vinyl halide/triflate with an aryl or vinyl boronic acid, which will act as an organic electrophile and an organometallic nucleophile respectively.[31] Notably, the coupling can be performed under mild conditions with excellent selectivity. Typically, the catalytic cyclic for the cross-coupling reaction of organometallics follows the sequence of an oxidative addition, followed by transmetalation and closed with a reductive elimination (Figure 10). While the general cycle is agreed upon, the details into each step are more disputed.

The first step involves the oxidative addition of the halide or other electrophiles to the active Pd(0) complex, to give a *trans*-palladium(II) complex ($R^1$-$Pd^{II}$-X). With decreasing reactivity in the order of iodide, triflate, bromine to chloride, oxidative addition generally is the rate-determining step, influenced by the strength of the C-X bond.[32] In the oxidative addition, the bond between the electrophile and its organic group is broken and two new bonds are formed with the Pd(0) complex, oxidizing palladium to Pd(II). Two mechanisms are possible for this step, either following a three-centered concerted mechanism or that of an $S_N2$.[31]

In the following transmetalation step, the organic group is transferred from the boronate to the Pd(II) complex, in a similar fashion of a ligand exchange between two metals. The detailed mechanism of the transmetalation is the most controversial, and only the importance of a base and the participation of the organoboron species are undisputed. From the role of the base, two possible pathways emerge, with the first beginning with the attack of the base on the organoboron species, followed by a nucleophilic attack on

the palladium halide complex by the anionic organoboronate (Figure 10, Pathway A). In the second pathway, the halide ligand of the Pd(II) complex is first substituted by the base and the new complex reacts with the organoborane (Figure 10, Pathway B). [31,33]

Finally, similar to oxidative addition, the reductive elimination goes through a three-coordinated transition state with two organic groups in *cis* position. A new bond between the aryl groups is formed, leading to a reduction of Pd(II) to Pd(0), regenerating the active catalyst.[31]

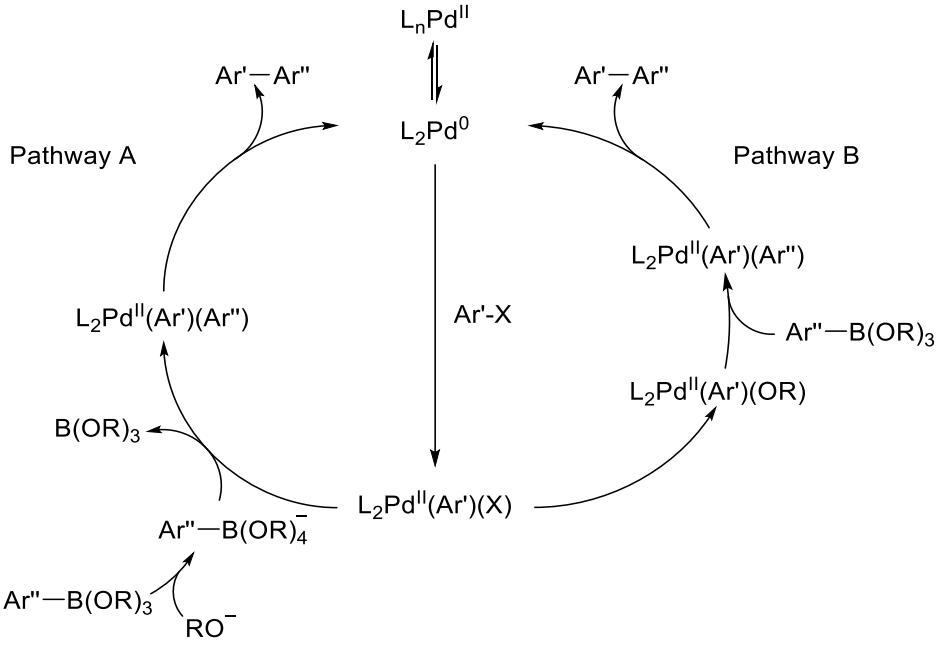


*Figure 10: Catalytic cycle of the Suzuki-Miyaura cross-coupling.*

### 2.1.2 Buchwald-Hartwig amination

The palladium mediated coupling of an amine to an aryl-halide is known as the Buchwald-Hartwig amination. Presently it is an important tool for the formation of C($sp^2$)-N bonds and emerged from the initial findings of couplings with aminostannanes and aryl halides.[34] These advances have had an impact on synthetic strategies in both academic research and industrial production. The success of the reaction can be attributed to the continuous development of its protocol and efforts to unravel the reaction.[35] The mechanism follows the general catalytic cycle of palladium-catalyzed cross couplings, with the active species being Pd(0) after initial dissociation of one phosphine ligand (Figure 11). In the first step the aryl-halide undergoes oxidative addition to the Pd(0) complex, oxidising it to Pd(II). The amines present can

coordinate to the palladium center, which can then be deprotonated by a base due to their enhanced acidity. The formed Pd(II) amido complex undergoes reductive elimination to give the product and close the catalytic cycle, restoring the active Pd(0) complex. Advancements in the catalysts have led to a broader substrate scope. Today, as a result of mechanistic studies, chelating bisphosphine ligands are commonly employed, as they prevent β-hydride elimination which could compete with the reductive elimination.[35]

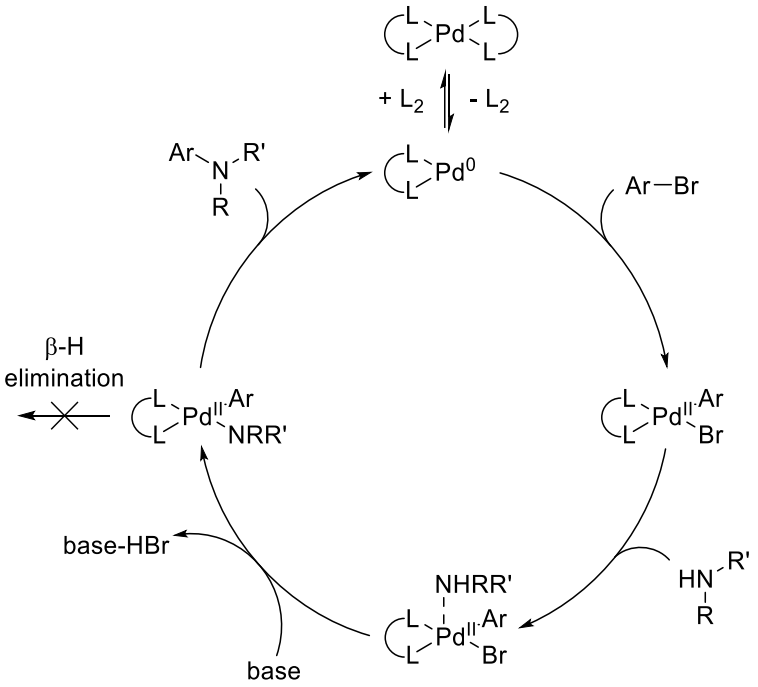


*Figure 11: Catalytic cycle of the Buchwald-Hartwig amination*

## 2.2 Ring-Opening Metathesis Polymerization

As a unique tool for the polymerization of cyclic monomers, ring-opening polymerization stands out with its capability to achieve polymers with a high molecular weight and narrow polydispersity.[36] The reaction is driven by the thermodynamically favored ring-opening, with the exception of six membered rings, due to the strain of the monomers' cyclic structure. Simply the ring strain is not enough to initiate the polymerization of cycloalkanes, due to the lack of a kinetic pathway for an initiator to open the ring. Subsequently, monomers with a considerable ring strain (>5kcal $mol^{-1}$), heteroatoms, or unsaturated moieties are ideal candidates.[36,37] For cycloalkenes to undergo ring-opening polymerization, a coordinating initiator based on transition metals is needed. As described by the given name of ring-opening metathesis polymerization (ROMP), the reaction follows the same initiation and reaction mechanism as in an olefin metathesis. Metathesis is the exchange of a C=C double bond controlled by the mediation of a metal and was unraveled

by Chauvin and revolutionized by Grubbs and Schrock, earning them the 2005 Nobel Prize in Chemistry.[38] Early transition metal catalysts suffered from little control over the polymerization or low functional group tolerance. Ru based catalysts proved useful due to their lower oxophilicity, than W or Mo based catalyst, and higher tolerance towards functional groups.[37] Particularly, with the Grubbs 3rd generation catalyst, these demands are met with more stable nitrogen-heterocyclic carbene ligands, while achieving high initiation rates due to the labile nature of the pyridine ligands.[37]

ROMP proceeds through three principal steps: initiation, propagation and termination (Figure 12). During initiation, the Ru catalyst coordinates to the monomer's double bond and undergoes a [2+2] cycloaddition forming a four-membered metallocyclobutane intermediate. Rearrangement of this intermediate generates a newly formed metal alkylidene that can propagate following the chain growth mechanism, acting as the active chain end for further monomer insertion. In the propagation stage, successive [2+2] cycloadditions drive the chain growth in a living manner until all monomers are consumed. When full conversion is ensured, the reaction is usually quenched by the addition of excess ethyl vinyl ether. In the termination the catalyst is displaced by the ethyl vinyl ether, which is incorporated in the polymer as the second end group. If quenching is omitted, incorporation of the metal catalyst into the polymer and inter- and intramolecular chain transfer will take place. This leads to degradation and a broader molecular weight distribution of the polymer.[36,37]

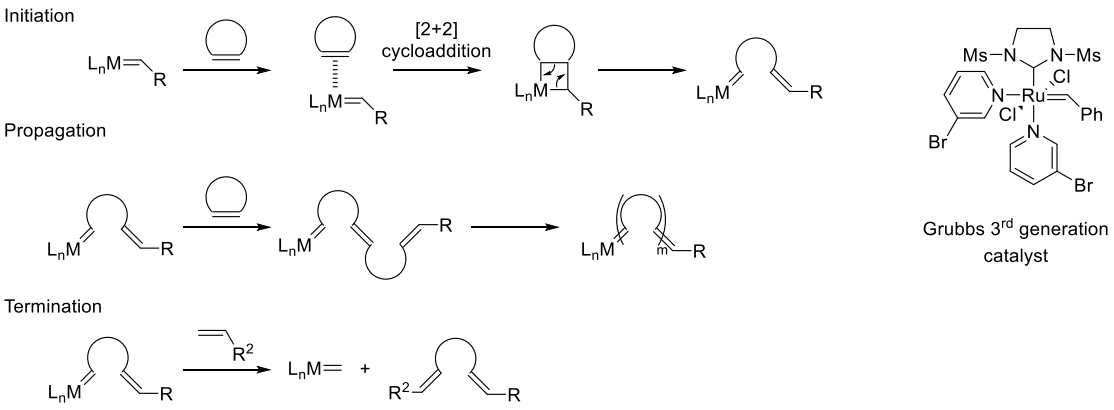


*Figure 12: The mechanism of ROMP and the structure of Grubbs 3rd generation catalyst.*

## 3. Aim of the Project

In the field of electrochromics, a wide range of colour based on different molecular classes have emerged as suitable candidates. Regardless of the variety, a systematic approach towards any colour for widely applicable electrochromic materials is missing. Currently, pre-specified goals are only reached through careful choice of candidates to find a perfect match and extensive fine-tuning of the materials.

Instead, focusing on a single class of molecules could be the pathway towards a broader colour palette, with unlimited options. This idea takes inspiration from nature, where only a few selected natural pigments are sufficient to produce the multitude of colours we see. A systematic approach, enabling rational design and mixing, requires only a select few colours to generate a wide palette. Furthermore, by focusing on a single molecule class, the coordination between the colours is simplified, as the behaviour and stability of the molecules will be similar. Phenothiazines are a versatile scaffold, being a small molecule that can be easily tuned through substitutions to change its spectroscopic and electronic properties. With the knowledge gained from fundamental research on this class, a rational approach to a new colour becomes possible. Toward this goal, the aim of this research was to develop a phenothiazine-based electrochromic colour palette and achieve new electrochromic hues through rational mixing. For the colour palette, simply aryl-substituted phenothiazines with a norbornene moiety are envisioned, mixed through ROMP with the polymer serving as the scaffold for the colours (Figure 13). First a synthetic pathway for the large-scale and efficient synthesis of these monomers must be established, followed by their full photophysical and electronic characterisation. Using the photophysical measurements, their colour is objectively described in the CIE colour space, allowing for a rational choice of the monomers to control the polymers final colour.

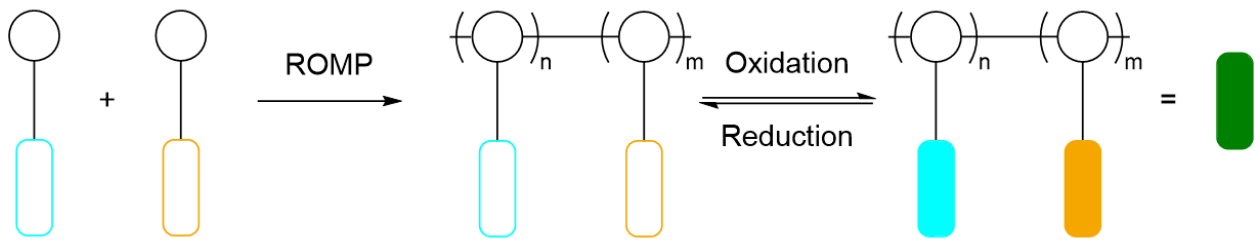


*Figure 13: Scheme of the subtractive mixing of two monomers by ring opening polymerization, to obtain a new hue.*

## 4. Retrosynthetic Analysis

The retrosynthetic pathway for the synthesis of phenothiazine based electrochomic polymers is displayed in Figure 14. To have the highest control over the polymerisation, the monomers with a phenothiazine core are polymerised by ROMP. For this a norbornene group is introduced and connected via a butyl chain spacer to the aryl-substituted phenothiazine core through alkylation of the amine. The norbornene group with its spacer is obtained in a Diels-Alder reaction of cyclopentadiene with 6-bromo-1-hexene. Since the reaction conditions of the Diels-Alder reaction are quite harsh, it is more efficient to connect the norbornene group to the spacer before the alkylation, even though the alkylation is very beneficial in increasing the solubility of the phenothiazine derivatives. A wide range of derivatives can be obtained by Suzuki-Miyaura cross-coupling with arylbronic acids, such as *o*-tolylboronic acid, *p*-tolylboronic acid, *m*-xyleneboronic acid and *p-tert*-butylphenylboronic acid. For the Suzuki-Miyaura cross-coupling the phenothiazine- or 1,9-dimethyl phenothiazine-core have to be brominated in the desired *para* position to the nitrogen atom. While phenothiazine is commercially available, 1,9-dimethyl can be obtained from 2,2'-dimethylphenylamine using the Bernthsen reaction conditions to close the heterocyclic ring with sulfur. At last, 2,2'-dimethylphenylamine is synthesized vie Buchwald-Hartwig coupling of *o*-toluidine and 2-bromotoluene.

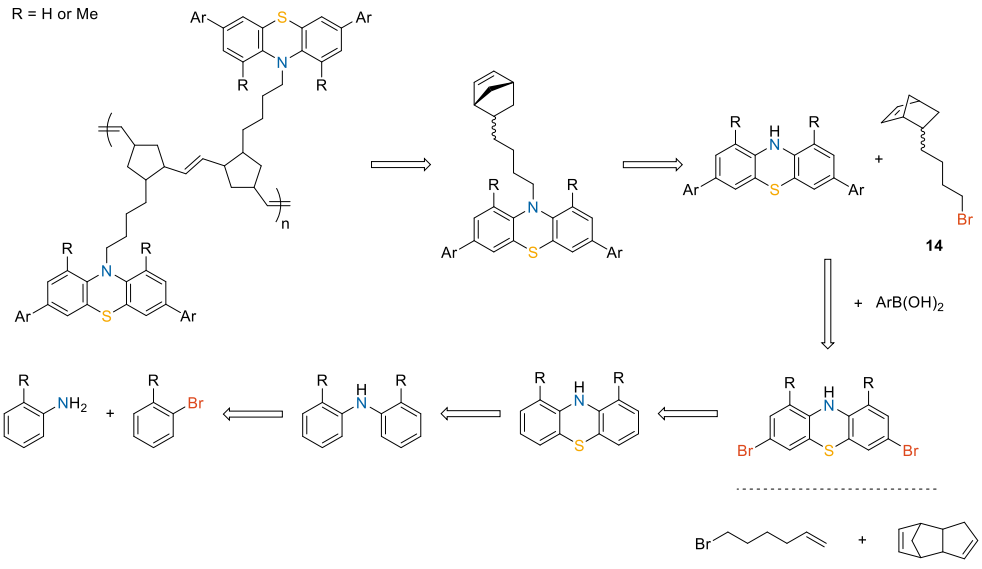


*Figure 14: Retrosynthetic plan towards phenothiazine based electrochromic polymers.*

# 5.Results and Discussion

## 5.1 Synthesis of Monomers with phenothiazine core

### 5.1.1 Bromination of phenothiazine

Brominated phenothiazine was used as the basis to expand the phenothiazine core with various aryl substituents. Specifically, the dibrominated phenothiazine species was used as the starting material for the following Suzuki-Miyaura coupling, acting as a gateway to a broad scope of phenothiazine derivatives with different electrochemical properties. Previously **1** had been successfully prepared in a large scale using bromine ($Br_2$) in AcOH (25 mmol, 75% yield) or *N*-bromosuccinimide (NBS) in THF (10 mmol, 74%).[39,40] The reaction outcome is overshadowed by the low solubility of dibrominated phenothiazine and the difficult separation of monobrominated phenothiazine species from the product mixture.[41] For the separation of large amounts of **10.1** from **10**, recrystallization in MePh followed by silica gel column chromatography gave the best result, and **10** was obtained in a yield of up to 40%.

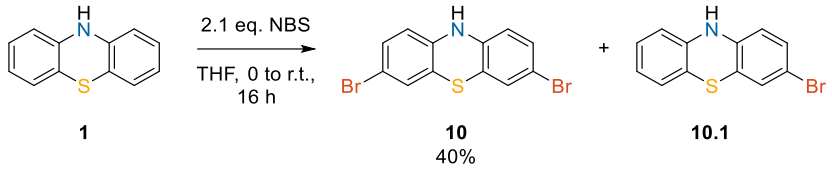


*Figure 15: Bromination of **1** with NBS.*

A more controlled approach is the bromination using tetrabutylammonium tribromide (TBATB) as a bromine source which is known for its high selectivity.[42] Previous protocols suggested a short reaction time (1 h) in polar aprotic solvents such as $CH_2Cl_2$, $CHCl_3$, $CH_3CN$ or THF.[43] For phenothiazine the short reaction time in the different solvents could not be observed (Table 1, Entry 1, 4, 7) and even an excess of TBATB had no effect on the conversion (Table 1, Entry 2, 3, 5, 6). After 16 h, only **10.1** could be observed (Table 1, Entry 7) and an increase of the reaction time to 72 h was needed for a full conversion of the starting material and product **10** was obtained in a yield of 76% (Table 1, Entry 8). On a scale of 2.5 mmol, increasing the reaction temperature to 60 °C significantly decreased the reaction time to 6 h (Table 1, Entry 9). For a larger scale of 10.0 mmol, the reaction time amounted to 16 h and the product was obtained in a yield of 75 % (Table 1, Entry 10)

Increasing the reaction temperature to 60 °C significantly decreased the reaction time to 6 h (Entry 9) and to 16 h for a larger scale of 10.0 mmol. The reaction proceeded with full conversion and the product was obtained in a yield of 75% (Entry 10).

*Table 1: Results for the bromination of **1** using TBATB.*

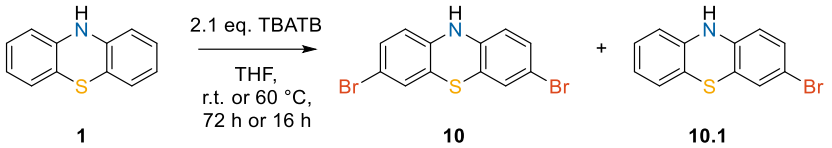


**1** **10** **10.1**

| Entry | **1**/mmol | TBATB/mmol | Solvent | T/°C | t/h | **10** Isol. yield |
|---|---|---|---|---|---|---|
| 1 | 1.0 | 2.1 | $CH_2Cl_2$ | r.t. | 3 | 0% |
| 2 | 1.0 | 2.5 | $CH_2Cl_2$ | r.t. | 3 | 0% |
| 3 | 1.0 | 3.0 | $CH_2Cl_2$ | r.t. | 3 | 0% |
| 4 | 1.0 | 2.1 | $CHCl_3$ | r.t. | 16 | 0% |
| 5 | 1.0 | 2.5 | $CHCl_3$ | r.t. | 16 | 0% |
| 6 | 1.0 | 3.0 | $CHCl_3$ | r.t. | 16 | 0% |
| 7 | 1.0 | 2.1 | THF | r.t. | 16 | 0% |
| 8 | 2.5 | 5.3 | THF | r.t. | 72 | 76% |
| 9 | 2.5 | 5.3 | THF | 60 | 6 | 69% |
| 10 | 10.0 | 21.1 | THF | 60 | 16 | 75% |

### 5.1.2 Suzuki-Miyaura Reaction

Following previously reported conditions for the Suzuki-Miyaura coupling of aryl substituents with compound **10**, product **11** was obtained only in a 1:1 ratio to the side product **11.1** that was formed through dehalogenation during the coupling (Table 2, Entry 1).[44] Besides affecting the yield, the mixture of **11** and **11.1** was difficult to separate and following the next step of the synthesis any amount of impurities would have undermined the SEC measurements. This led to an investigation into the reaction protocol to inhibit dehalogenation. As the base plays an important role in the dehalogenation, *i.e.* first substituting the halide of the Pd(II) complex upon oxidative addition, alternatives were investigated (Table 2).[45] Using KOH as base, the ratio of **11** to **11.1** only improved to 6:4 and with NaAc the conversion of the starting material was very low (Table 2, Entry 2, 3). The conversion of the starting material improved with increasing equivalents of $^t$BuOK as base, with only minor formation of **11.1** (Table 2, Entry 4-6). With six equivalents of $^t$BuOK full conversion of the starting material was achieved, but only a mixture of products was obtained, with **11.1** being the major product (Table 3, Entry 7). Ultimately, eliminating hydride sources by changing the solvent

to dimethoxyethane:water (6:1) and using $Cs_2CO_3$ as base limited the dehalogenation to a minimum (Table 2, Entry 8).

*Table 2: Results of the Suzuki-Miyaura cross-coupling of **10** with p-tolylboronic acid.*

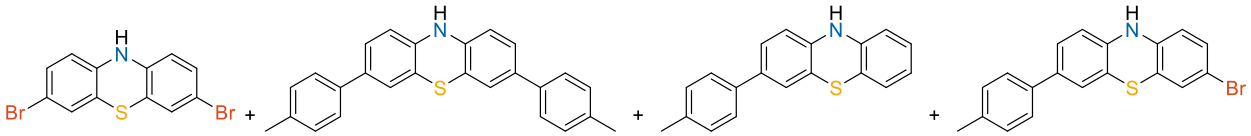


$C_{12}H_7Br_2NS$
357.06 g/mol
**10**

$C_{26}H_{21}NS$
379.52 g/mol
11

$C_{19}H_{15}NS$
289.40 g/mol
11.1

$C_{19}H_{14}BrNS$
368.29 g/mol
11.2

| Entry | Base | **2**/mmol | Solvent | T/°C | t/h | Ratio **10**/11/11.1/11.2 |
|---|---|---|---|---|---|---|
| 1 | 15 eq. $K_2CO_3$ | 0.084 | 2-ethoxyethanol :water (10:1) | 130 | 18 | 0/50/50/0 |
| 2 | 5. eq. KOH | 0.084 | 2-ethoxyethanol :water (10:1) | 130 | 5 | 0/60/40/0 |
| 3 | 3 eq. NaAc | 0.084 | THF | 80 | 2 | 74/2/0/24 |
| 4 | 2 eq. KO$^t$Bu | 0.084 | THF | 80 | 2 | 11/21/0/68 |
| 5 | 3 eq. KO$^t$Bu | 0.084 | THF | 80 | 2 | 3/55/3/40 |
| 6 | 2 eq. KO$^t$Bu | 0.084 | THF | 80 | 2 | 16/27/0/57 |
| 7 | 6 eq. KO$^t$Bu | 0.084 | THF | 80 | 2 | 0/34/49/17 |
| 8 | 4 eq. $Cs_2CO_3$ | 0.084 | dimethoxyethane :water (6:1) | 85 | 2 | 0/96/4/0 |

The optimized reaction conditions from the coupling with *p*-tolyl-boronic acid were employed for the coupling of compound **10** with *m*-tolyl-boronic acid and *m*-xylene-boronic acid.

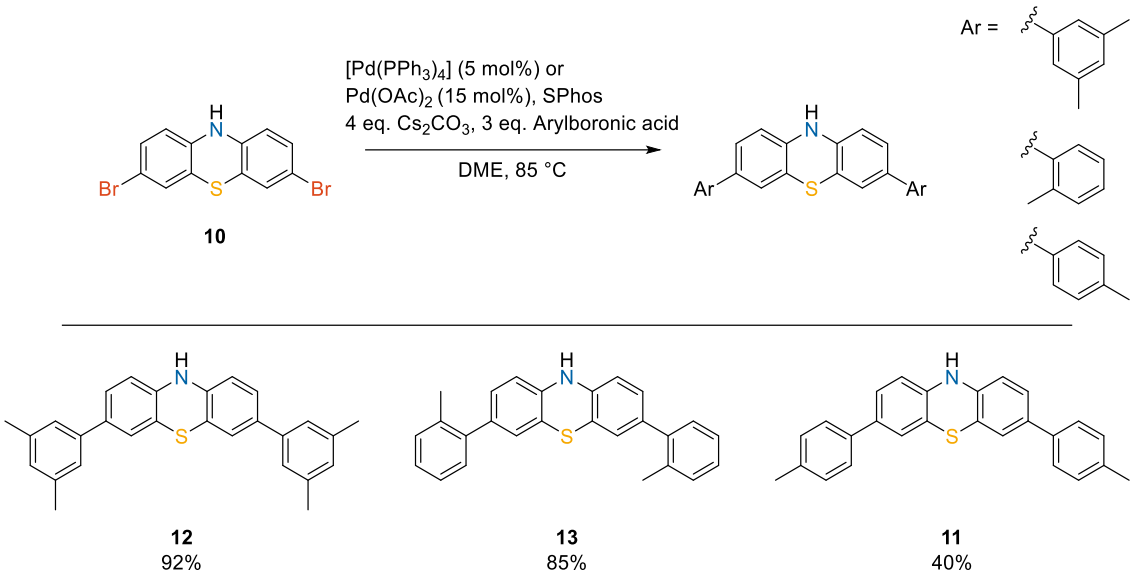


*Figure 16: Results and scope of the Suzuki-Miyaura cross-coupling of **10** with m-xyleneboronic acid, o-tolylboronic acid and p-tolylboronic acid.*

### 5.1.3 Alkylation

Following the protocol by Espinet et al., molecule **14** was prepared and obtained in a yield of 30%.[46] As previously reported, the product was obtained as an isomeric mixture of *endo*- (major) and *exo*- (minor) in a ratio of *endo*:*exo* = 75:25. The alkylation was first attempted with KOH as a base to deprotonate the amine but only worked reliably for 3,7-di-3,5-dimethylphenyl-10*H*-phenothiazine (**3**) which was obtained in an 82% isolated yield. On TLC several fluorescent spots could be observed, suggesting a mixture of side products. As an alternative, the alkylation was attempted using LiHMDS to give the respective lithium ammonium salt, which was then transferred to molecule **14**. During several attempts, either no reaction was observed, or an inseparable mixture of products was obtained. At last, using a weaker base such as $Cs_2CO_3$ in $CH_3CN$ afforded products **4** and **5** were obtained in a yield of 87% and 40%, respectively.

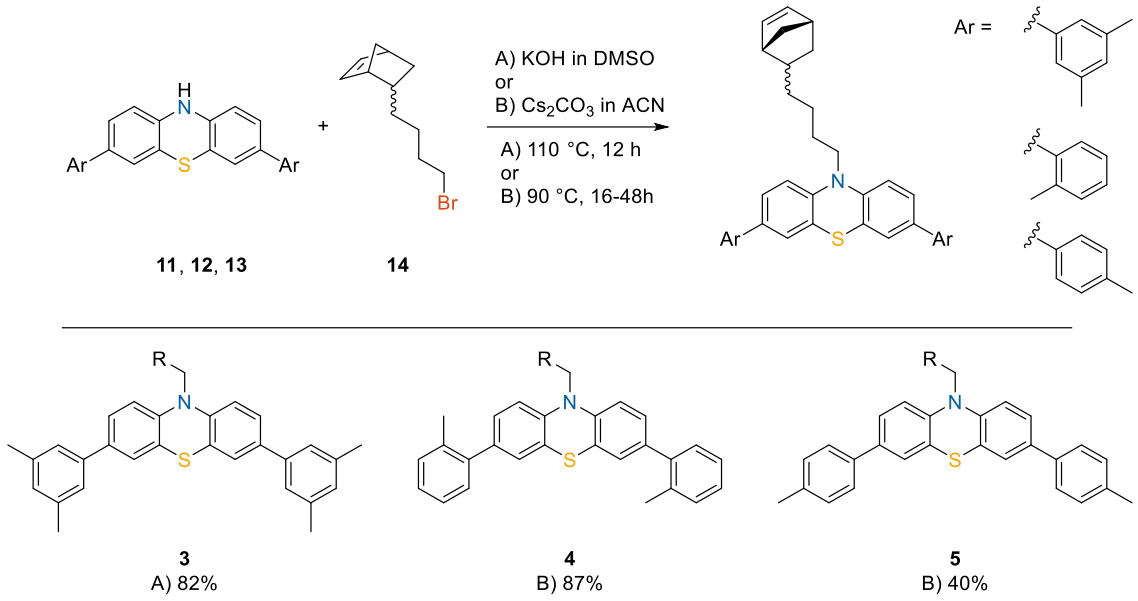


*Figure 17: Results and substrate scope for the alkylation of **11, 12, 13** with **14**.*

## 5.2 Synthesis of Monomers with 1,9-dimethyl-phenothiazine core

### 5.2.1 Synthesis of 1,9-dimethyl-phenothiazine

Derivatives of phenothiazine were studied by incorporating methyl groups in the 1,9-positions, which upon their oxidation could influence the planarisation of the radical cation. Compound **15** was synthesised *via* Buchwald-Hartwig amination of *o*-toluidine and 2-bromotoluene and obtained with a 96% yield. The following heterocyclic ring closure of **15** with $S_8$ gave product **2** with a 34% yield. By increasing the $S_8$ equivalents from 1.1 to 2.0 in the Bernthsen reaction, the yield of **2** was increased to 50%. However, when scaling up the reaction from 5.0 mmol to 11.5 mmol, the yield reduced to 34%.

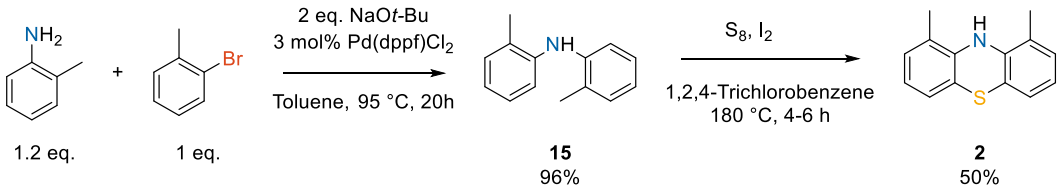


*Figure 18: Reaction scheme of the Buchwald Hartwig amination of o-toluidine and 2-bromotoluene, followed by the Bernthsen reaction of **15**, affording **2**.*

### 5.2.2 Bromination of 1,9-dimethyl-phenothiazine

The reaction conditions used for the bromination of **1** were initially employed for compound **2**, however after 48 h only starting material and different oxidized species of **2** were observed by $^1$H-NMR. These suggested

that free radical bromination of the methyl groups in the 1,9-positions was occurring. The reaction temperature was then lowered to 40 °C, but only low conversion to product **16** and monobrominated side-product was observed on TLC after 48 h. To promote the formation of the bromonium ion, new reaction conditions were sought out, using $Br_2$ in AcOH with $FeBr_3$ as catalyst. At room temperature, after 36 h product **16** was obtained in a yield of 51% (Table 3, Entry 1). By lowering the reaction temperature to 0 °C at the beginning of the reaction, the yield increased to 59% (Table 3, Entry 2), but prolonging the reaction time had no positive effect (Table 3, Entry 3). Overall, the yield was affected by the purification procedure, as only crystallization from EtOH was suitable. When compound **16** was subjected to silica gel column chromatography, oxidation could be observed and only a small fraction of the product was isolated (Table 3, Entry 4).

*Table 3: Results for the optimization of the bromination of **2**.*


**2** **16** 59%

| Entry | **13**/mmol | T/°C | t/h | **16** Isol. yield |
|---|---|---|---|---|
| 1 | 0.3 | r.t. | 36 | 51% |
| 2 | 0.3 | 0 to r.t. | 36 | 59% |
| 3 | 0.3 | 0 to r.t. | 96 | 43% |
| 4 | 0.9 | r.t. | 36 | 6% |

### 5.2.3 Suzuki-Miyaura Reaction

Using the previously reported optimized procedure for the Suzuki-Miyaura reaction, products **17** and **18** were obtained in a yield of 98% and 64%, respectively. Since from the bromination of compound **2**, only small amounts of starting material **16** were obtained, the reactions were only performed on a scale of 0.1 mmol.

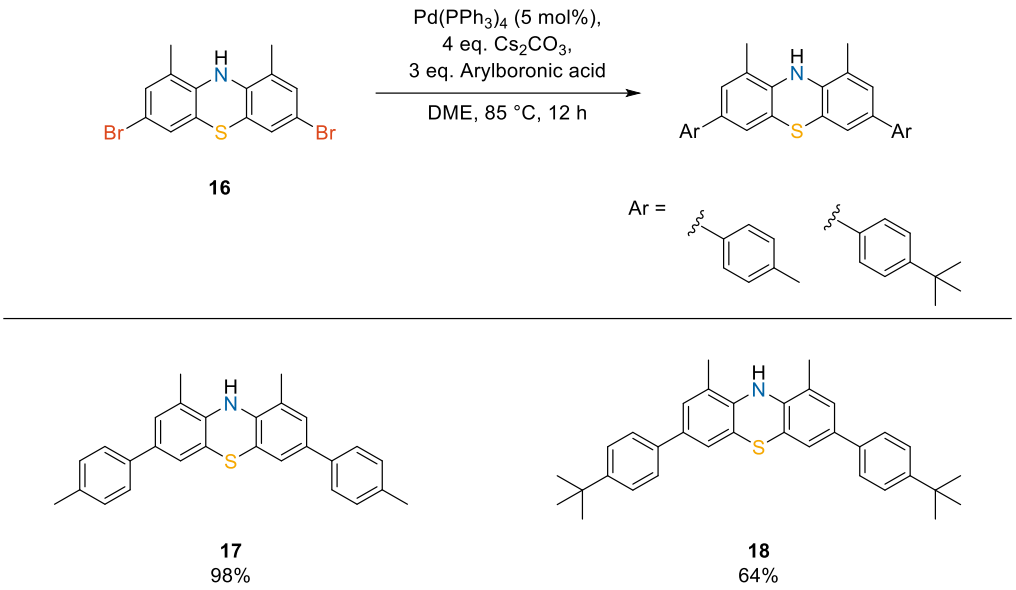


*Figure 19: Results for the Suzuki-Miayaura cross-coupling of **16** with o-tolylboronic acid and tert-butylphenylboronic acid.*

### 5.2.4 Alkylation of 1,9-dimethyl-phenothiazine derivatives

Based on the previous findings, the employed conditions for the alkylation were using $Cs_2CO_3$ as base in $CH_3CN$ instead of KOH in DMSO. The weaker base and lower reaction temperature employed in the protocol lead to less degradation and unconverted starting material could be recovered. Previously, during the purification of the alkylation, excess starting material **14** had to be washed out with MeOH or $CH_3CN$, also leading to removal of product. To minimize the loss of the product during purification, the equivalents of **14** were reduced from 3.0 to 1.3, simplifying the isolation of product **6** and **7** from the crude. Due to the reduced equivalents of **14** the reaction time was prolonged to 48 h until no change in the conversion of the starting material **17** or **18** could be observed anymore on TLC.

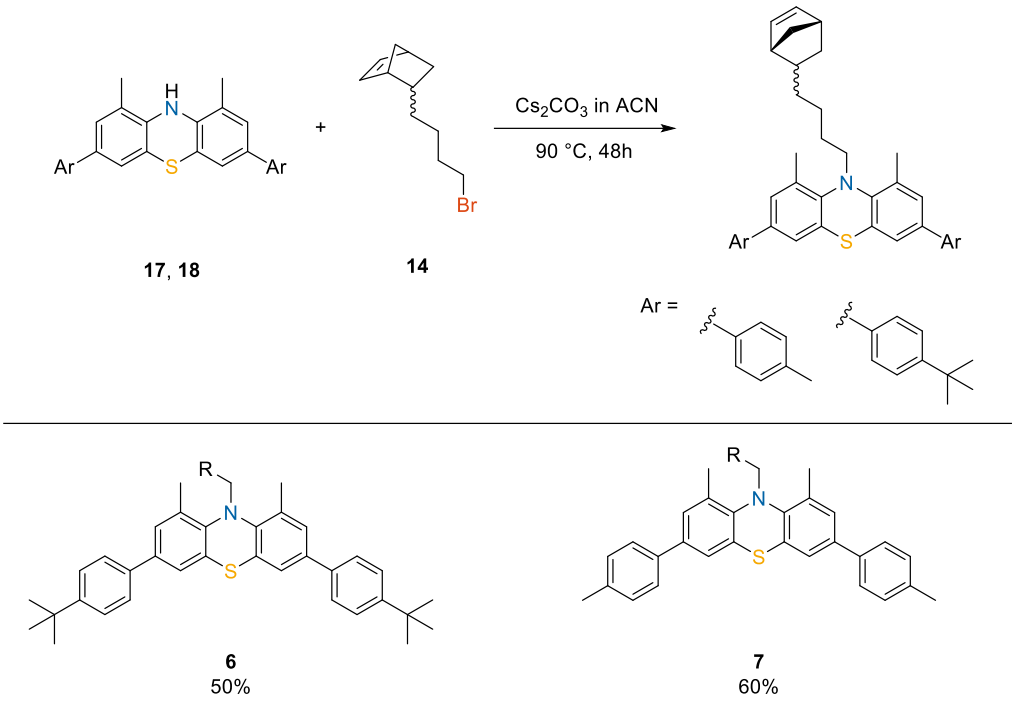


*Figure 20: Results for the alkylation of **17** and **18** with **14**.*

### 5.3.1 Photophysical characterization of monomers

UV–vis spectroscopy of synthesised monomers was investigated in their neutral state to understand their initial absorption and analyse their colour before oxidation. Furthermore, the previously synthesised monomer **19**, consisting of the native phenothiazine core, was included for comparison (Figure 22). Monomers **3**, **4**, **5**, **6**, **7**, and **19** exhibited an absorption band centered at 336, 321, 336, 326, 326, and 310 nm respectively, with all substituted monomers exhibiting a bathochromic shift compared to the native monomer **19**. The shift is due to the extended conjugation by the aryl substituents in the 3,7-positions, resulting in bathochromic shifts of 26 nm for monomers **3** and **5**, and 11 nm for monomer **4.** In monomer **4**, the ortho-methyl group on the aryl substituent introduces steric hindrance, forcing the phenyl ring to rotate out of plane with respect to the phenothiazine core (Figure 21). This torsion reduces π-conjugation, leading to a smaller bathochromic shift compared to the more planar and conjugated monomers 3 and 5. In analogous biphenyl systems, the correlation between an increasing torsion angle and a hypsochromic shift on the $\lambda_{max}$ was demonstrated, with a 90° torsion angle leading to a 68 nm hypsochromic shift.[47]

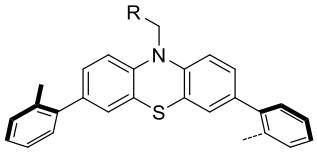


*Figure 21: Possible twisted geometry of monomer **4**, showing the hindered conjugation between the phenothiazine core and its aryl substituents.*

For both monomers **6** and **7**, the bathochromic shift is 16 nm, which is lower than that of **3** and **5**. Besides the aryl substituents in the 3,7-positions extending the conjugated system, the methyl groups in the 1,9-positions have an hypsochromic effect on the $\lambda_{max}$, which is in accordance with literature.[26] The optical bandgap ($E_g^{00}$) can be estimated from the onset of the lowest energy absorption using the formula $E_g^{00} = \left(\frac{hc}{\lambda_{onset}}\right) \approx 1240/\lambda_{onset}$ (Table 4) and gives insight into the colour of the monomers in their neutral state. Since the highest energy wavelength of visible light is 380 nm, $E_g^{00}$ must be approximately larger than 3.26 eV for the monomers to be colourless.[12] This is the case for monomers **19**, **4**, **6**, and **7**, exhibiting $E_g^{00}$ of 3.46, 3.28, and 3.38 eV, respectively, making them appear colorless. Meanwhile, monomers **3** and **5** exhibit $E_g^{00}$ of 3.00 and 2.97 eV, respectively, and both appear yellow.

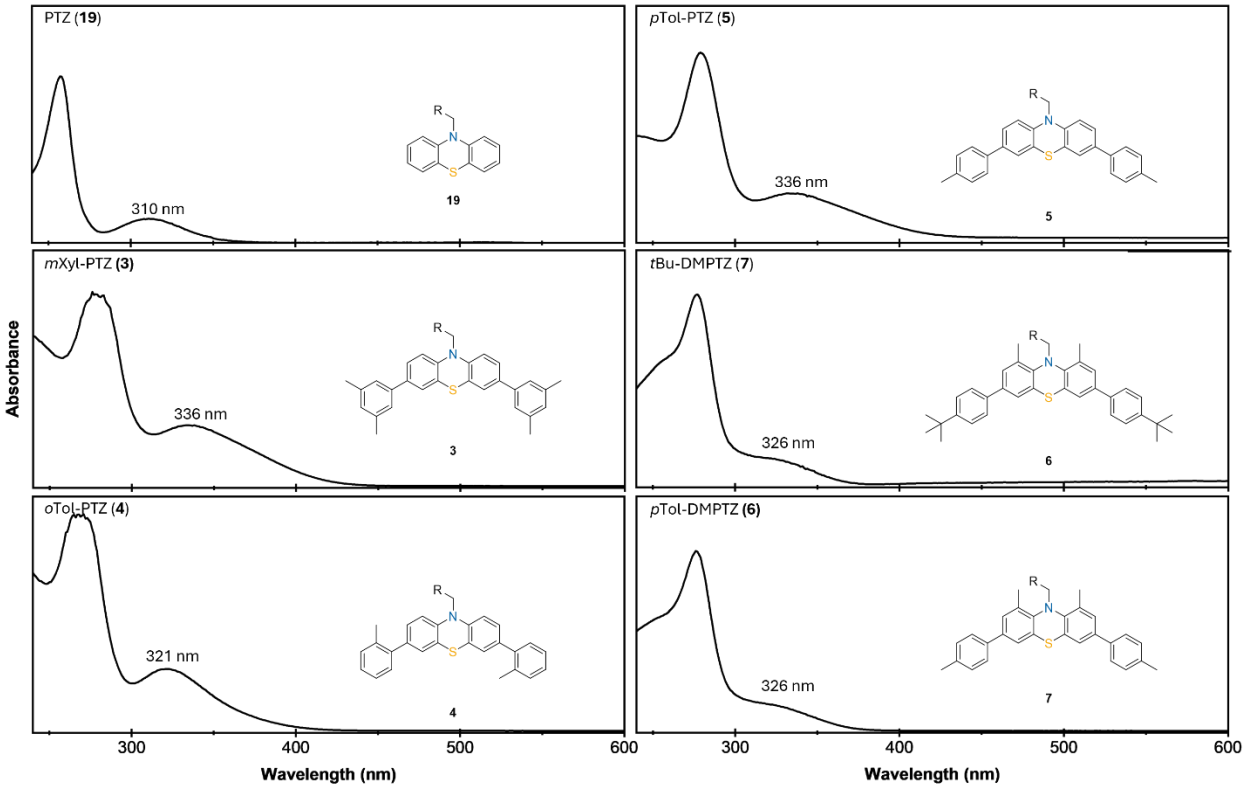


*Figure 22: UV-Vis of the neutral (0.00 V) monomer species **3, 4, 5, 6, 7, 19** and the respective values for $\lambda_{max}$.*

Following the characterisation of the monomers in the neutral state, the redox properties were investigated via cyclic voltammetry (CV) using decamethylferrocene/decamethylferrocenium ($DmFc/DmFc^+$) as an internal reference and $CH_2Cl_2$ as a solvent at rt. The initial studies showed that all monomers exhibited a single-electron reversible oxidation process ($E^{ox}_{1/2}$)(Figure 24 left), except for monomer **6** which displayed another oxidation process at 0.85 V (vs $DmFc/DmFc^+$). This additional oxidation process could be due to impurity, which was not detected in the $^1$H-NMR or mass spectrum of monomer **6**. Since the additional oxidation process occurs at a lower oxidation potential than the first oxidation of monomer **6**, it is not possible to oxidise monomer **6** selectively without oxidising the impurity. Hence, further spectroelectrochemical characterisation of monomer **6** was not performed. All monomers exhibit at least one irreversible oxidation process from 0.0 – 2.0 V. The oxidation potential of the first irreversible process ($E^{ox}_{irrev}$) was determined at the onset of the anodic wave. All monomers displayed a similar limit in the range of 1.30 to 1.50 V. The reversibility of the first oxidation is fully supported with a peak-to-peak separation ($\Delta_{p\text{-}p}$) values ranging from 81 to 100 mV and linear correlation between the peak current ($I_a$) and square root of scan rate ($\sqrt{v}$) (Figure 24 right).

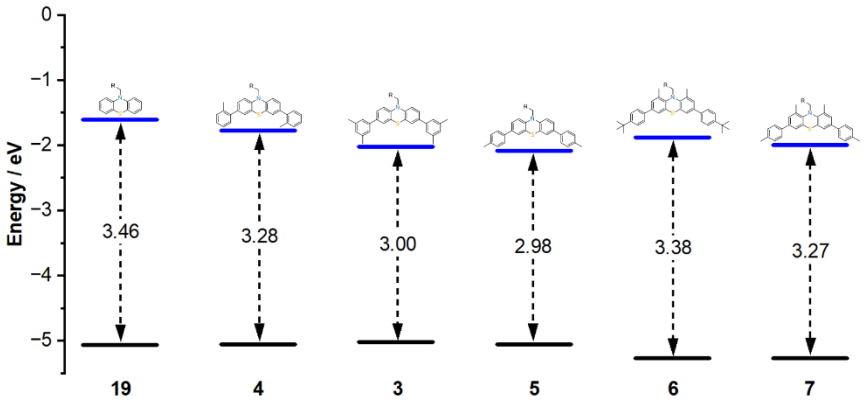


*Figure 23: From the halfwave oxidation potential ($E_{1/2}^{ox}$) and optical bandgap ($E_{00}^{g}$) estimated HOMO and LUMO profiles of the monomers.*

*Table 4:Summary of the oxidation potential ($E_{1/2}^{ox}$), optical bandgap ($E_{00}^{g}$) and associated frontier molecular orbital energies (HOMO, LUMO). The HOMO was calculated with: $E_{HOMO} = -\left(E_{\frac{1}{2}}^{ox} - 0.54\right) - 4.8$, and the LUMO using the optical bandgap: $E_{LUMO} = E_{HOMO} + E_{00}^{g}$.*

| Entry | Monomer | $E_{1/2}^{ox}\ (V)$ | $E_{00}^{g}(eV)$ | $E_{HOMO}\,(eV)$ | $E_{LUMO}\,(eV)$ |
|---|---|---|---|---|---|
| 1 | PTZ (**19**) | 0.80 | 3.46 | –5.06 | –1.60 |
| 2 | mXyl-PTZ (**3**) | 0.76 | 3.00 | –5.02 | –2.02 |
| 3 | *o*Tol-PTZ (**4**) | 0.79 | 3.28 | –5.05 | –1.77 |
| 4 | *p*Tol-PTZ (**5**) | 0.79 | 2.97 | –5.05 | –2.08 |
| 5 | *t*Bu-DMPTZ (**6**) | 1.00 | 3.27 | –5.26 | –1.99 |
| 6 | *p*Tol-DMPTZ (**7**) | 1.00 | 3.38 | –5.26 | –1.88 |

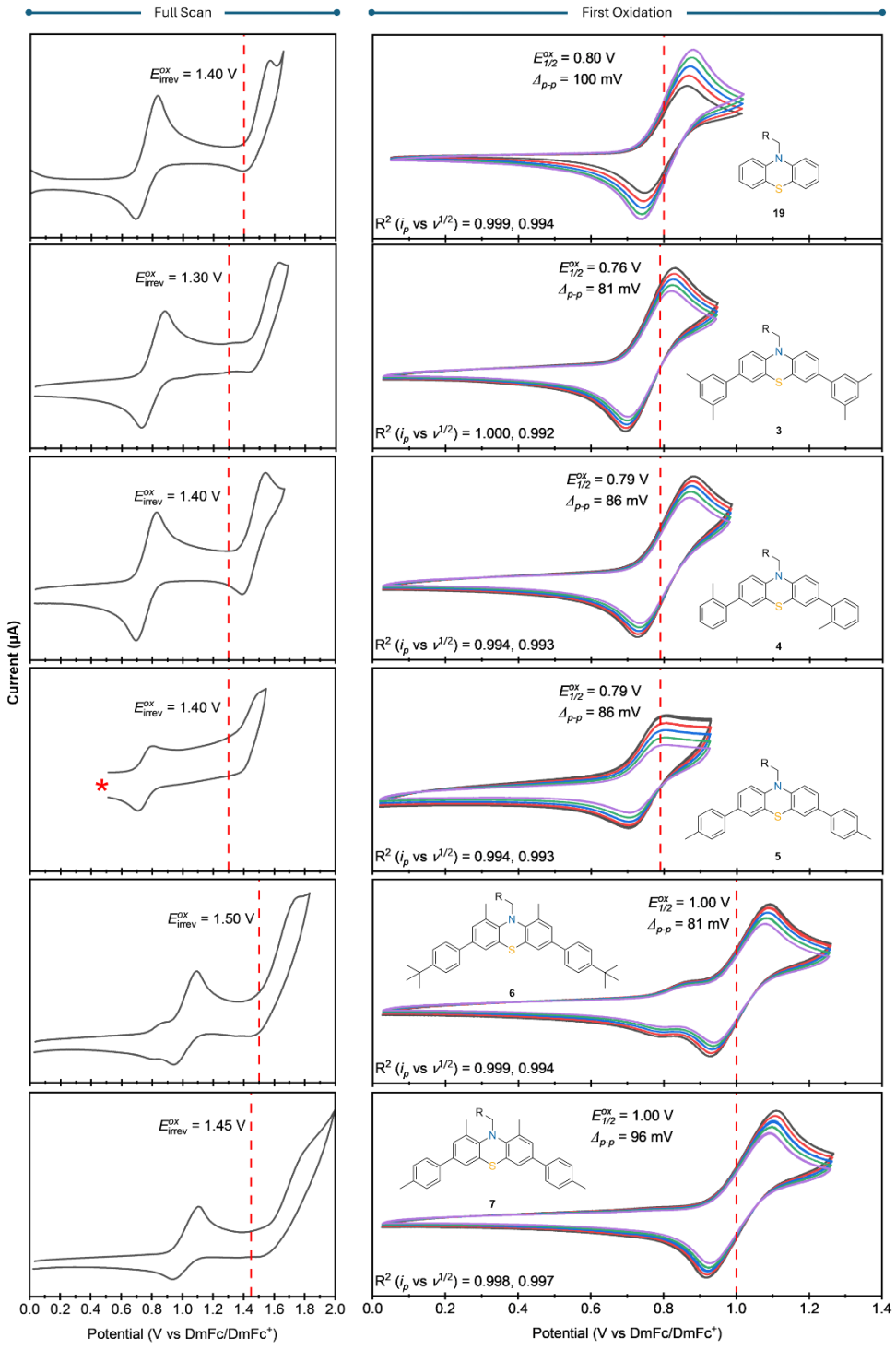


*Figure 24 Cyclic voltammetry of monomers **3**, **4**, **5**, **6**, and **7** (1 mM). Scan rate: 100 mV/s. Solvent: $CH_2Cl_2$. Supporting electrolyte: $TBAPF_6$. Working electrode: 7 $mm^2$ platinum disk. Counter electrode: Platinum wire. DmFc is used as an internal reference standard. * $E^{ox}_{1/2}$ = half-wave oxidation potential, calculated using the formula $E^{ox}_{1/2} = (E_{pa} + E_{pc})/2$ , where $E_{pa}$ and $E_{pc}$ are the anodic and cathodic peak potential, respectively. $E^{ox}_{irrev}$ = first irreversible oxidation potential, determined at the onset of the first irreversible oxidation. $\Delta_{p-p}$ = peak-to-peak separation, the difference between the anodic and cathodic peak potentials.*

As summarized in Table 5, monomers **19**, **3**, **4** and **5** showed a halfwave potential from 0.76 V to 0.80 V (vs DmFc/DmFc$^+$), while monomers **6** and **7** have a noticeably higher $E^{ox}_{1/2}$ at 1.00 V (Figure 24 right). Based on the optical bandgap ($E_g^{00}$) and first oxidation potential ($E_{1/2}^{ox}$), the highest occupied molecular orbital (HOMO) and lowest unoccupied molecular orbital (LUMO) energy levels of the monomers were estimated, as summarized in Table 4 and Figure 23. The higher oxidation potential of monomers **6** and **7** is related to their lower HOMO energy of –5.26 V, while the other monomers exhibit similar HOMO energy levels ranging from –5.02 V to –5.06 V (Figure 23, Table 4). As previously stated, the geometry of phenothiazine changes during the oxidation from bend to planar, which is limited by the methyl groups in the 1 and 9 positions, lowering the energy of the HOMO.[26] For the LUMO, compared to monomer **19**, lower energy levels were observed for the aryl-substituted monomers **3**, **5**, **6**, and **7**, in the range of –1.88 V to –2.08 V , due to the extended conjugation.[48] Only monomer **4** exhibits a LUMO energy level closer to that of the native monomer **19**, of –1.77 V compared to the –1.60 V (Figure 23, Table 4). The higher torsion angle (Figure 21) decreases the degree of electron π-delocalization, destabilizing the LUMO and increasing the energy gap.[47]

Following the study of the electrochemical data, *in situ* spectroelectrochemical (SEC) measurements were performed for monomers **19**, **3**, **4**, **5**, and **7** to gain insight into the electronic properties of their oxidized species. Upon oxidation, all monomers exhibited a clear bleaching of their characteristic absorption band at 310–336 nm, accompanied by the concomitant appearance of a broad absorption band, tailing to the NIR region ($\lambda_{max}$= 865, 699, 630, 712, 866 nm for monomers **19**, **3**, **4**, **5**, and **7**, respectively). This new absorption band confirms the formation of radical cation of the monomers, **19**$^{\cdot+}$, **3**$^{\cdot+}$, **4**$^{\cdot+}$, **5**$^{\cdot+}$, and **7**$^{\cdot+}$ upon oxidation. Since the electronic excitation of the radical cations is a transition from the SOMO–n (Single Occupied Molecular Orbital) to the SOMO, which was before the oxidation the HOMO, the energy of the first electronic transition is significantly lowered, compared to their neutral species, as shown in the overall bathochromic shift of all radical cations. These transitions have been previously characterised through computational studies and confirmed that the transitions from lower MOs (*i. e.,* SOMO–n) to the SOMO can be assigned to the absorption at longer wavelengths.[49] Since the radical cations exhibit multiple absorption bands, their color depends on their position and relative intensities of these visible absorption bands. Although the $\lambda_{max}$ of monomer **19**$^{\cdot+}$ is centered at 865 nm, its relative intensity is significantly lower (~7×) compared to the absorption band at 515 nm, making its colour red. Radical cations **3**$^{\cdot+}$ and **5**$^{\cdot+}$ exhibited similar visible absorption band centered at 483 and 699 nm for **3**$^{\cdot+}$, and 485 and 712 nm for **5**$^{\cdot+}$, resulting in similar colour that can be described as green. On the other hand, monomer **4**$^{\cdot+}$ exhibited visible absorption peaks at 476 and 630 nm, resulting in cyan colour. The hypsochromic shift of 69 and 82 nm between the $\lambda_{max}$ of **4**$^{\cdot+}$ vs **3**$^{\cdot+}$ and **5**$^{\cdot+}$, respectively, is due to the limited conjugation of **4**$^{\cdot+}$ with the sterically hindering

*ortho*-tolyl group disturbing the planarization of the radical cation. Finally, monomer **7**$^{\cdot+}$ exhibited absorption bands at 442, 583, and 866 nm, resulting in a brown/purple colour. Here, the electron donating effect of the methyl groups in 1,9-positions resulted in the decrease of the energy level of the SOMO (previous HOMO), lowering the first energy transition (*i.e.,* SOMO–n to SOMO), which results in a longer $\lambda_{max}$ compared to the other radical cations.[26]

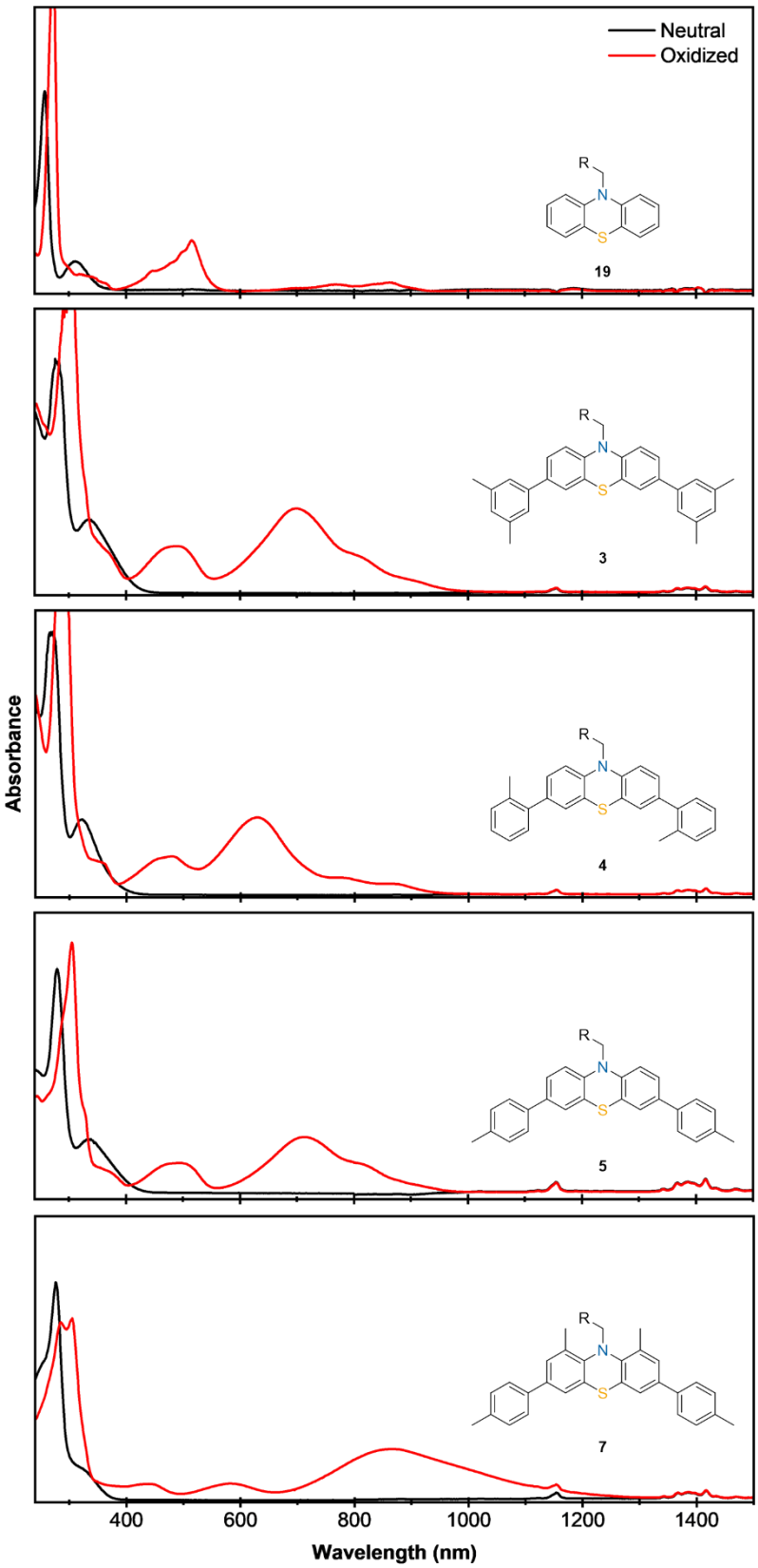


*Figure 25: UV-Vis of the neutral (0.00 V) and oxidized species (1.10 V) of the monomers **19**, **3**, **4**, **5** and **7**.*

### 5.3.2 Tristimulus values and colour mixing

To provide a quantitative colour description, the tristimulus values xyY of for the observed colour of the radical cations were determined. Initially, the x and y values of the complimentary/absorbed colour of the radical cations was calculated from the absorbance spectra (Table 5, columns 2 and 3), using the software "ColorCalculator" from Osram. Then, the x,y values of the observed colour were calculated, using equation (1), as specified in Table 5 (columns 4 and 5) and plotted in the CIE 1931 plot.

$$x_{vis} = 0.66 - x_{comp},\ y_{vis} = 0.66 - y_{comp} \quad (1)$$

Here $x_{vis}$ and $y_{vis}$ are the x and y values of the observed colour, while $x_{comp}$ and $y_{comp}$ are the x and y values of the complimentary/absorbed colour of the radical cations.

*Table 5: Summary of the x,y values of the complimentary/absorbed ($x_{comp}$ and $y_{comp}$) and observed ($x_{vis}$ and $y_{vis}$) color of the radical cations. The $x_{vis}$ and $y_{vis}$ values of the observed colour displayed in the CIE 1931 plot, which was generated with python using the "colour-science 0.4.6" package.*

| | Complimentary | | Visible | |
|---|---|---|---|---|
| Radical Cation | $x_{comp}$ | $y_{comp}$ | $x_{vis}$ | $y_{vis}$ |
| **19**$^{\cdot+}$ | 0.123 | 0.341 | 0.537 | 0.319 |
| **3**$^{\cdot+}$ | 0.331 | 0.284 | 0.329 | 0.377 |
| **4**$^{\cdot+}$ | 0.387 | 0.336 | 0.273 | 0.324 |
| **5**$^{\cdot+}$ | 0.325 | 0.319 | 0.335 | 0.341 |
| **7**$^{\cdot+}$ | 0.336 | 0.329 | 0.324 | 0.331 |

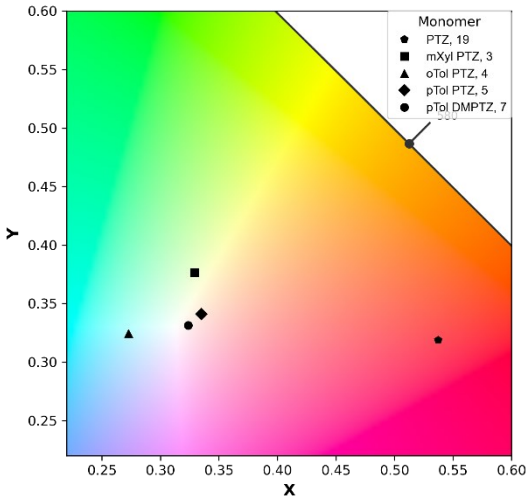


The $x_{vis}$ *and* $y_{vis}$ values of the observed colour of the radical cations, **19**$^{\cdot+}$, **3**$^{\cdot+}$, **4**$^{\cdot+}$, **5**$^{\cdot+}$, and **7**$^{\cdot+}$, confirm their red, green, cyan, green, and purple colour. Building on these colors, the monomers can be strategically copolymerized to generate the highly sought-after black colour, upon oxidation. For the choice of the monomers, several parameters, such as $E_{1/2}^{ox}$, observed colour, visible absorption spectra, and molar absorption coefficient (ε) were considered. First, monomer **7** was excluded from the copolymerization since it showed a 0.2 V higher oxidation potential than the other monomers (Table 4), which could lead to an offset in the oxidation of the copolymer. Since there is a great offset between the visible absorbance

spectra of **19**$^{\cdot+}$ with **3**$^{\cdot+}$, **4**$^{\cdot+}$ and **5**$^{\cdot+}$, it is hypothetically possible to copolymerize them at a certain ratio to achieve black. However, since **4**$^{\cdot+}$ has a much lower ε than that of **19**$^{\cdot+}$, **3**$^{\cdot+}$, and **5**$^{\cdot+}$, monomer **4** was excluded as it will require a disproportionately high **4**:**19** molar ratio to achieve black (Table 6). Furthermore, monomer **4** was also excluded to avoid the absorption of one monomer to be very dominant in dictating the color of the copolymer. Finally, between the remaining monomers (**3** and **5**) that can be copolymerised with **19**, monomer **3** was preferred due to its greater observed solubility.

*Table 6: The values for the $\lambda_{max}$ (nm) and the molar extinction coefficient ε ($M^{-1}$ $cm^{-1}$) of the neutral and oxidised species of monomer **3**, **4**, and **19**.*

| | Neutral | | Oxidised | |
|---|---|---|---|---|
| Compound | $\lambda_{max}$ (nm) | ε ($M^{-1}$ $cm^{-1}$) | $\lambda_{max}$ (nm) | ε ($M^{-1}$ $cm^{-1}$) |
| mXyl-PTZ (**3**) | 332 | 6197 | 699 | 7186 (699 nm)<br>3955 (486 nm) |
| *o*Tol-PTZ (**4**) | 321 | 5059 | 630 | 5265 (630 nm)<br>2581 (475 nm) |
| PTZ (**19**) | 311 | 6244 | 515 | 10,391 (515 nm) |

To determine the ratio of **19**:**3** to achieve black, a previously developed method was used to predict the subtractive mixing of two different coloured monomers as part of a copolymer. This method is under the assumption that the spectrochemical properties of the radical species is maintained upon copolymerization. The x,y values of the mixed colour ($x_m$, $y_m$) could be calculated from the coordinates ($x_a$, $y_a$ for monomer a and $x_b$, $y_b$ for monomer b) of two different coloured monomers (A, B) and their respective luminance value ($Y_a$, $Y_b$ for monomer a and b, respectively). The coordinates were obtained as stated before using the software "ColorCalculator", while the luminance value can be obtained as followed from the color matching function of the luminance:

$$Y = K[P(\lambda_1)\bar{y}(\lambda_1) + P(\lambda_2)\bar{y}(\lambda_2) + \cdots + P(\lambda_n)\bar{y}(\lambda_n)] = K\sum P\bar{y}.^{12} \quad (2)$$

Here $K$ (683 lm $W^{-1}$) is a constant which is derived from the luminous sensitivity of the eye; $\lambda_n$ is the wavelength at *n* nm; $\bar{y}$ is the colour-matching function as defined and tabulated for each wavelength in the range of 360-830 nm by CIE and $P$ the relative spectral power distribution for $\lambda_n$ which is equal to the absorbance:

$$P = A = \varepsilon c l \tag{3}$$

and thus, applied to the luminance:

$$Y = K \sum \varepsilon c l \bar{y}. \tag{4}$$

The targeted observed colour is dependent on the parameters of the different coloured monomers which are summarised in the generalised equation for the mixing of two colours ($x_a$, $y_a$ and $x_b$, $y_b$):

$$x_m = \frac{\frac{x_a}{y_a} \cdot Y_a + \frac{x_b}{y_b} \cdot Y_b}{\frac{\cdot Y_a}{y_a} + \frac{\cdot Y_b}{y_b}} \text{ and } y_m = \frac{Y_a + \cdot Y_b}{\frac{Y_a}{y_a} + \frac{Y_b}{y_b}}. \tag{5}$$

With the definition of the luminance value $Y$ in equation (4) the following equation could be derived from equation (4):

$$x_m = \frac{x_a y_b c_a \Sigma \epsilon_a \bar{y} + x_b y_a c_b \Sigma \epsilon_b \bar{y}}{y_b c_a \Sigma \epsilon_a \bar{y} + y_a c_b \Sigma \epsilon_b \bar{y}} \text{ and } y_m = \frac{y_a y_b [c_a \Sigma \epsilon_a \bar{y} + c_b \Sigma \epsilon_b \bar{y}]}{y_b c_a \Sigma \epsilon_a \bar{y} + y_a c_b \Sigma \epsilon_b \bar{y}} \tag{6}$$

Using equation (6) the CIE xyY coordinates of the copolymer could be calculated.

Following the previously described method, it was calculated that to achieve black ($x_m$ = 0.333, $y_m$ = 0.333), a **19**/**3** ratio of 1:24 must be used in the copolymerization. This ratio accounts for the larger ε of **19**$^{\cdot+}$ and ensuring an equal contribution between **3**$^{\cdot+}$ and **19**$^{\cdot+}$ in the visible region and to possibly achieve black. For reference, two different copolymers were synthesized at **19**/**3** ratio of 1:240 and 2:23.

### 5.3.2 Polymerisation

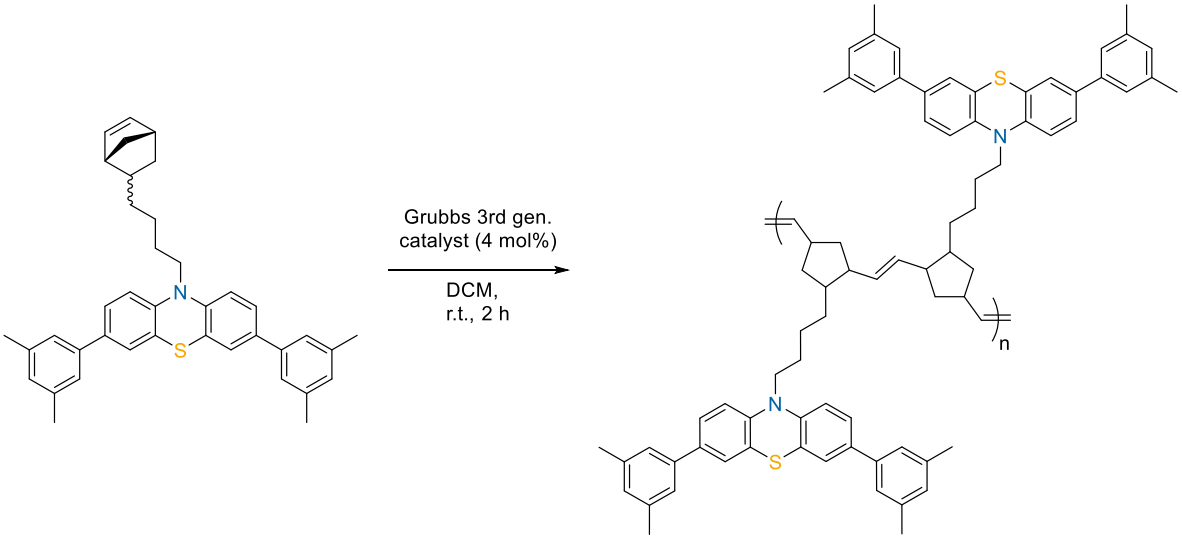


*Figure 26: Reaction scheme for the polymerisation of **3**.*

First, a reliable protocol for the polymerisation was developed, to ensure a degree of polymerisation (DP) of 25 monomeric units. The optimisation was performed by producing homopolymers of monomer **3** (Figure 26), since it was the most abundant (0.82 mmol, 456.0 mg). During testing it became apparent that a larger scale would be beneficial, as the accurate weighing in of the catalyst became the limiting factor (Table 7, Entry 1, 2). With the goal of achieving a reliable DP of 25±1, the error margin for the catalyst weight was less than 5%. Increasing the scale from 0.03 mmol to 0.06 mmol, gave a homopolymer of monomer **3** with a DP of 25 and a PDI of 1.06 (Table7, Entry 3) (Gel permeation chromatography results are shown in Figure S30, S31, and S32)

*Table 7: Results for the polymerisation of **3**.*

| Entry | Scale/mmol | **3**/mg | Grubbs 3rd. gen/mg | Mn | Mw | PDI | DP |
|---|---|---|---|---|---|---|---|
| 1 | 0.03 | 16.7 | 1.06 | 19892 | 20610 | 1.04 | 36 |
| 2 | 0.03 | 16.7 | 1.06 | 16417 | 17067 | 1.04 | 29 |
| 3 | 0.06 | 33.3 | 2.12 | 13970 | 14740 | 1.06 | 25 |

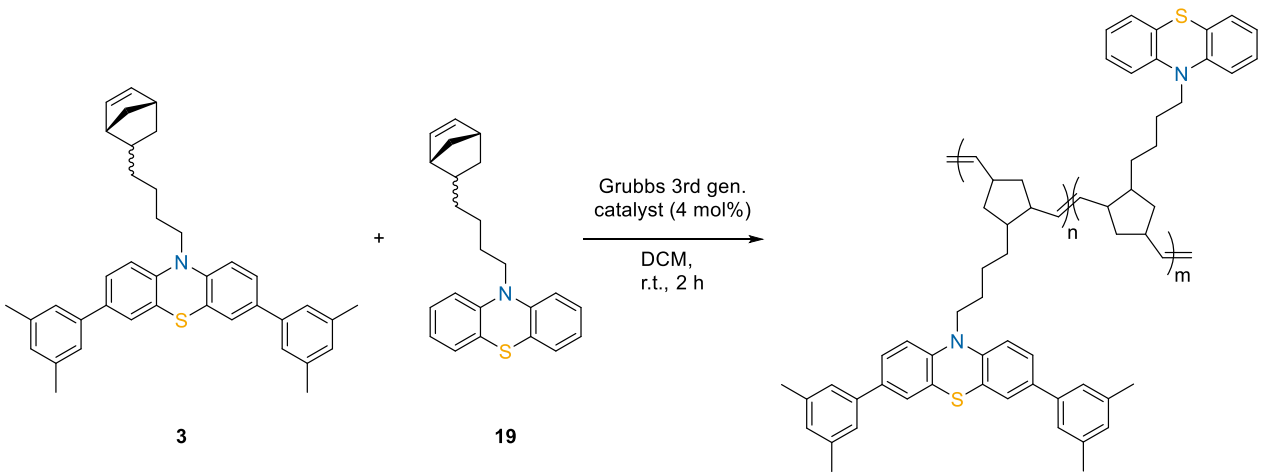


*Figure 27: Reaction for the copolymerisation of monomer **3** and **19**.*

With the results from the homopolymers of **3**, copolymers of monomers **3** and **19** were produced with **19**/**3** ratios of 1:240, 1:24 and 2:23 on a scale of 0.06 mmol. All copolymers exhibited a narrow PDI of around 1.05. However, for the copolymers with a **19**/**3** ratio of 1:24 and 2:23, a DP of 46 was observed corresponding to an increase in the DP of ~90% relative to the targeted DP of 25 (Table 8, Figure 28). The DP in ROMP is generally controlled by catalyst loading. This DP increase implies that only ~50% of the intended catalyst was effectively present, which could be due to the degradation of the catalyst.

*Table 8: Summary of the results from the copolymerization of **3** and **19**, with* $DP_n = \frac{M_n}{M_{repeat}}$ *and* $M_{repeat} = \frac{n_A M_A + n_B M_B}{n_A + n_B}$.

| Entry | Ratio **19**/**3** | Scale/mmol | Mn | Mw | PDI | DP |
|---|---|---|---|---|---|---|
| 1 | 1:240 | 0.06 | 13592 | 14263 | 1.05 | 24 |
| 2 | 1:24 | 0.06 | 24920 | 25904 | 1.04 | 46 |
| 3 | 2:23 | 0.06 | 24951 | 25872 | 1.04 | 46 |

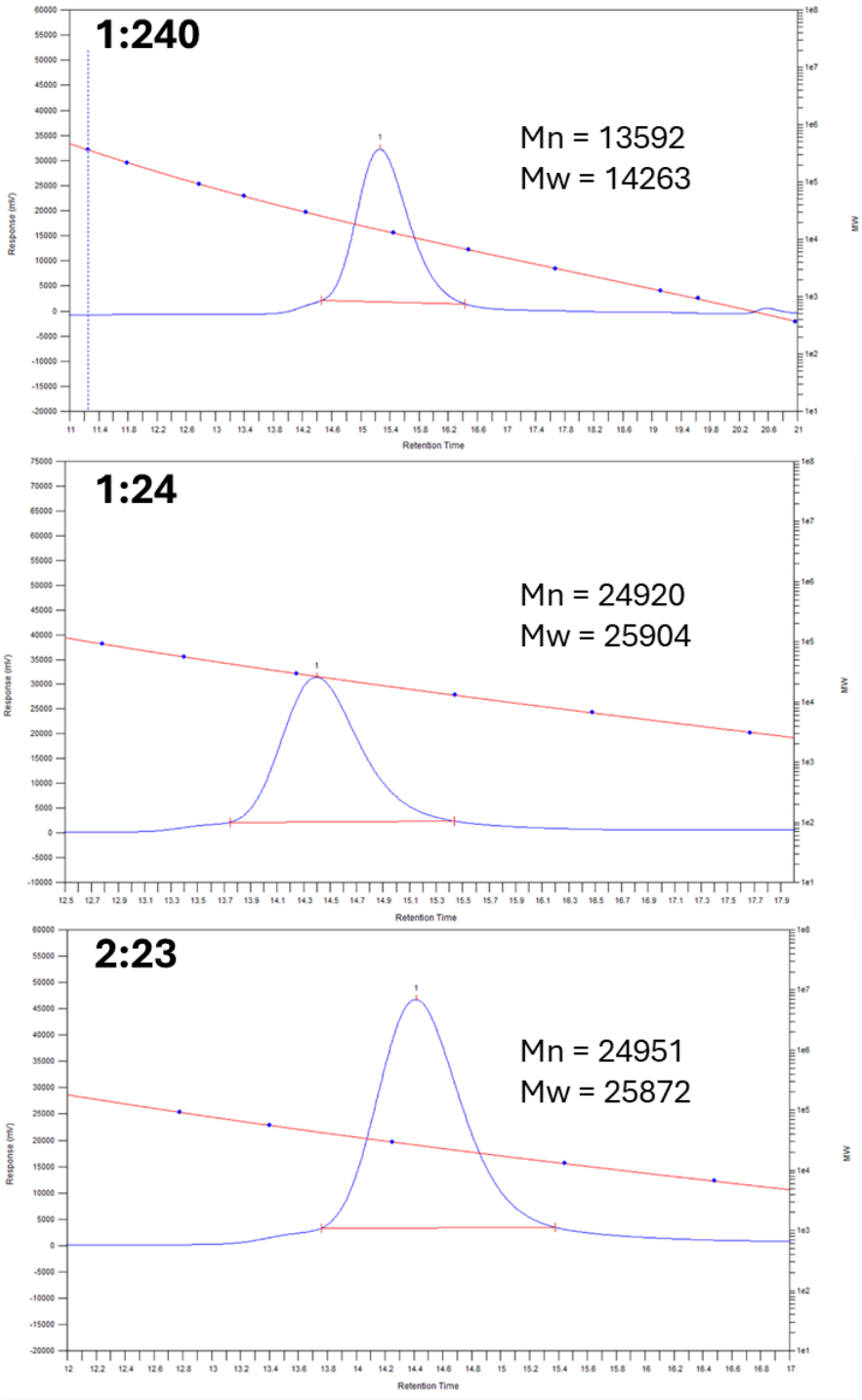


*Figure 28: Gel permeation chromatography results (GPC) for the copolymerisation of monomer **19** and **3** in the respective ratios of 1:24, 2:23 and 1:240.*

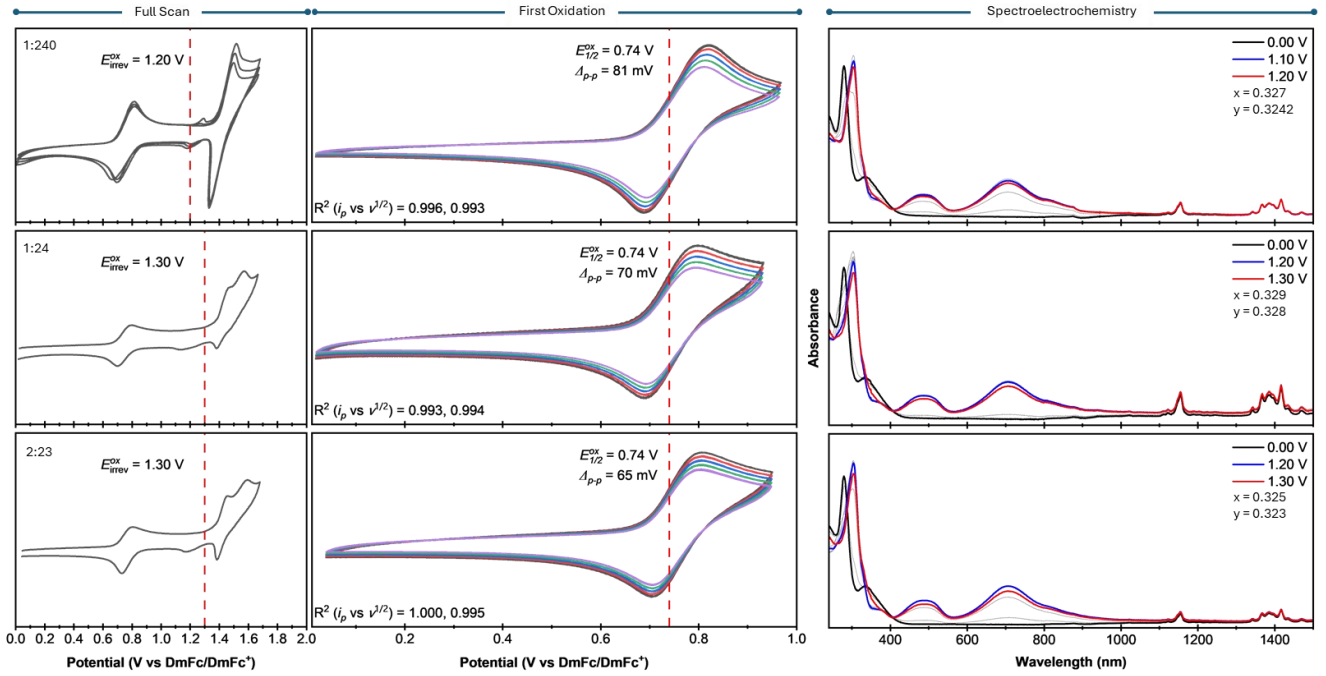


*Figure 29: Summary of the photophysical characterization of the copolymers with monomers **19** and **3** in the respective ratios of 1:240, 1:24 and 1:23.*

Initially, the redox properties of the copolymers were investigated. All copolymers exhibited a reversible single-electron oxidation at $E^{ox}_{1/2}$ = 0.74 V, as confirmed in Figure 29 (center). The $E^{ox}_{1/2}$ of the copolymers is consistent with the $E^{ox}_{1/2}$ values of monomers **3** (0.76 V) and **19** (0.80 V). Here, the $E^{ox}_{1/2}$ of the monomers are within 0.04 V, making it impossible to resolve them in cyclic voltammetry. The copolymers with a **19**/**3** ratio of 1:24 and 2:23 showed the same $E^{ox}_{irrev}$ of 1.30 V, while the copolymer with a **19**/**3** ratio of 1:240 exhibited a $E^{ox}_{irrev}$ slightly lower of 1.20 V (Figure 29, left). Following the electrochemical characterization, *in situ* SEC measurements of the copolymers were performed. Surprisingly, the UV-vis-NIR spectra of the oxidised copolymers closely matched that of **3**$^{\cdot+}$; with no contribution of monomer **19**$^{\cdot+}$ being visible. Furthermore, the $x_m$,$y_m$ coordinates of the copolymers were determined using the "ColorCalculator" software and equation (1) (Table 9). The failed oxidation of **19** to **19**$^{\cdot+}$ in the copolymers could possibly be due to slower oxidation kinetics for monomer **19**, which exhibits a slightly higher $E^{ox}_{1/2}$ of 0.04 V. In non-conducting redox polymers the charge transport relies on localized hopping and ion ingress, both of which are kinetically limited.[50] It is hypothesised that upon oxidation of monomer **3** units, a high local positive charge environment is created and disfavors oxidation of neighboring monomer **19** units, effectively blocking their oxidation. In addition, restricted electrolyte penetration in the copolymer matrix could lead to a situation

where only the thermodynamically easier site undergoes oxidation, while the slightly more demanding process remains kinetically suppressed.

*Table 9: Summary of the predicted ($x_{predicted}$ and $y_{predicted}$) and experimental ($x_{vis}$ and $y_{vis}$) observed colour of the radical cations. The $x_{vis}$ and $y_{vis}$ values of the experimental observed colour displayed in the CIE 1931 plot, which was generated with python using the "colour-science 0.4.6" package.*

| Copolymer ratio (**19**:**3**) | $x_{predicted}$ | $y_{predicted}$ | $x_{vis}$ | $y_{vis}$ |
|---|---|---|---|---|
| 1:240 | 0.330 | 0.376 | 0.332 | 0.335 |
| 1:24 | 0.338 | 0.374 | 0.331 | 0.332 |
| 2:23 | 0.346 | 0.372 | 0.335 | 0.336 |

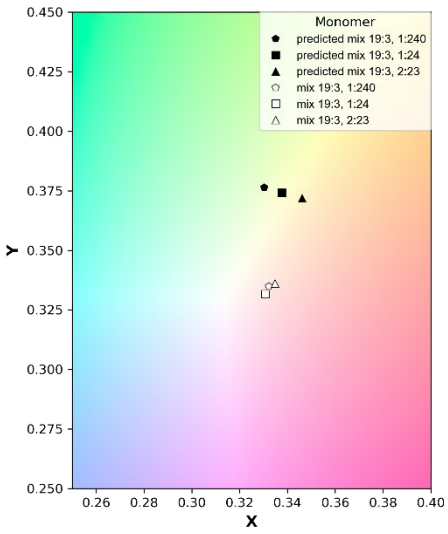

## 5.4 Conclusion and outlook

In this work five novel phenothiazine-based monomers (**3**, **4**, **5**, **6** and **7**), for use in electrochromic polymers, were synthesised on a scale of up to 0.81 mmol (**3**). For 3,7 aryl-subsituted phenothiazines monomers bearing a norbornene moiety for ROMP, a reliable and adaptive synthetic pathway for large-scale production was established by optimising key steps of the synthesis. Furthermore, monomers with a 1,9-dimethylphenothaizine core were explored and synthesized (**6**, **7**). For all monomers the photophysical properties were characterised and possible trends based on their structure established. It was determined that through the coherent extension and manipulation of the monomer's conjugation, the absorption of their respective radical cations can be controlled. By introducing a slight torsion angle, radical cation $\mathbf{4}^{\cdot+}$ exhibited a maximum hypsochromic shift of 80 nm compared to $\mathbf{3}^{\cdot+}$ and $\mathbf{5}^{\cdot+}$, giving them distinctly different colours. Besides the absorption, the tuneability of the oxidation potential through the introduction methyl groups in the 1,9-positions of phenothiazine was demonstrated. For monomer **7** a 0.2 V higher oxidation potential than its phenothiazine-based counterpart **5** could be observed. Through the determination of their optical bandgap, sought-after electrochromic materials that switch from a bleached to a coloured state was obtained for the three monomers **4**, **6** and **7**. The results on the substituent effects on the phenothiazine core are crucial for a systematic design of future monomers.

With the results from the SEC measurements the electrochromic monomers were plotted in the CIE colour space to study the rational subtractive mixing towards new hues. A protocol for polymerization of novel monomers was established and based on these findings; three copolymers were obtained with a narrow PDI of 1.05. This result demonstrated the possibility of how the composition of electrochromic polymers can be closely controlled. This reliable and reproducible protocol will be useful in the future kinetic studies of the phenothiazine-based electrochromic polymers.

# 6. Experimental Section

## Instrumentation

**Thin layer chromatography (TLC)** analysis was performed using the ALUGRAAM Xtra SIL G UV254 aluminum sheets with silica gel 60 and fluorescent indicator. For visualisation of the spots ultraviolet light (254 or 366 nm) or a permanganate stain were used.

**Flash column chromatography** was performed using the MAcherey-Nagel silica gel 60 (particle size: 40-63 µm). The analyte was transferred onto the column using Sigma-Aldrich Celite 545 (particle size: >125.30 µm).

**Nuclear magnetic resonance spectroscopy (NMR)** measurements were conducted at the NMR Centre of the Faculty of chemistry of the University of Vienna. The NMR spectra were recorded on Bruler spectrometers AV NEO 400, AV III 600 or AV III HD 700, and the samples prepared in NMR samples tube made from borosilicate glass, by dissolving them in deuterated solvents. $^{1}H$ NMR spectra were recorded at 400, 600 or 700 MHz and $^{13}C$ NMR spectra at 101, 151 or 176 MHz. All chemical shifts (δ) are reported in ppm, using tetramethylsilane as a reference. In the recorded spectra, the deuterated solvents were used as internal reference ($CD_2Cl_2$: $\delta_H$: 5.32 ppm, $\delta_C$: 53.84 ppm; $(CD_3)_2SO$: $\delta_H$: 2.50 ppm, $\delta_C$: 39.52 ppm). The multiplicity of Signals is denoted as followed: s: singlet, d: doublet, dd: doublet of doublets, t: triplet, m: multiplet and bs: broad signal.

**Infrared spectra (IR)** were recorded using the Bruker Alpha FT-IR spectrometer in attenuated total reflectance (ATR) mode. The most dominant absorption bands are reported using the unit wavenumber ($cm^{-1}$).

**High-resolution mass spectrometry (HRMS)** were recorded at the Mass Spectrometry Centre of the University of Vienna. LDI-timsTOF and MALDI-timsTOF measurements were performed using a Bruker Autoflex Speed LD-timsTOF or MALDI-timsTOf, where a Matrix (DCTB = 2-[(2E)-3-(4-tert butylphenyl)-2-methylprop-2-enylidene]malononitrile) was added to the analyzed substance. ESI measurements were recorded on a Bruker maXis UHR ESI-Qq-TOF mass spectrometer in the positive ion mode and gas-chromatography mass analysis measured on an Agilent 7200B GC/Q-TOF mass spectrometer.

**Ultraviolet-Visible (UV-Vis) absorption spectroscopy** was measured an on Agilent Cary 5000 UV-Vis-NIR Spectrophotometer in double beam mode with a matched pair of quartz absorbance cuvettes (1 x 1 cm). All absorption measurements were performed at room temperature in $CH_2CL_2$, unless specified otherwise.

**Cyclic voltammetry (CV)** measurements and experiments were performed at room temperature in $CH_2CL_2$, using an Autolab PGSTAT204 potentiostat (Metrohm, DE). The cell used was an conventional three-electrode electrochemical cell connected to an argon source and an oil bubbler. Prior to measurements dry argon gas was bubble for 15 min through the sample solution and the setup continuously flushed with argon. Furthermore, the argon flow was diverted through an additional bubbler filled with solvent in front of the setup to prevent evaporation. For the working electrode a Platinum S5 disk (3 mm diameter) was used, Pt wire as auxiliary electrode, and an Ag/AgCl electrode as reference. From ethanol freshly recrystallized tetrabutylammonium hexafluorophosphate (Alfa Aesar, TBAPF6) was used as an supporting electrolyte at a concentration of 0.1M and decamethylferocene (Sigma Aldrich) was used as an internal reference. The half wave potentials were calculated using the following formula $E_{1/2} = \frac{(E_{pa} + E_{pc})}{2}$ where $E_{pa}$ is the peak anodic potential and $E_{pc}$ the peak cathodic potential. With the formula $E_{HOMO} = -\left(E_{\frac{1}{2}}^{ox} - 0.54\right) - 4.8$, where $E_{\frac{1}{2}}^{ox}$ is the half-wave oxidation potential (vs $Fc/Fc^+$) and 4.8 is the HOMO energy of ferrocene in vacuum, the HOMO energy was calculated. The oxidation potentials were referenced vs $Fc/Fc^+$, by experimentally determining the potential of the $DmFc/DmFc^+$ redox couple (-0.54 V vs $Fc/Fc^+$).

Spectroelectrochemical characterization was performed using a thin layer quartz cuvette (path length of 1 mm) equipped with an optically transparent platinum minigrid working electrode, platinum wire auxiliary electrode, and an Ag/AgCl reference electrode.

### Materials and Methods

Chemicals were purchased from Sigma Aldrich, Acros Organics, TCI, Alfa Aesar, Fluorochem, Thermo Fisher Scientific and BLDpharm and used as is without further purification. Anhydours toluene, thetrahydrofuran (THF) and dichloromethane ($CH_2Cl_2$) were dried using a MBraun SP-800 solvent purification system. Degassing of solvents was preformed either bubbling argon through the solution for 15-30 min using a balloon or by *freeze-pump-thaw* (After freezing the solvent, it was put under dynaic vacuum for 15 min and the cycles repeated at least three times). To achieve anhydrous conditions, reactions were performed in Schlenk-tubes and the reaction vessel stored in an oven before use 120 °C for at least 12h before use. Additionally, the reaction vessel was further dried using a heat gun and purged with argon. As an alternative to Schlenk tubes in high pressure reactions, microwave tubes sealed with a microwave cap were used. Alternative to the use of Schlenk line techniques, inert conditions were achieved using an argon-filled MBraucn LabStar glove box when stated.

**3,7-dibromo-10H-phenothiazine (10)**

**With *N*-Bromosuccinimide**

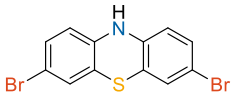

In a 250 ml oven dried double necked round-bottomed flask charged with argon, phenothiazine (10 mmol, 2.0 g) was dissolved in 20 ml of dry, degassed THF and cooled to 0 °C. NBS (20 mmol, 3.75 g) was dissolved in 40 ml of dry, degassed THF and added to the stirred phenothiazine solution with an addition funnel over the span of one hour. After the addition, the reaction mixture was allowed to warm to room temperature and left to stir for 16 h under the protection form light. To the reaction mixture, 100 ml of a saturated aqueous thiosulphate solution was added and stirred for one hour, after which the aqueous phase was extracted three times with 100 ml of $CH_2Cl_2$. The organic layers were combined and the solvent removed in *vacuo*. The crude product was purified via silica gel column chromatography (eluent gradient: *n*-heptane/$CH_2Cl_2$/EtOAc = 8:2:0.2 → 6:4:0.2) and recrystallized in MePh, yielding the product as greenish crystals (1.5 g, **41%** yield).

**With Tetrabutylammonium tribromide**

In a 250 ml oven dried double necked round-bottom flask charges with argon, phenothiazine (10 mmol, 2.0 g) was dissolved in 100 ml of dry, degassed THF. To the stirred solution tetrabutylammonium tribromide (21.1 mmol, 10.2 g) was added at once and the reaction mixture heated to 70 °C and stirred for 16 h. After this period, 100 ml of a saturated aqueous solution of thiosulphate was added and the mixture stirred vigorously for 1 h to quench the reaction. The aqueous and the organic phase were separated and the organic phase washed with 200 ml of water five times and once with 200 ml of brine. The organic phase was dried over $MgSO_4$, filtrated and the solvent removed in *vacuo*. The crude product was purified via silica gel column chromatography (eluent gradient: *n*-heptane/$CH_2Cl_2$/EtOAc = 8:2:0.2 → 6:4:0.2) and recrystallised in MePh, yielding the product as greenish crystals (2.7 g, **75%** yield). $^1$H-NMR (400 MHz, DMSO-$d_6$) δ: 8.84 (bs, 1H), 7.16 (d, J = 2.3 Hz, 1H), 7.13 (q, J = 2.3, 3H), 6.58 (d, J = 8.4 Hz, 2H).

**Suzuki-Miyaura Coupling General Procedure (A)**

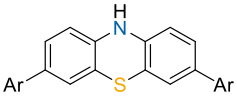

3,7-dibromo-10H-phenothiazine (1 mmol, 357.0 mg),$Cs_2CaO_3$ (4 mmol, 1.3 g) and 3 mmol of the respective boronic acid were suspended in 3 ml of a solvent mixture of $CH_2Cl_2$/water (6:1) and degassed by freeze-pump-thaw. $Pd(PPh_3)_4$ (5 mol%) was then added, and the reaction mixture was heated to 85 °C for 12 h. After cooling down, the mixture was diluted with water and

EtOAc, and the aqueous layer extracted three times with EtOAc. The combined organic layers were washed with brine, dried over $MgSO_4$, filtered and the solvent removed in *vacuo*.

**3,7-di-2-methylphenyl-10H-phenothiazine (13)**

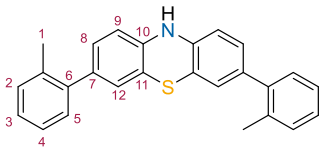

3,7-di-2-methylphenyl-10H-phenothiazine was prepared following the general procedure **A** and the crude product purified using silica gel column chromatography (eluent: *n*-heptane/$CH_2Cl_2$/EtOAc = 8:2:0.1 → 2:8:0.1). The product was obtained as a white powder (321.0 mg, **85%** yield). $^1$H NMR (600 MHz, DMSO) δ 8.79 (s, 1H$^{amine}$), 7.30 – 7.10 (m, 8H$^{2, 3, 4, 5}$), 6.98 (dd, *J* = 8.1, 2.0 Hz, 2H$^{9}$), 6.89 (d, *J* = 2.0 Hz, 2H$^{12}$), 6.77 (d, J = 8.1 Hz, 2H$^{8}$), 2.23 (s, 6H$^{1}$). $^{13}$C NMR (151 MHz, DMSO-$d_6$) δ: 140.83 (C$^{10}$), 140.37 (C), 134.91 (C), 134.67 (C$^{7}$) 130.30 (C$^{2-5}$), 129.25 (C$^{2-5}$), 128.34 (C$^{9}$), 127.02 (C$^{2-5}$), 126.55 (C$^{12}$), 125.91 (C$^{2-5}$), 116.17 (C$^{11}$), 114.13 (C$^{8}$), 20.23 (C$^{1}$). IR (cm$^{-1}$): 3396, 3376, 3011, 1467, 1392, 1293, 1273, 1242, 1143, 818, 766, 752, 729, 687, 644, 567, 503, 455. $C_{26}H_{21}NS$ [M$^+$]: 379.1389, found 379.1384.

**3,7-di-4-methylphenyl-10H-phenothiazine (11)**

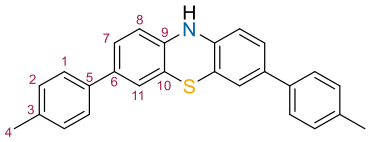

3,7-di-4-methylphenyl-10H-phenothiazine was prepared following the general procedure **A** and the crude product purified using silica gel column chromatography (eluent: *n*-heptane/EtOAc/$CH_2Cl_2$ = 8:0.1:2 → 2:0.1:8). The product was obtained as a yellow powder (214.0 mg, **40%** yield. $^1$H NMR (600 MHz, DMSO) δ 8.77 (s, 1H$^{amine}$), 7.46 (d, *J* = 8.1 Hz, 4H$^{1}$), 7.28 (dd, *J* = 8.2, 2.1 Hz, 2H$^{8}$), 7.24 – 7.17 (m, 4H$^{2}$), 7.21 (s, 2H$^{11}$), 6.74 (d, *J* = 8.2 Hz, 2H$^{7}$), 2.31 (s, 6H$^{4}$). $^{13}$C NMR (151 MHz, DMSO) δ 140.70 (C$^{9}$), 136.25 (C$^{5}$), 136.03 (C$^{3}$), 133.69 (C$^{6}$), 129.43 (C$^{2}$), 125.59 (C$^{8}$), 125.56 (C$^{1}$), 123.85(C$^{11}$), 116.76 (C$^{10}$), 114.74 (C$^{7}$), 20.62 (C$^{4}$).$^{13}$C NMR. IR (cm$^{-1}$): 3376, 2912, 1495, 1311, 1258, 1202, 805, 499, 417. $C_{26}H_{21}NS$ [M$^+$]: 379.1389, found 379.1388.

**3,7-di-3,5-dimethylphenyl-10H-phenothiazine (12)**

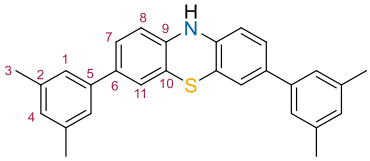

3,7-di-3,5-dimethylphenyl-10H-phenothiazine was prepared following general procedure **A** and the crude product was purified using silica gel column chromatography (eluent: *n*-heptane/$CH_2Cl_2$/EtOAc = 8:2:0.1 → 2:8:0.1). The product was obtained as a yellow powder (375.0 mg , **92%** yield). $^1$H-NMR (600 MHz, $CD_2Cl_2$) δ: 7.25 (m, 2H$^{7}$), 7.24 (m, 2H$^{8}$), 7.14 (s, 4H$^{1}$), 6.96 (s, 2H$^{4}$), 6.64 (s, 2H$^{11}$), 6.00 (bs, 1H$^{amine}$), 2.35 (s, 12H$^{3}$). $^{13}$C NMR (151 MHz, $CD_2Cl_2$) δ: 140.84 (C$^{5}$), 140.09 (C$^{9}$), 138.782 (C$^{2}$), 136.31 (C$^{6}$), 128.99 (C$^{4}$), 126.39 (C$^{8}$), 125.40 (C$^{7}$), 124.49 (C$^{1}$), 118.62 (C$^{10}$), 115.04 (C$^{11}$), 21.51 (C$^{3}$). IR (cm$^{-1}$): 3410, 3002, 1850, 1602, 1490, 1230, 800, 410. $C_{28}H_{25}NS$ [M$^+$]: 407.1702, found 407.1706.

**5-(4-bromobutyl)bicyclo[2.2.1]hept-2-ene (14)**

This procedure was carried out as described in literature.[46]

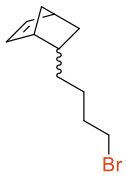


In an argon charged10-20 ml round bottom microwave vial diclyopentadien (30 mmol, 3.96 g) and 6-bromo-1-hexene (60 mmol, 8.0 ml) were heated to 200 C for 72 h and stirred vigorously. Upon completion, the crude product was purified by fractional distillation under reduced pressure (145 °C, 0.3 mbar)and followed by silica gel column chromatography (eluent: *n*-heptane/EtOAc = 1% EtOAc). The product was obtained as a clear oil in an isomeric mixture of 75:25, endo/exo (2.08 g, **30%** yield). $^{1}$H NMR (400 MHz, $CD_2Cl_2$) δ 6.16 – 6.05 (m, 1H), 6.03-5.90 (m, 1H), 3.41 (t, *J* = 6.9 Hz, 2H), 2.76 - 2.51 (m, 2H), 1.99 (m 1H), 1.93 – 1.73 (m, 3H), 1.55 – 1.00 (m, 7H), 0.49 (m, 1H). $^{13}$C NMR (101 MHz, $CD_2Cl_2$) δ 137.374, 137.201, 136.581, 132.626, 49.906, 46.756, 45.799, 45.538, 43.012, 42.347, 39.062, 38.988, 34.610, 34.247, 33.502, 32.743, 27.568. $C_{11}H_{17}Br$: 229.16, found 228.0502.

**3,7-2-methylphenyl-10-(5-(4-bromobutyl)bicyclo[2.2.1]hept-2-ene)-phenothiazine (4)**

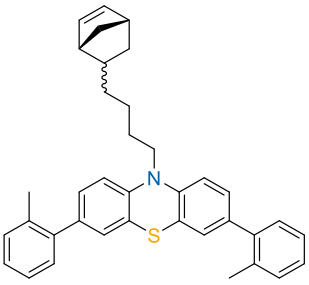


After drying 3,7-di-2-methylphenyl-10H-phenothiazine (0.8 mmol, 304.0 mg), 5-(4-bromobutyl)bicyclo[2.2.1]hept-2-ene (1.6 mmol, 238.0 mg) and $Cs_2CaO_3$ (6.4 mmol, 2.08 g) in an oven dried 100 ml Schlenk tube over argon, they were dissolved in 24 ml of $CH_3CN$ and heated to 90 °C for 16 h. The progress of the reaction was monitored continuously and upon completion the mixture cooled down to room temperature, diluted with water and EtOAc and washed with water and brine. The crude product was purified using silica gel column chromatography (eluent: *n*-heptane/EtOAc = 1% EtOAc) and the product precipitated by dissolving the product in minimal $CH_2Cl_2$ upon the addition of an excess of $CH_3OH$ sonicating the content. After washing the product three more times with $CH_3OH$, the product was obtained as a greenish powder (358.0 mg, **85%** yield). Due to the *endo*/*exo* isomeric mixture, a detailed assignment in the $^{1}$H-NMR and $^{13}$C-NMR is not possible. For the $^{1}$H-NMR integration is possible, when regarding the isomeric mixture as whole. $^{1}$H NMR (600 MHz, $CD_2Cl_2$) δ 7.31 – 7.06 (m, 12H), 6.95 (m, 2H), 6.14 – 6.06 (m, 1H), 6.00 - 5.88 (m, 1H), 3.93 (m, 2H), 2.76 (1, 1H), 2.28 (s, 6H), 2.07 – 1.77 (m, 4H), 1.51 – 1.38 (m, 2H), 1.39 – 1.07 (m, 5H), 0.50 m, 1H). $^{13}$C NMR (151 MHz, $CD_2Cl_2$) δ 144.38, 141.24, 137.29, 137.23, 136.60, 136.55, 135.82, 132.69, 132.67, 130.71, 130.00, 128.62, 128.27, 127.55, 126.17, 124.53, 115.34, 49.88, 47.77, 47.75, 46.73, 45.77, 45.53, 43.00, 42.34, 39.13, 39.08, 36.48,

34.75, 33.34, 32.71, 27.42, 27.39, 26.49, 26.24, 20.69. IR ($cm^{-1}$): 2928, 2350, 1463, 1392, 1329, 1254. $C_{37}H_{37}NS$ [$M^+$]: 527.2641, found 527.2638.

**3,7-di-4-methylphenyl-10-(5-(4-bromobutyl)bicyclo[2.2.1]hept-2-ene)-phenothiazine (5)**

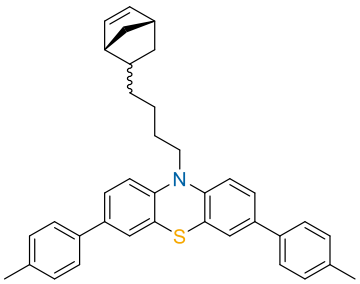

3,7-di-4-methylphenyl-10H-phenothiazine (0.8 mmol, 304.0 mg), 5-(4-bromobutyl)bicyclo[2.2.1]hept-2-ene (1.04 mmol, 238.0 mg) and $Cs_2CaO_3$ (6.4 mmol, 2,08 g) were dried in an oven dried 100 ml Schlenk tube over argon for 30 min. The content was suspended in 30 ml of $CH_3CN$ and heated to 90 °C for 48 h, while the progress of the reaction was monitored by TLC. Upon completion, the mixture was cooled down to room temperature and diluted with water and EtOAc. After washing the reaction mixture with 100 ml of water and 100 ml of brine, the organic layer was dried with $MgSO_4$, filtered and the solvent removed in *vacuo*. The crude product was purified using silica gel column chromatography (eluent: *n*-heptane/EtOAc = 1% EtOAc), followed by precipitation from $CH_3OH$ to remove starting material. The product was carefully washed three more times with $CH_3OH$ and obtained as a yellow powder (192.0 mg, **45%** yield). Due to the *endo*/*exo* isomeric mixture, a detailed assignment in the $^1$H-NMR and $^{13}$C-NMR is not possible. For the $^1$H-NMR integration is possible, when regarding the isomeric mixture as whole.$^1$H NMR (600 MHz, $CD_2Cl_2$) δ 7.47 – 7.43 (m, 4H), 7.41 – 7.35 (m, 4H), 7.23 (d, *J* = 7.7 Hz, 4H), 6.93 (m, 2H), 6.07 (m, 1H), 6.00 - 5.88 (m, 1H), 3.89 (m, 2H), 2.75 (s, 1H), 2.37 (s, 6H), 2.04 – 1.95 (m, 1H), 1.89 – 1.76 (m, 3H), 1.50 – 1.06 (m, 7H), 0.49 (m, 1H).$^{13}$C NMR (151 MHz, $CD_2Cl_2$) δ 144.48, 137.32, 137.29, 137.26, 136.54, 135.61, 135.60, 132.67, 129.87, 126.54, 126.02, 125.72, 125.70, 125.08, 125.05, 115.98, 115.94, 49.87, 47.82, 46.71, 45.78, 45.77, 45.51, 42.99, 42.32, 39.13, 39.08, 39.07, 36.48, 34.76, 33.35, 32.69, 27.41, 26.46, 26.23, 21.18. IR ($cm^{-1}$): 2920, 1490, 1320, 1230, 800, 470, 410. $C_{37}H_{37}NS$ [$M^+$]: 527.2641, found 527.2639.

**3,7-di-3,5-dimethylphenyl-10-(5-(4-bromobutyl)bicyclo[2.2.1]hept-2-ene)-phenothiazine (3)**

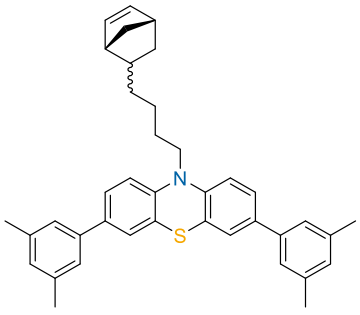

In an oven dried 15 ml microwave vial 3,7-di-3,5-dimethylphenyl-10H-phenothiazine (1.0 mmol, 408.0 mg), 5-(4-bromobutyl)bicyclo[2.2.1]hept-2-ene (3 mmol, 687.0 mg) and KOH (8.0 mmol, 449.0 mg) were dried over argon for 15 minutes. Proceeding, the content was dissolved in 4 ml of DMSO and heated to 110 °C for 16 h. After cooling down, the crude was poured into 100 ml of ice-cold water and stirred for 30 min. To the mixture 100 ml of $CH_2Cl_2$ was added and stirred for an additional 30 min. The layers were separated, and the organic layer collected, dried with $MgSO_2$, filtered and the solvent removed in *vacuo*. The product was purified using

silica gel column chromatography (eluent: *n*-heptane/EtOAc = 1% EtOAc) and precipitated from the obtained oil by sonicating the content in $CH_3CN$ . The precipitated product was collected with ultra-centrifugation (3600 rpm, 30 min) and washed three times with acetonitrile and the product obtained as a yellow powder (456.0 mg, **82%** yield). Due to the *endo*/*exo* isomeric mixture, a detailed assignment in the $^1$H-NMR and $^{13}$C-NMR is not possible. For the $^1$H-NMR integration is possible, when regarding the isomeric mixture as whole. $^1$H NMR (600 MHz, $CD_2Cl_2$) δ 7.42 – 7.35 (m, 4H), 7.17 (s, 4H), 6.99 – 6.90 (m, 4H), 6.07 (m, 1H), 6.00 - 5.88 (m, 1H), 3.90 (m, 2H), 2.74 (1, 1H), 2.36 (s, 12H), 2.00 (dh, *J* = 12.1, 4.2 Hz, 1H), 1.90 – 1.74 (m, 3H), 1.51 – 1.06 (m, 7H), 0.49 (m, 1H).$^{13}$C NMR (151 MHz, $CD_2Cl_2$) δ 144.58, 140.08, 138.73, 137.30, 137.23, 136.55, 135.92, 135.91, 132.68, 129.00, 126.20, 125.93, 125.92, 125.01, 124.98, 124.62, 115.89, 49.88, 47.83, 46.72, 45.79, 45.52, 43.00, 42.33, 39.14, 39.09, 39.08, 36.50, 34.77, 33.35, 32.70, 27.42, 26.47, 26.24, 21.53, 21.52. IR ($cm^{-1}$): 2928, 1599, 1463, 1332, 1253, 880, 847, 824, 702, 465. $C_{39}H_{41}NS$ [$M^+$]: 555.2954, found 555.2954.

**2-methyl-*N*-(2-methylphenyl)aniline (15)**

The procedure was adapted from literature.[51]

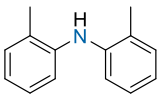

An oven dried, argon flushed 250 ml Schlenk tube was charged with o-Toluidine (15 mmol, 1.6 ml), 2-Bromotoluene (12.5 mmol, 1.5 ml) and NaO$^t$Bu (25 mmol, 2.4 g). The content was dissolved in 50 ml of MePh and degassed by freeze-pump-thaw. To the mixture, $Pd(dppf)Cl_2$ (0.375 mmol, 274 mg) was added and the solution heated to 95 °C for 20 h. After cooling down the reaction mixture, the solvent was evaporated in *vacuo*, the crude product dissolved in $CHCl_3$ and after filtration the filtrate collected, and the solvent removed again in *vacuo*. The crude product was purified using silica gel column chromatography (eluent: *n*-heptane/$CH_2Cl_2$ = 2% $CH_2Cl_2$) and the product obtained as a yellow oil (2.37 g, **96%** yield). $^1$H NMR (400 MHz, $CD_2Cl_2$) δ 7.24 (d, *J* = 8.7 Hz, 2H), 7.14 (t, *J* = 7.7 Hz, 2H), 7.04 – 6.88 (m, 4H), 5.24 (s, 1H), 2.30 (s, 6H). $^{13}$C NMR (101 MHz, $CD_2Cl_2$) δ 142.52, 131.17, 128.14, 127.12, 121.74, 118.63, 17.97. $C_{14}H_{15}N$ [M+H]: 198.1277, found 198.1273.

**1,9-dimethyl-10H-phenothiazine (2)**

The procedure was adapted from literature.[51]

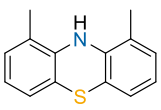

In an oven dried 250 ml Schlenk tube 2-methyl-*N*-(2-methylphenyl)aniline (5 mmol, 0.98 g), sulfur (10 mmol, 2.56 g) and $I_2$ (0.5 mmol, 0.127 g) were dissolved in 5 ml of1,2,4-trichlorobenzene and the mixture heated to 180 °C for 16 h. After letting the solution cool down, the mixture was diluted with EtOAc and filtered. The filtrate was collected and after removal of

the solvent in *vacuo*, the crude product purified using silica gel column chromatography (eluent: *n*-heptane/EtOAc = 2% EtOAc). The product was obtained as a yellow powder (0.57 g, **50%** yield). $^{1}$H NMR (400 MHz, $CD_2Cl_2$) δ 6.90 (dd, *J* = 18.6, 7.6 Hz, 4H), 6.77 (t, *J* = 7.6 Hz, 2H), 5.84 (s, 1H), 2.25 (s, 6H). $^{13}$C NMR (101 MHz, $CD_2Cl_2$) δ 140.51, 129.30, 125.00, 122.51, 122.33, 118.35, 17.03. $C_{14}H_{13}$ [$M^+$]: 227.0763, found 227.0761.

**3,7-dibromo-1,9-dimethyl-10H-phenothiazine (16)**

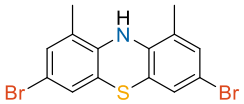


In an oven dried, argon charged 25 ml round bottom flaks, 3,7-dibromo-1,9-dimethyl-10H-phenothiazine (0.3 mmol, 68.2 mg) and $FeBr_3$ (0.03 mmol, 8.9 mg) were dissolved in 10 ml of glacial AcOH. The solution was cooled to 0 °C and $Br_2$ (0.9 mmol, 0.05 ml) in 5 ml of glacial AcOH was added dropwise with a syringe. After the addition, the solution was allowed to warm up to room temperature and stirred for 72 h under the protection from light. Afterwards, 10 ml of an aqueous saturated solution of $Na_2SO_3$ was added and the mixture stirred for 2 h. The crude product was extracted from the aqueous solution with 50 ml of EtOAc, dried with $MgSO_4$ and after filtration the solvent removed in *vacuo*. After recrystallisation from EtOH the product was obtained as a grey powder (68.0 mg, **59%** yield). $^{1}$H NMR (400 MHz, $CD_2Cl_2$) δ 7.05 (s, 2H), 6.98 (s, 2H), 5.74 (s, 1H), 2.20 (s, 6H). $^{13}$C NMR (101 MHz, $CD_2Cl_2$) δ 139.282, 131.927, 127.166, 124.181, 119.844, 114.276, 16.846. $C_{14}H_{12}NSBr_2$[$M^+$]: 385.9031, found 385.9026.

**3,7-di(4-*tert*-butylphenyl)-1,9-dimethyl-10H-phenothiazine (18)**

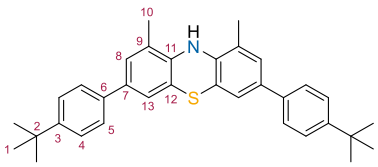


3,7-dibromo-1,9-dimethyl-10H-phenothiazine (0.1 mmol, 38.5 mg), $Cs_2CaO_3$ (0.4 mmol, 130.0 mg) and 4-*tert*-butylphenylboronic acid (0.3 mmol, 53.4 mg) were suspended in 2 ml of a solvent mixture of dimethoxyethane/water (6:1) and degassed by freeze-pump-thaw. Afterwards, 10 mol% $Pd(PPh_3)_4$ (0.01 mmol, 11.6 mg) was added and the reaction mixture heated to 85 °C for 12 h. After cooling down, the mixture was diluted with water and EtOAc, and the aqueous layer extracted three times with EtOAc. The combined organic layers were washed with brine, dried over $MgSO_4$, filtered and the solvent removed in *vacuo*. The crude product was purified using silica gel column chromatography (eluent: *n*-heptane/EtOAc = 1% EtOAc) and the product obtained as a yellow powder. (32.5 mg, **66%** yield) $^{1}$H NMR (700 MHz, $CD_2Cl_2$) δ 7.47 (d, *J* = 8.7 Hz, 4H[4]), 7.44 (d, *J* = 8.7 Hz, 4H[5]), 7.18 (s, 2H[8]), 7.15 (s, 2H[13]), 5.90 (s, 1H[amine]), 2.32 (s, 6H[10]), 1.35 (s, 18H[1]). $^{13}$C NMR (176 MHz, $CD_2Cl_2$) δ 150.394 (C[3]), 139.264 (C[11]), 137.462 (C[6]), 135.358 (C[9]), 127.889 (C[8]), 126.199 (C[5]), 126.112 (C[4]), 123.159 (C[13]), 122.546 (C[7]), 118.590

($C^{12}$), 34.780 ($C^{2}$), 31.493 ($C^{1}$), 17.244 ($C^{10}$). IR ($cm^{-1}$): 3447, 2962, 2903, 1488, 1470, 1324, 831. $C_{34}H_{37}NS$: 491.2641, found 491.2636.

**3,7-bis(4-methylphenyl)-1,9-dimethyl-10H-phenothiazine (17)**

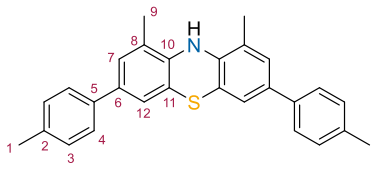

3,7-bis(4-methylphenyl)-1,9-dimethyl-10H-phenothiazine was prepared following the same procedure as for 3,7-di(4-*tert*-butylphenyl)-1,9-dimethyl-10H-phenothiazine, with 4-methylphenylboronic acid (0.3 mmol, 40.8 mg) as the respective boronic acid used in the coupling. The crude product was purified using silica gel column chromatography (eluent: *n*-heptane/EtOAc = 1% EtOAc) and the product was obtained as a brown powder (40.0 mg, **98%** yield). $^{1}$H-NMR (600 MHz, $CD_2Cl_2$) Sδ: 7.42 (d, *J* = 8.2 Hz, 4H$^{4}$), 7.22 (d, *J* = 7.8 Hz, 4H$^{3}$), 7.17 (s, 2H$^{7}$), 7.13 (s, 2H$^{12}$), 5.89 (s, 1H, H$^{amine}$), 2.37 (s, 6H$^{1}$), 2.32 (s, 6H$^{9}$). $^{13}$C-NMR (151 MHz, $CD_2Cl_2$) δ: 139.22 ($C^{10}$),137.49 ($C^{5}$), 137.15 ($C^{2}$), 135.45 ($C^{6}$), 129.82 ($C^{3}$), 127.83 ($C^{7}$), 126.41 ($C^{4}$), 123.12 ($C^{12}$), 122.54 ($C^{8}$), 118.57 ($C^{11}$), 21.16 ($C^{1}$), 17.23 ($C^{9}$).IR ($cm^{-1}$): 3453, 2913, 1468, 1318, 869, 814, 715, 529, 496, 426. $C_{28}H_{25}NS$ [$M^{+}$]: 407.1702, found 407.1701.

**3,7-di(4-*tert*-butylphenyl)-1,9-dimethyl-10-(5-(4-bromobutyl)bicyclo[2.2.1]hept-2-ene)**

**-phenothiazine (6)**

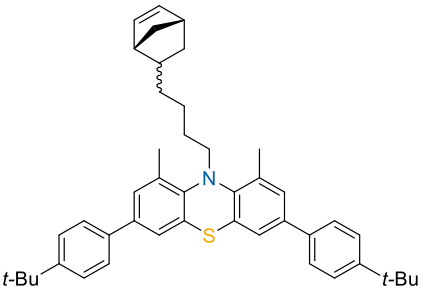

In an oven dried, argon flushed, 15 ml Schlenk tube, 3,7-di(4-*tert*-butylphenyl)-1,9-dimethyl-10H-phenothiazine (0.04 mmol, 19.7 mg), 5-(4-bromobutyl)bicyclo[2.2.1]hept-2-ene (0.052 mmol, 11.9 mg) and $Cs_2CO_3$ (0.32 mmol, 104 mg) were dried over argon for 15 min. After dissolving the compounds in 15 ml of dry $CH_3CN$, the reaction mixture was heated to 90 °C for 48 h, while the progress of the reaction was monitored by TLC. After cooling down, the content was diluted in water and EtOAc and the organic layer washed one with 25 ml of water and once with 25 ml of brine. After drying the organic layer with $MgSO_4$, the solution filtered, and the solvent removed in *vacuo*. The crude product was purified using silica gel column chromatography (eluent: *n*-heptane) and the product was obtained as a white powder (12.8 mg, **50%** yield). Due to the *endo*/*exo* isomeric mixture, a detailed assignment in the $^{1}$H-NMR and $^{13}$C-NMR is not possible. For the $^{1}$H-NMR integration is possible, when regarding the isomeric mixture as whole. $^{1}$H NMR (600 MHz, $CD_2Cl_2$) δ 7.53 – 7.49 (m, 4H), 7.45 (m, 4H), 7.32 (m, 4H), 6.08 – 5.93 (m, 1H), 5.83 (m, 1H), 3.54 – 3.36 (m, 2H), 2.73(s, 1H), 2.48 (m, 6H), 1.92 – 1.83 (m, 1H), 1.76 (m, 1H), 1.68 – 1.48 (m, 4H), 1.35 (s, 18H), 1.33 – 1.11 (m, 6H), 0.98 (m, 2H), 0.40 (m, 1H).$^{13}$C NMR (151 MHz, $CD_2Cl_2$) δ 150.70, 144.12, 144.07, 137.63,

137.61, 137.56, 137.18, 134.66, 134.64, 134.24, 134.22, 132.71, 128.49, 126.67, 126.13, 123.23, 55.89, 49.82, 46.71, 45.77, 45.48, 42.95, 42.28, 39.19, 39.17, 36.86, 35.12, 34.81, 33.35, 32.68, 32.67, 31.49, 29.80, 26.90, 26.72, 18.99. IR ($cm^{-1}$): 3055, 2959, 2864, 1459, 1362, 1266, 829, 738, 563. $C_{45}H_{53}NS$ [M+]: 639.3893, found 639.3891.

**3,7-bis(4-methylphenyl)-1,9-dimethyl-10-(5-(4-bromobutyl)bicyclo[2.2.1]hept-2-ene)-phenothiazine (7)**

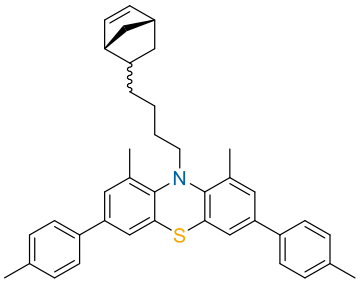


3,7-bis(4-methylphenyl)-1,9-dimethyl-10H-phenothiazine (0.04 mmol, 16.3 mg), 5-(4-bromobutyl)bicyclo[2.2.1]hept-2-ene (0.052 mmol, 11.9 mg) and $Cs_2CO_3$ (0.32 mmol, 104 mg) were dried over argon for 15 min in an oven dried, argon flushed 15 ml Schlenk tube. Upon the addition of 15 ml of dry $CH_3CN$, the reaction mixture was heated to 90 °C for 48 h, and the reaction progress monitored continuously by TLC. Afterwards, the mixture was diluted with water and $CH_3CN$ and the organic layer washed once with 25 ml of water and once with 25 ml of brine. The organic layer was dried with $MgSO_4$, filtered and the solvent removed in *vacuo*. The crude product was purified using silica gel column chromatography (eluent: *n*.heptane) and the product was obtained as a white powder (13.4 mg ,60% yield). Due to the *endo*/*exo* isomeric mixture, a detailed assignment or integration in the $^1$H-NMR and $^{13}$C-NMR is not possible. $^1$H NMR (600 MHz, $CD_2Cl_2$) δ 7.46 (m), 7.34 – 7.28 (m, 4H), 7.24 (m), 6.03 (m), 5.83 (m), 3.51 – 3.38 (m), 2.73 – 2.63 (m), 2.56 – 2.33 (m), 1.91 – 1.83 (m), 1.75 (m), 1.62 – 1.53 (m), 1.37 – 1.11 (m), 1.06 – 0.92 (m), 0.39 (m). $^{13}$C NMR (151 MHz, $CD_2Cl_2$) δ 144.07, 144.04, 137.71, 137.69, 137.58, 137.48, 137.21, 137.17, 136.47, 134.64, 134.22, 132.70, 129.86, 129.85, 128.41, 126.89, 126.88, 123.17, 55.91, 49.83, 49.82, 46.70, 45.78, 45.77, 45.47, 42.97, 42.95, 42.27, 39.18, 39.16, 36.85, 35.13, 35.12, 33.34, 32.69, 32.68, 29.77, 26.89, 26.73, 26.72, 21.21, 21.19, 18.99, 18.97. IR ($cm^{-1}$): 2917, 1459, 1301, 1251, 1147, 874, 813, 717, 505. $C_{39}H_{41}NS$ [M+]: 555.2954, found 555.2957.

**Homopolymer General Procedure (B)**

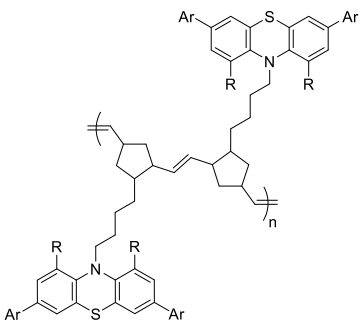


Grubbs' third generation catalyst (0.0024 mmol, 2.12. mg) was weighed in a 15 ml microwave vial inside of the glovebox. A solution of dissolved monomer (0.06 mmol) in degassed $CH_2Cl_2$ (3 ml) was transferred with a syringe to the catalyst and the solution stirred for two hours at room temperature. To stop the polymerisation, 1 ml of ethyl vinyl ether was added and the reaction mixture stirred for 30 min before the addition of $CH_3OH$

(5 ml). After stirring the mixture for another 30 min, the precipitated monomer was collected by centrifugation (500 rpm, 15 min) and washed with 20 ml of $CH_3OH$ four times.

**Co-Polymer General Procedure (C)**

Analogous to the Homopolymer, Grubbs' third generation catalyst (0.0024 mmol, 2.12 mg) was weighed in a 15 ml microwave vial inside of the glovebox. A solution of the dissolved monomers (total 0.06 mmol) in degassed $CH_2Cl_2$ (3 ml) was transferred with a syringe to the catalyst and the solution stirred for two hours at room temperature. To stop the polymerization, 1 ml of ethyl vinyl ether was added and the reaction mixture stirred for 30 min before the addition $CH_3OH$ (5 ml). After stirring the mixture for another 30 min, the precipitated monomer was collected by centrifugation (500 rpm, 15 min) and washed with 20 ml of $CH_3OH$ four times.

## 7. Literature


1. Mortimer RJ. Electrochromic materials. *Chem Soc Rev*. 1997;26:147-156.

2. Xu JW, Chua MH, Shah KW. *Electrochromic Smart Materials*.; 2019.

3. Gu C, Jia AB, Zhang YM, Zhang SXA. Emerging Electrochromic Materials and Devices for Future Displays. *Chem Rev*. 2022;122(18):14679-14721. doi:10.1021/acs.chemrev.1c01055

4. Deb SK. A Novel Electrophotographic System. *Appl Opt*. 1969;8(S1):192. doi:10.1364/ao.8.s1.000192

5. Eh ALS, Tan AWM, Cheng X, Magdassi S, Lee PS. Recent Advances in Flexible Electrochromic Devices: Prerequisites, Challenges, and Prospects. *Energy Technol*. 2018;6(1):33-45. doi:10.1002/ente.201700705

6. Guarr TF, Theiste DA, Ash KL, Driscroll DI, Luten HA. Variable transmission electrochromc window and assocated aircraft window system. 2014;2(12).

7. Gustafsson JC, Liedberg B, Inganfis O. In situ spectroscopic investigations of electrochromism and ion transport in a poly (3,4-ethylenedioxythiophene) electrode in a solid state electrochemical cell. *Solid State Ionics*. 1994;69(2):145-152.

8. Dioxythiophenes E rich, Dyer AL, Craig MR, Babiarz JE, Kiyak K, Reynolds JR. Orange and Red to Transmissive Electrochromic Polymers Based on. Published online 2010:4460-4467. doi:10.1021/ma100366y

9. Polymers E, Amb CM, Dyer AL, Reynolds JR. Navigating the Color Palette of Solution-Processable. Published online 2011:397-415. doi:10.1021/cm1021245

10. Chen D, Tong Z, Rao Q, Liu X, Meng H, Huang W. High-Performance Black Copolymers Enabling Full Spectrum Control in Electrochromic Devices. *Nat Commun* . 2024;15(1):1-9. doi:10.1038/s41467-024-52430-2

11. Souza VHR, Schmidt A, Zarbin AJG. A tunable color palette of electrochromic materials achieved through an ingenious stacking of ordinary conducting polymers. *Journals Metrials Chem A*. 2023;11(35):18853-18861. doi:10.1039/d3ta02860g

12. Malacara D. *Color Vision and Colorimetry: Theory and Applications*.; 2002.

13. Aristotle. *Minor Works: On Colours. On Things Heard. Physiognomics. On Plants. On Marvellous Things Heard. Mechanical Problems. On Indivisible Lines. The Situations and Names of Winds. On Melissus, Xenophanes, Gorgias*. MA: Harvard University Press; 1936.

14. Paddie W. The Trichromatic Theory of Colour Vision. *Nature*. 1923;112(2805):163-164.

15. Kulyk O, Rocard L, Maggini L, Bonifazi D. Synthetic strategies tailoring colours in multichromophoric organic nanostructures. *Chem Soc Rev*. 2020;49(23):8400-8424. doi:10.1039/c9cs00555b

16. Bernthsen A. Zur Kenntniss des Methylenblau und verwandter Farbstoffe. *Berichte der Dtsch Chem Gesellschaft*. 1883;16(2):2896-2904.

17. McDowell JJH. The Crystal and Molecular Structure of Phenothiazine. *Acta Crystallogr*. 1976;32(1):5-10.

18. Singhabhandhu A, Robinson PD, Fang JH, Geiger WE. Crystal and Molecular Structures of Ion Radical Molecular Complexes with Phenothiazine and Phenoxazine . Effects of Donor-Acceptor Separation oh the Molecular Properties. *Inorg Chem*. 1975;14(2):318-323.

19. Eicher T, Hauptmann S, Speicher A. *The Chemistry of Heterocycles : Structure, Reactions, Syntheses, and Applications*. 2nd ed.; 2003.

20. Kazemi F, Mohamadnia Z, Kaboudin B, Karimi Z. Photodegradation of methylene blue with a titanium dioxide/polyacrylamide photocatalyst under sunlight. *J Appl Polym Sci*. 2016;133(19). doi:10.1002/app.43386

21. Clarke BD, Gilbert BC, Hanson P, Kirk CM. The Influence of the Structure and the Conformation of the Side-chain on the Properties of Phenothiazine Cation-radicals substituted at Nitrogen. *J Chem Soc Perkin Trans 2*. Published online 1978:1103-1110.

22. Wagner E, Filipek S, Kalinowski MK. Visible absorption spectra of the phenothiazine radical cation and its 10-substituted derivatives - Short communication. *Monatshefte für Chemie Chem Mon*. 1988;119(8-9):929-932. doi:10.1007/BF00810102

23. Narayana KA, Casselman MD, Elliott CF, et al. N-Substituted Phenothiazine Derivatives:How the Stability of the Neutral and Radical Cation Forms Affects Overcharge Performance in Lithium-Ion Batteries. *ChemPhysChem*. 2015;16(6):1179-1189.

24. Attanayake NH, Kaur AP, Suduwella TM, Elliott CF, Parkin SR, Odom SA. A stable, highly oxidizing

radical cation. *New J Chem*. 2020;44(42):18138-18148. doi:10.1039/d0nj04434b

25. Li XS, MU TW, Guo QX, Liu YC. A Theoretical Study on the Structure and Properties of Phenothiazine Derivatives and their Radical Cations. *Res Chem Intermed*. 2000;26(4):375-384.

26. Casselman MD, Elliott CF, Modekrutti S, et al. Beyond the Hammett Effect: Using Strain to Alter the Landscape of Electrochemical Potentials. *ChemPhysChem*. 2017;18(16):2142-2146. doi:10.1002/cphc.201700607

27. Sailer M, Gropeanu R adrian, Mu TJJ, Der O chemisches I. Practical Synthesis of Iodo Phenothiazines. A Facile Access to Electrophore Building Blocks Markus. 2003;(5):7509-7512.

28. Barkschat CS, Müller TJJ. Synthesis and Electronic Properties of 3-Aryl 10H-Phenothiazines. *Stud UBB Chem*. 2016;61:55-72.

29. Tu X, Fu X, Jiang Q. The synthesis and electrochemical properties of anodic electrochromic materials phenothiazine derivatives and their electrochromic devices. 2010;31:150-154. doi:10.1016/j.displa.2010.05.001

30. Miyaura N, Yamada K, Suzuki A. A NEW STEREOSPECIFIC CROSS-COUPLING BY THE PALLADIUM-CATALYZED REACTION OF 1-ALKENYLBORANES WITH 1-ALKENYL OR l-ALKYNYL HALIDES. *Tetrahedron Lett*. 1979;20(36):3437-3440.

31. D'Alterio MC, Casals-Cruañas È, Tzouras N V., Talarico G, Nolan SP, Poater A. Mechanistic Aspects of the Palladium-Catalyzed Suzuki-Miyaura Cross-Coupling Reaction. *Chem - A Eur J*. 2021;27(54):13481-13493. doi:10.1002/chem.202101880

32. Suzuki A, Miyaura N. Palladium-Catalyzed Cross-Coupling Reactions of Organoboron Compounds. *Chem Rev*. 1995;95(7):2457-2483.

33. Martin R, Buchwald SL. Palladium-catalyzed suzuki-miyaura cross-coupling reactions employing dialkylbiaryl phosphine ligands. *Acc Chem Res*. 2008;41(11):1461-1473. doi:10.1021/ar800036s

34. Paul F, Patt J, Hartwig JF. Palladium-Catalyzed Formation of Carbon-Nitrogen Bonds. Reaction Intermediates and Catalyst Improvements in the Hetero Cross-Coupling of Aryl Halides and Tin Amides. *J Am Chem Soc*. 1994;116(13):5969-5970.

35. Dorel R, Grugel CP, Haydl AM. The Buchwald–Hartwig Amination After 25 Years. *Angew Chemie - Int Ed*. 2019;58(48):17118-17129. doi:10.1002/anie.201904795

36. Odian G. *Principles of Polymerization*. 4th ed.; 2004.

37. Sutthasupa S, Shiotsuki M, Sanda F. Recent advances in ring-opening metathesis polymerization, and application to synthesis of functional materials. *Polym J*. 2010;42(12):905-915. doi:10.1038/pj.2010.94

38. Hérisson JL, Chauvin Y. Catalyse de transformation des oléfines par les complexes du tungstène. *Die Makromol Chemie*. 1970;141(3487):161-176. http://doi.wiley.com/10.1002/macp.1971.021410112

39. Williams GT, Sedgwick AC, Sen S, et al. Boronate ester cross-linked PVA hydrogels for the capture and H2O2-mediated release of active fluorophores. *Chem Commun*. 2020;56(41):5516-5519. doi:10.1039/d0cc01904f

40. Tung-Sheng H, Jhen-Yi W, Cheng-Chung C. Synthesis of a Photostable Near-Infrared-Absorbing Photosensitizer for Selective Photodamage to Cancer Cells. *Chem - A Eur J*. 2014;20(31):9709-9715.

41. Sailer M, Franz AW, Müller TJJ. Synthesis and electronic properties of monodisperse oligophenothiazines. *Chem - A Eur J*. 2008;14(8):2602-2614. doi:10.1002/chem.200701341

42. Gao S, Bethel TK, Kakeshpour T, Hubbell GE, Jackson JE, Tepe JJ. Substrate Controlled Regioselective Bromination of Acylated Pyrroles Using Tetrabutylammonium Tribromide (TBABr3). *J Org Chem*. 2018;83(16):9250-9255. doi:10.1021/acs.joc.8b01251

43. Berthelot J, Fournier M. Bromation stéréosélective d'alcynes par le tribromure de tétrabutylammonium. *Can J Chem*. 1986;64(3):603-607. doi:10.1139/v86-097

44. Zhang W, Feng X, Zhang C, Jia Q, Liu X, Zhou K. Activity of N-H in phenothiazine derivatives: synthesis and applications in fluoride ions sensing and electrochromism. *J Mater Chem C*. 2023;11(8):2949-2956. doi:10.1039/d2tc04079d

45. Navarro O, Marion N, Oonishi Y, Kelly III RA, Nolan SP. Suzuki-Miyaura, r-Ketone Arylation and Dehalogenation Reactions Catalyzed by a Versatile N-Heterocyclic Carbene-Palladacycle Complex. *J Org Chem*. 2006;71(2):685-692.

46. Martínez-Arranz S, Alḃeniz AC, Espinet P. Versatile route to functionalized vinylic addition polynorbornenes. *Macromolecules*. 2010;43(18):7482-7487. doi:10.1021/ma101137z

47. Vonlanthen D, Rudnev A, Mishchenki A, et al. Conformationally Controlled Electron Delocalization

in n-Type Rods: Synthesis, Structure, and Optical, Electrochemical, and Spectroelectrochemical Properties of Dicyanocyclophanes. *Chem - A Eur J*. 2011;17(26):7236-7250.

48. Hanson K, Roskop L, Djurovich PI, Zahariev F, Gordon MS, Thompson ME. A Paradigm for Blue- or Red-Shifted Absorption of Small Molecules Depending on the Site of π-Extension. *J Am Chem Soc*. 2010;132(45):16247–16255.

49. Christensen JA, Phelan BT, Chaudhuri S, Acharya A, Batista VS, Wasielewski MR. Phenothiazine Radical Cation Excited States as Super-oxidants for Energy-Demanding Reactions. *J Am Chem Soc*. 2018;140(15):5290-5299. doi:10.1021/jacs.8b01778

50. Ma T, Easley AD, Thakur RM, Mohanty KT, Wang C, Lutkenhaus JL. Nonconjugated Redox-Active Polymers : Electron Transfer Mechanisms , Energy Storage , and Chemical Versatility. *Annu Rev ofChemical Biomol Eng*. 2023;14:187-216.

51. Gao M, Tian Y, Li X, et al. The Effect of Molecular Conformations and Simulated “Self-Doping” in Phenothiazine Derivatives on Room-Temperature Phosphorescence. *Angew Chemie - Int Ed*. 2023;62(5).

# 8. Appendix

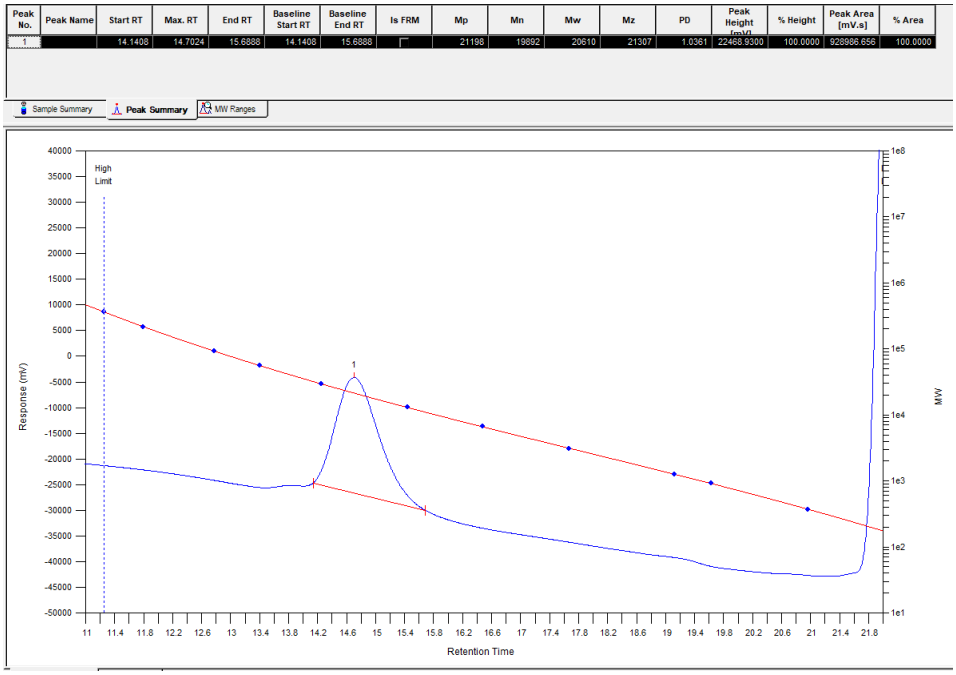


Figure 30: GPC results of the homopolymer using monomer **3** (Table 7, Entry 1) (scale: 0.03 mmol, DP=36).

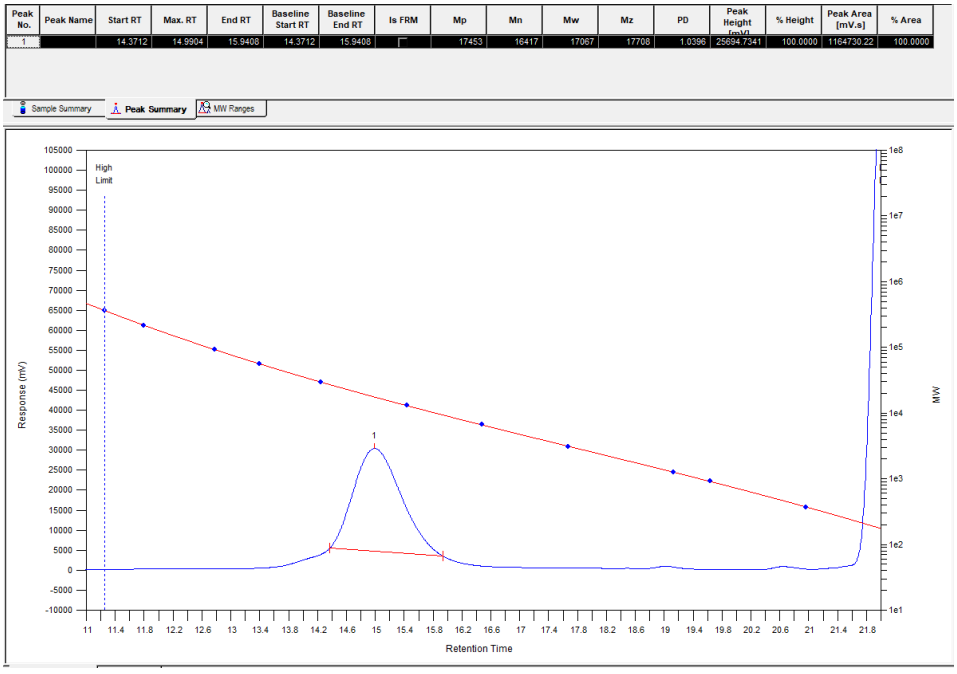


Figure 31: GPC results of the homopolymer using monomer **3** (Table 7, Entry 2) (scale: 0.03 mmol, DP=29).

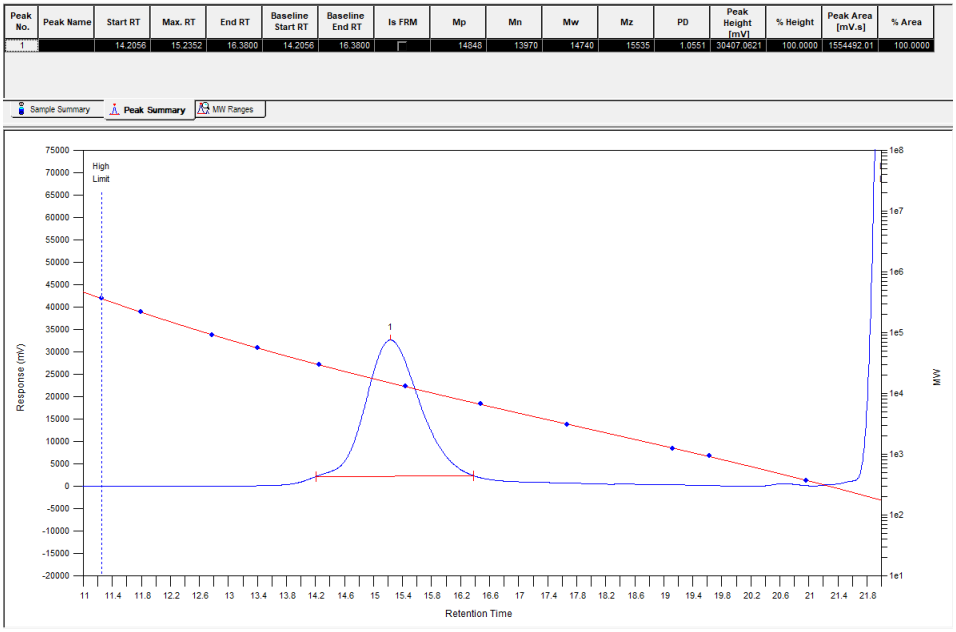


Figure 32: GPC results of the homopolymer using monomer **3** (Table 7, Entry 3) (scale: 0.03 mmol, DP=25).

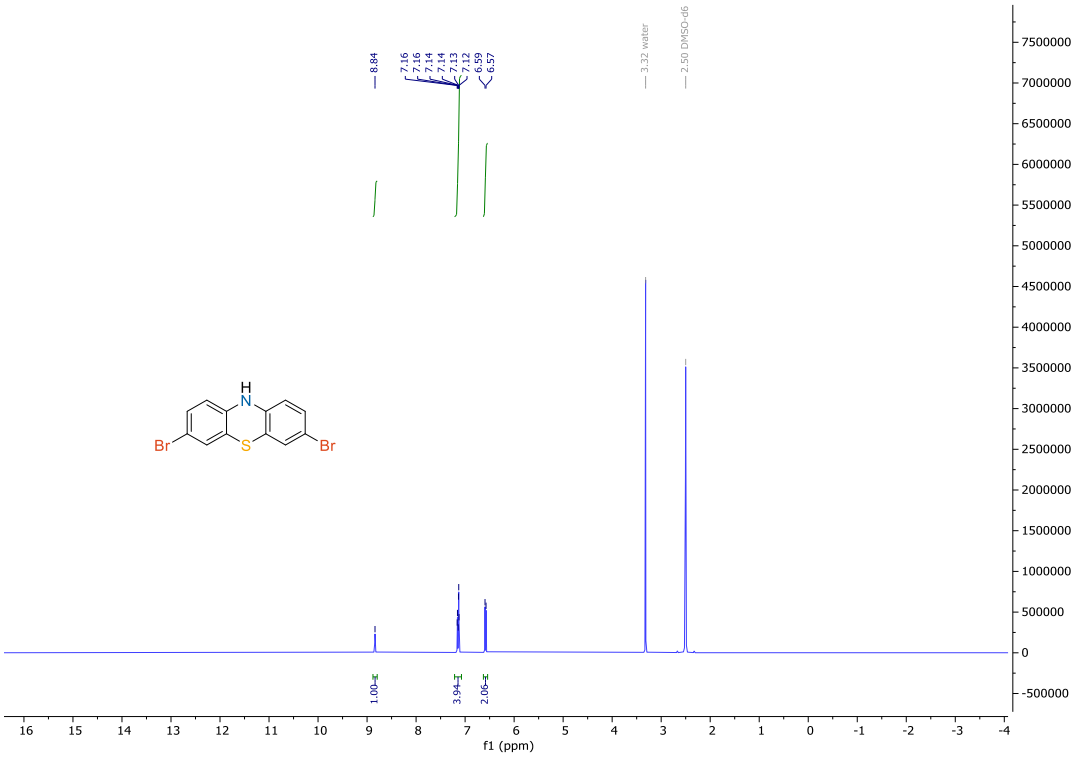


*Figure 33: $^{1}$H-NMR spectrum of **10** in DMSO-$d_6$.*

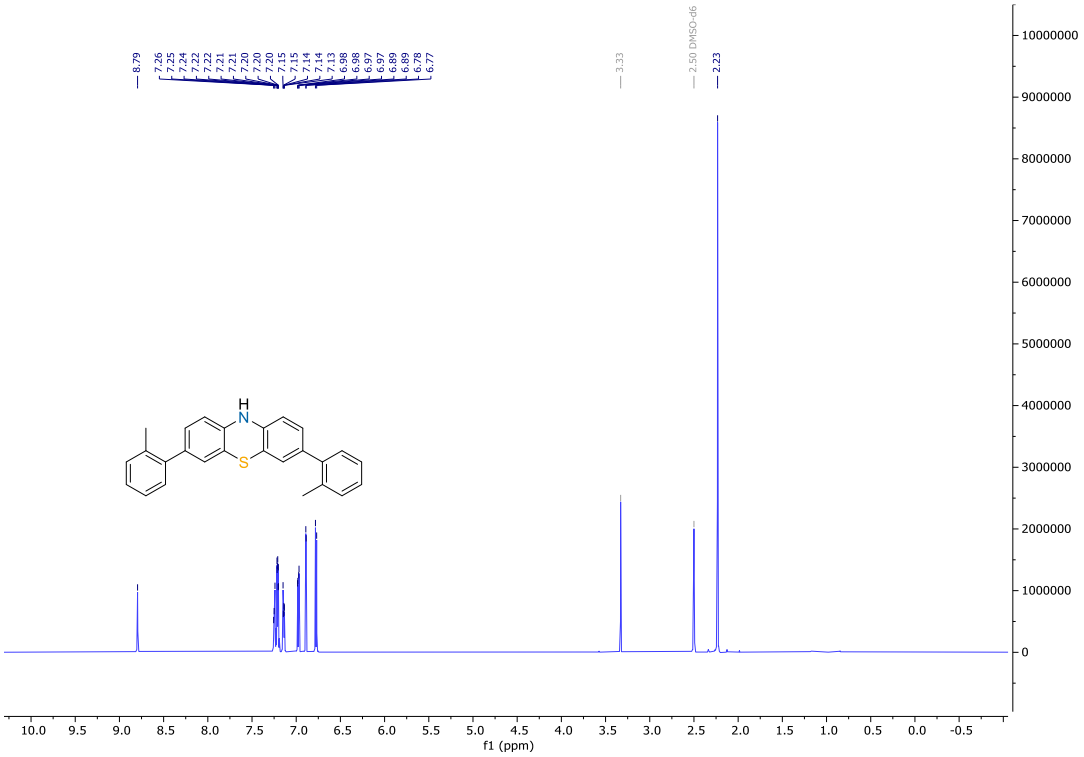


*Figure 34: [1]H-NMR spectrum of **13** in DMSO-$d_6$.*

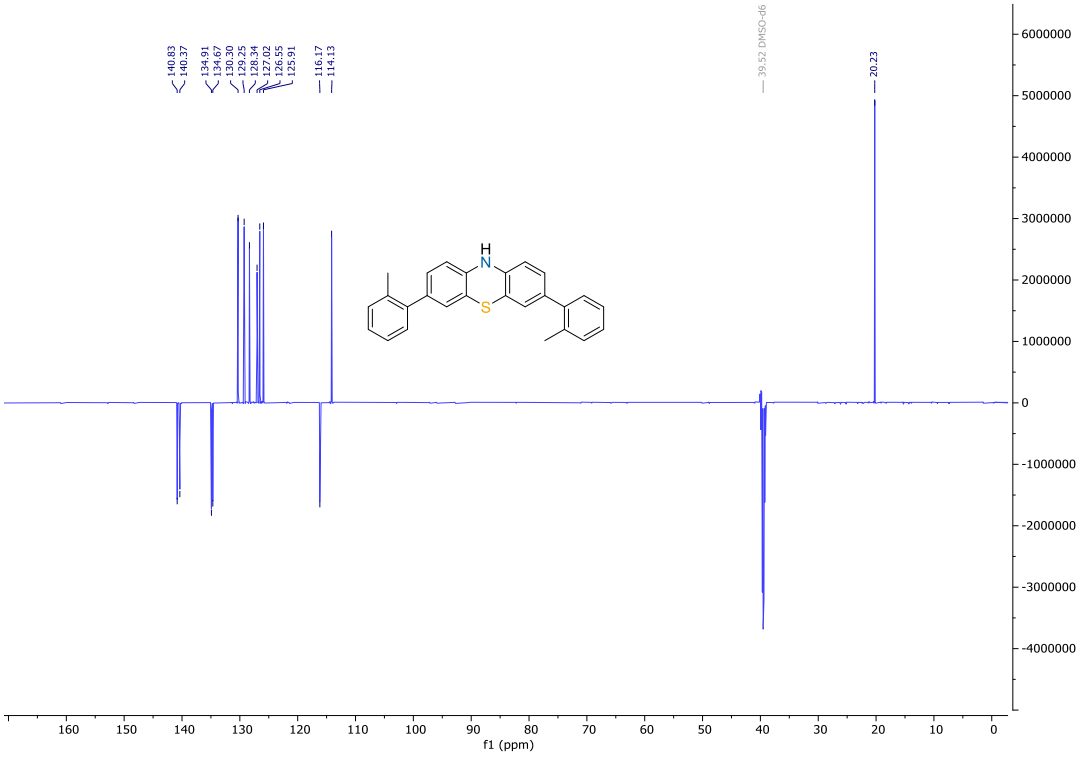


*Figure 35: [13]C-NMR spectrum of **13** in DMSO-$d_6$.*

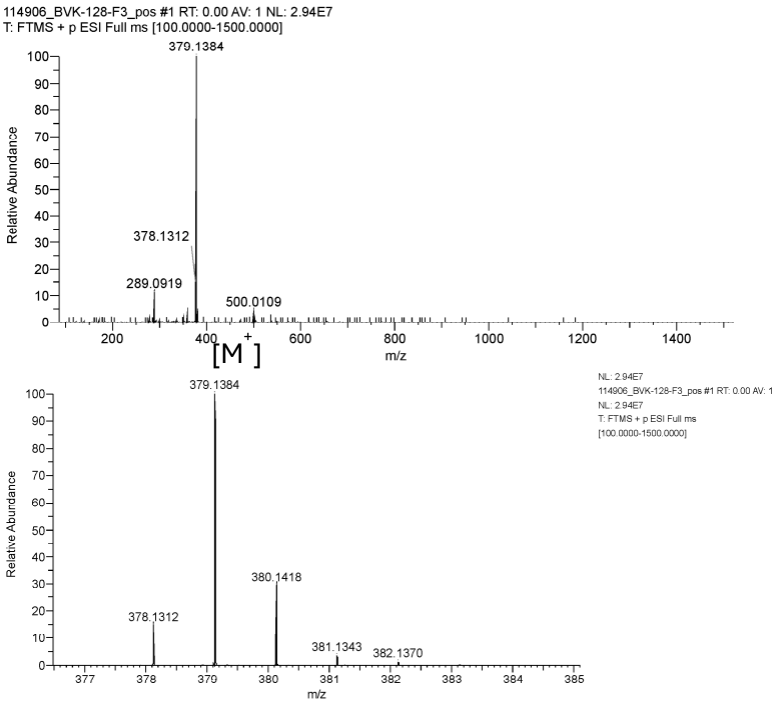


*Figure 36: HRMS (ESI) of **13**.*

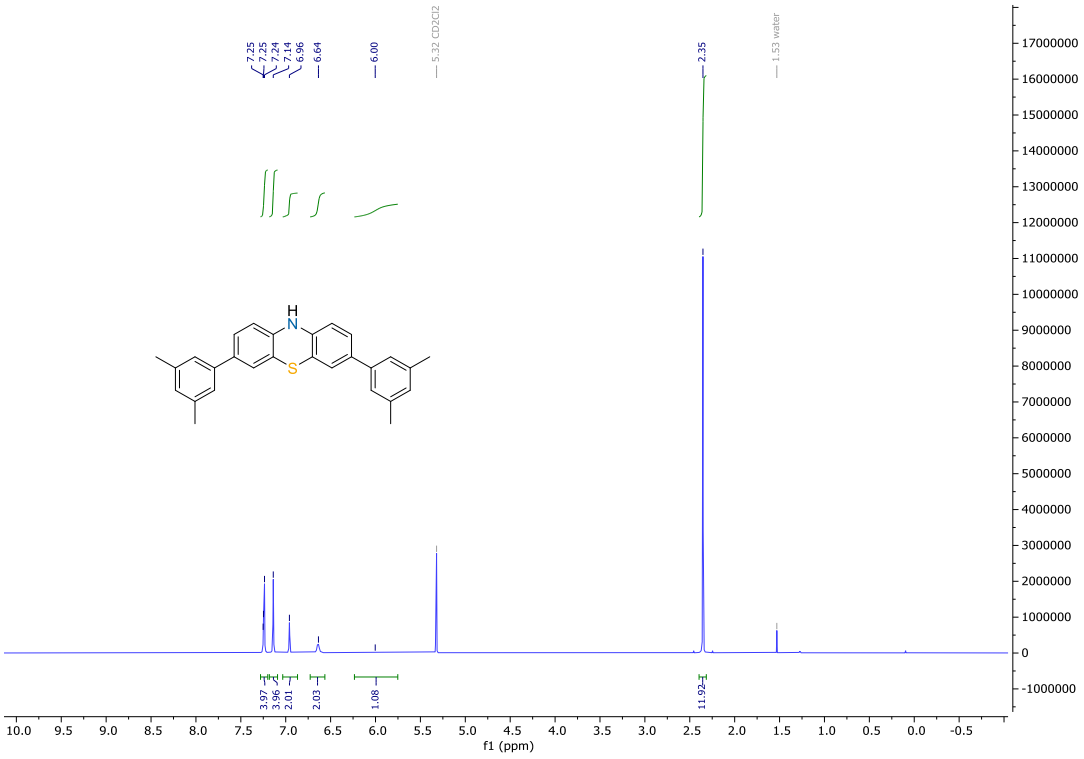


*Figure 37: $^1$H-NMR spectrum of **12** in $CD_2Cl_2$.*

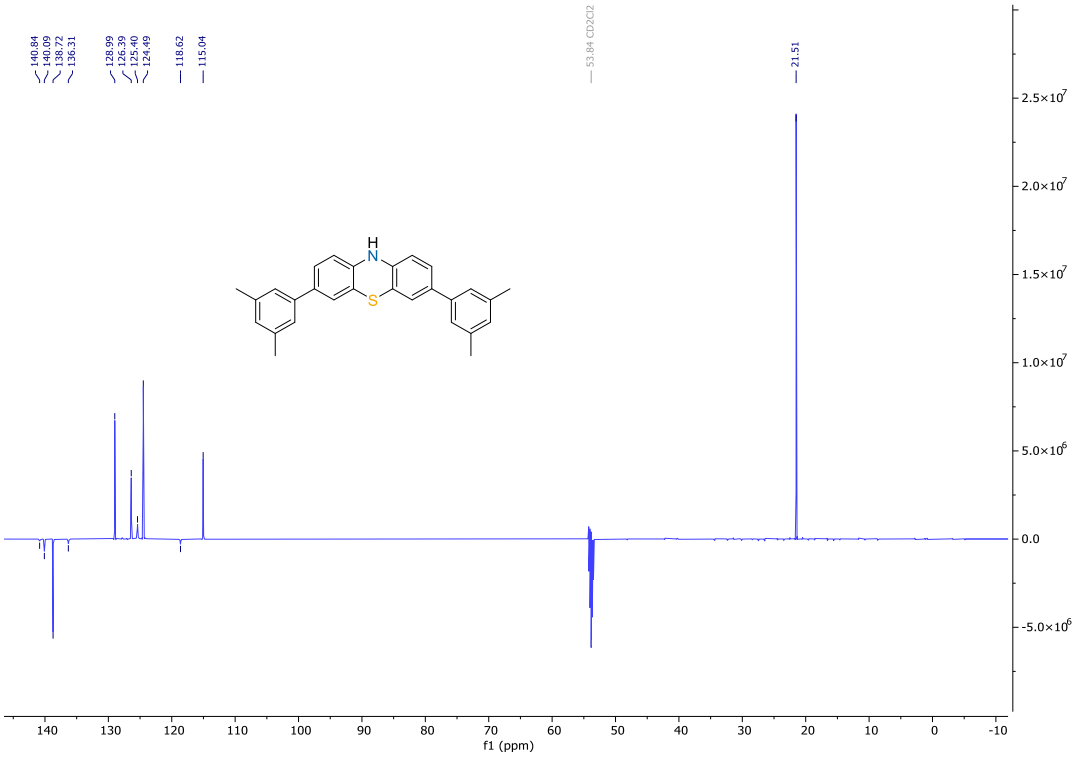


*Figure 38 $^{13}$C-NMR spectrum of **12** in $CD_2Cl_2$.*

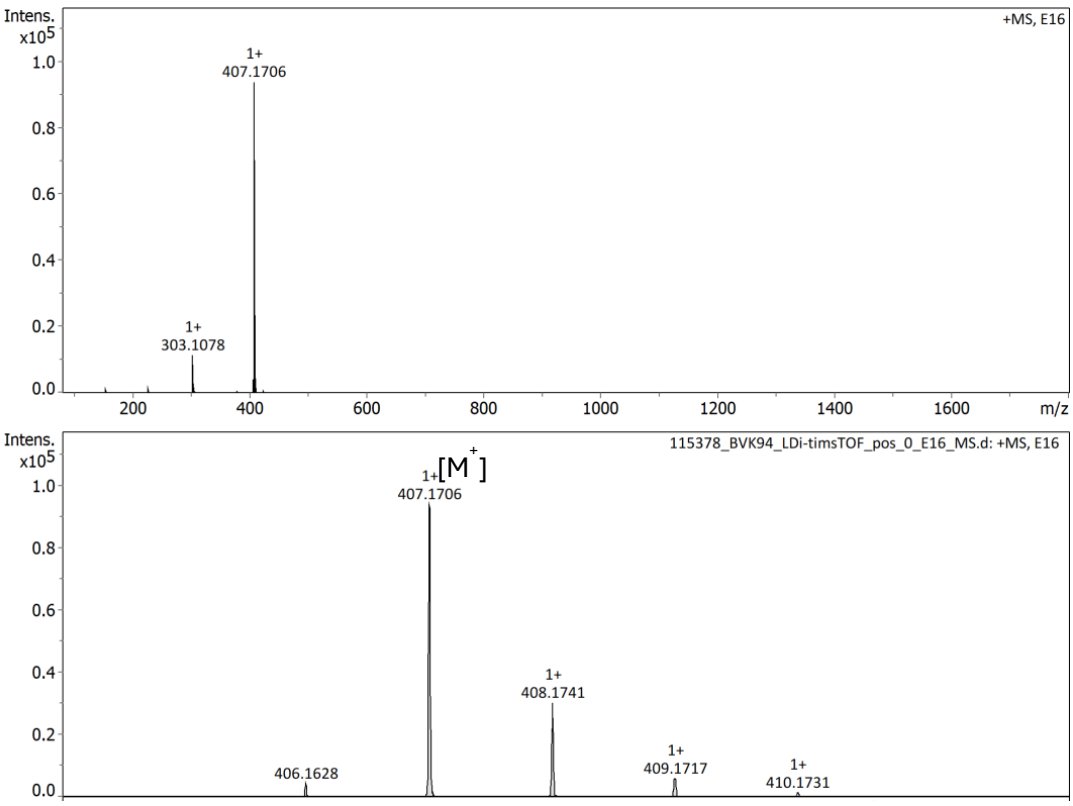


*Figure 39: HRMS (MALDI-timsTOF) mass spectrum of **12**.*

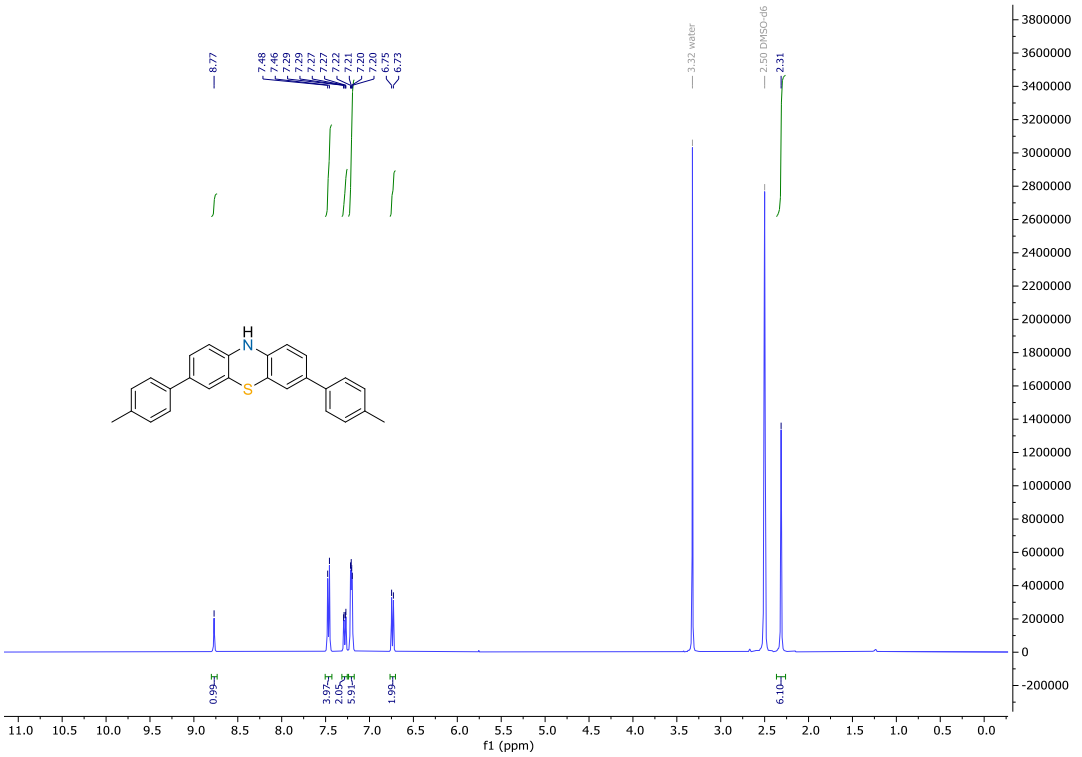


*Figure 40: $^{1}$H-NMR spectrum of **11** in DMSO-$d_6$.*

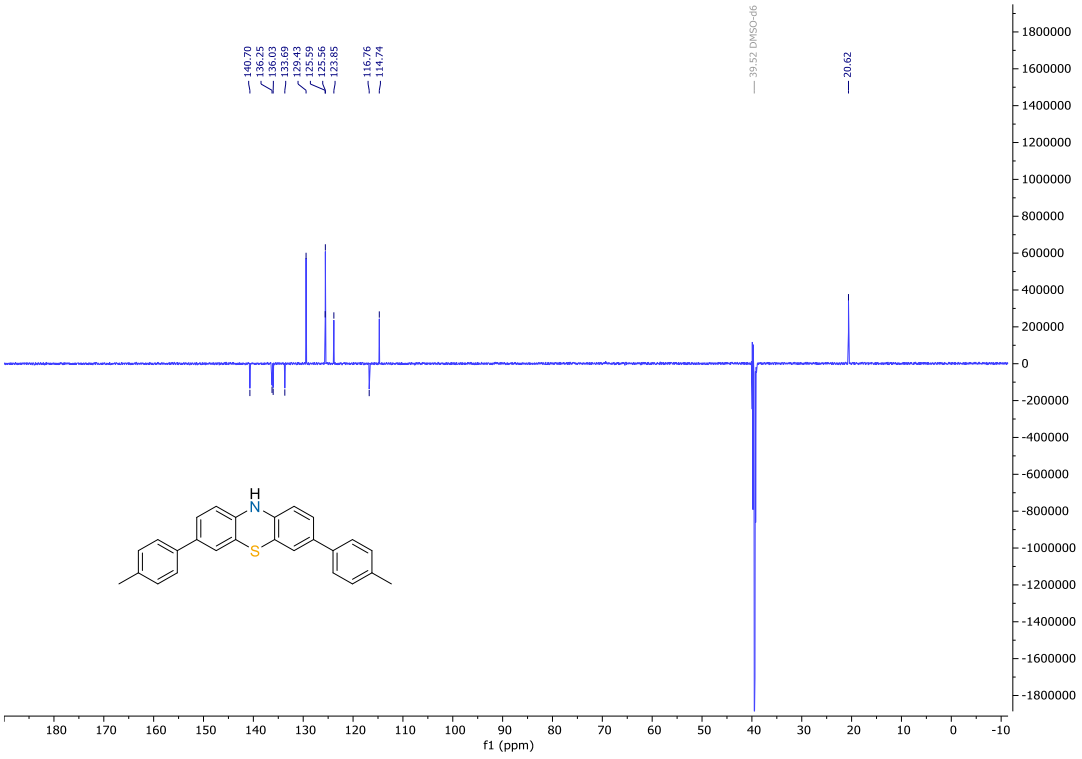


*Figure 41 $^{13}$C-NMR spectrum of **11** in DMSO-$d_6$.*

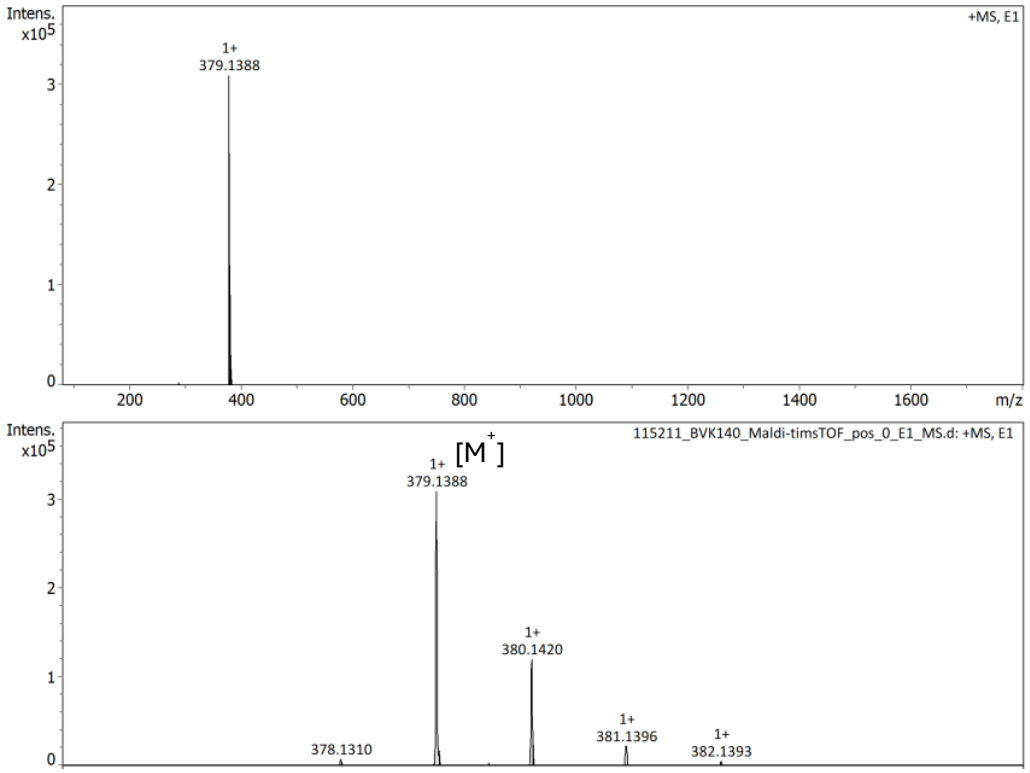


*Figure 42: HRMS (MALDI-timsTOF) mass spectrum of **11**.*

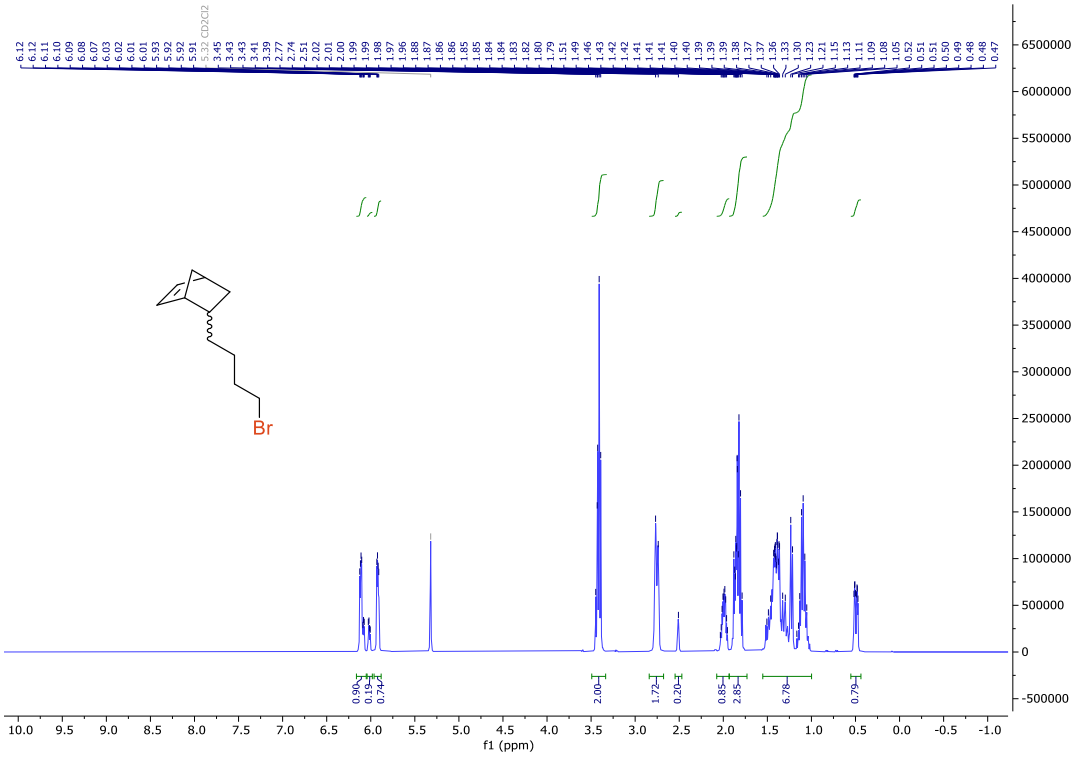


*Figure 43 $^1$H-NMR spectrum of **14** in $CD_2Cl_2$.*

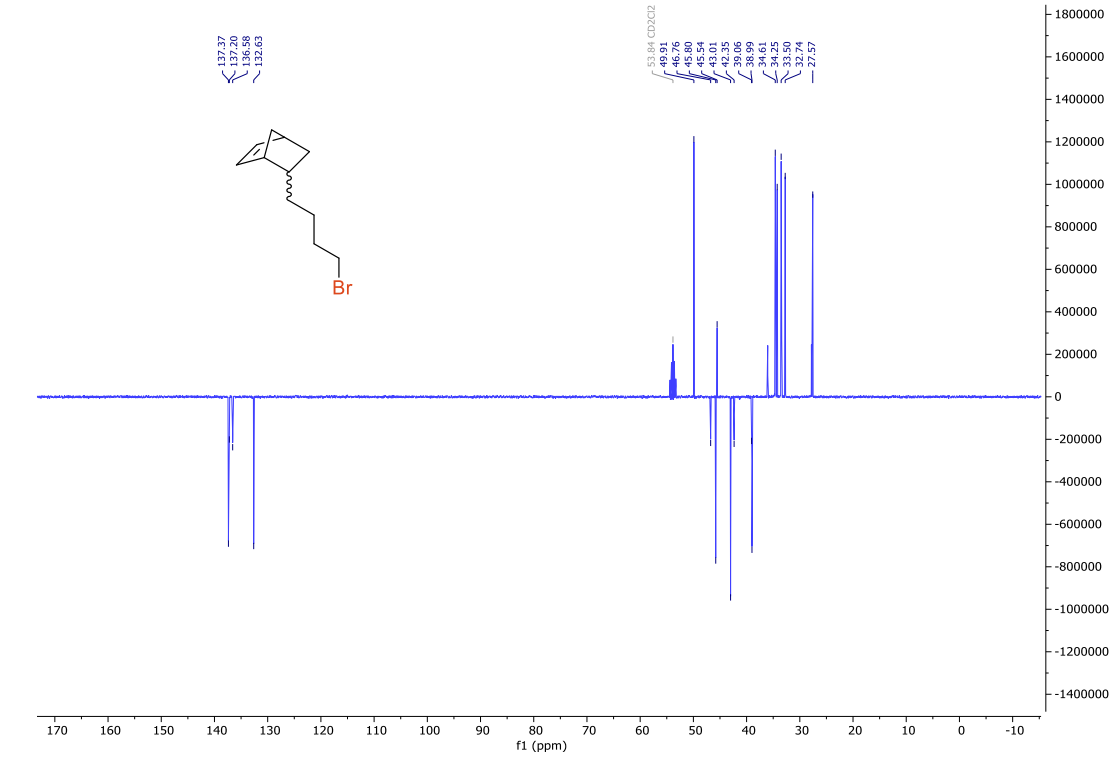


*Figure 44: $^{13}$C-NMR spectrum of **14** in $CD_2Cl_2$.*

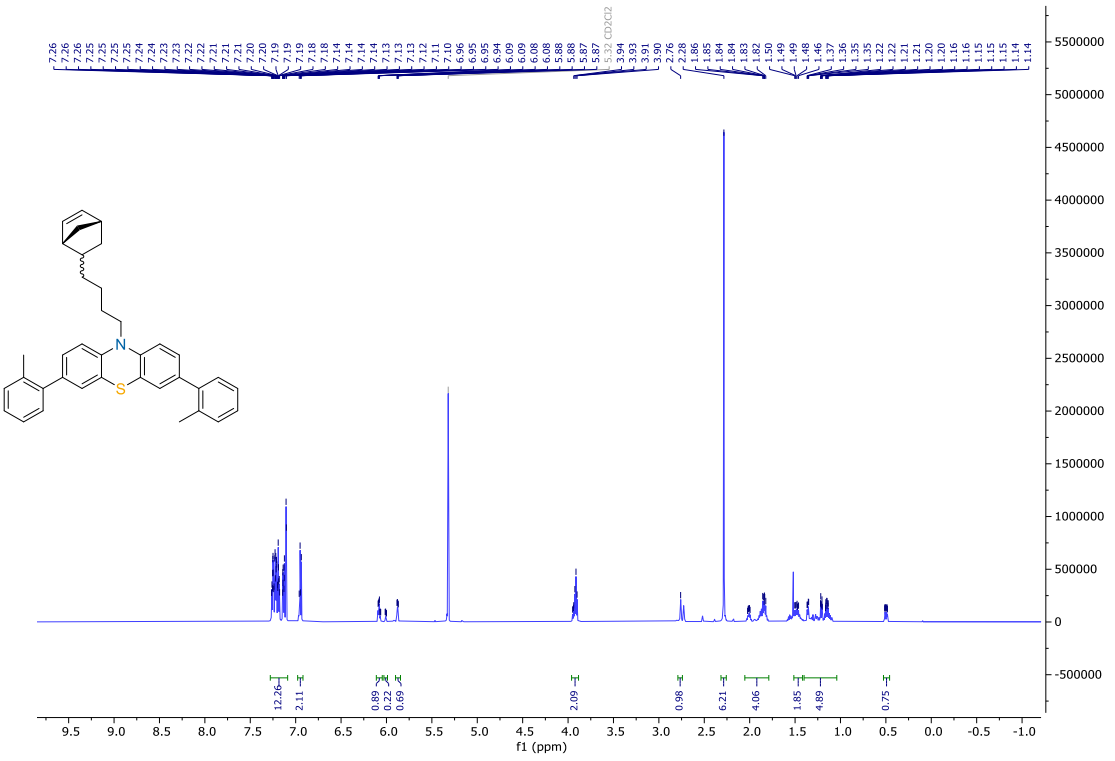


*Figure 45: $^{1}$H-NMR of **4** in $CD_2Cl_2$.*

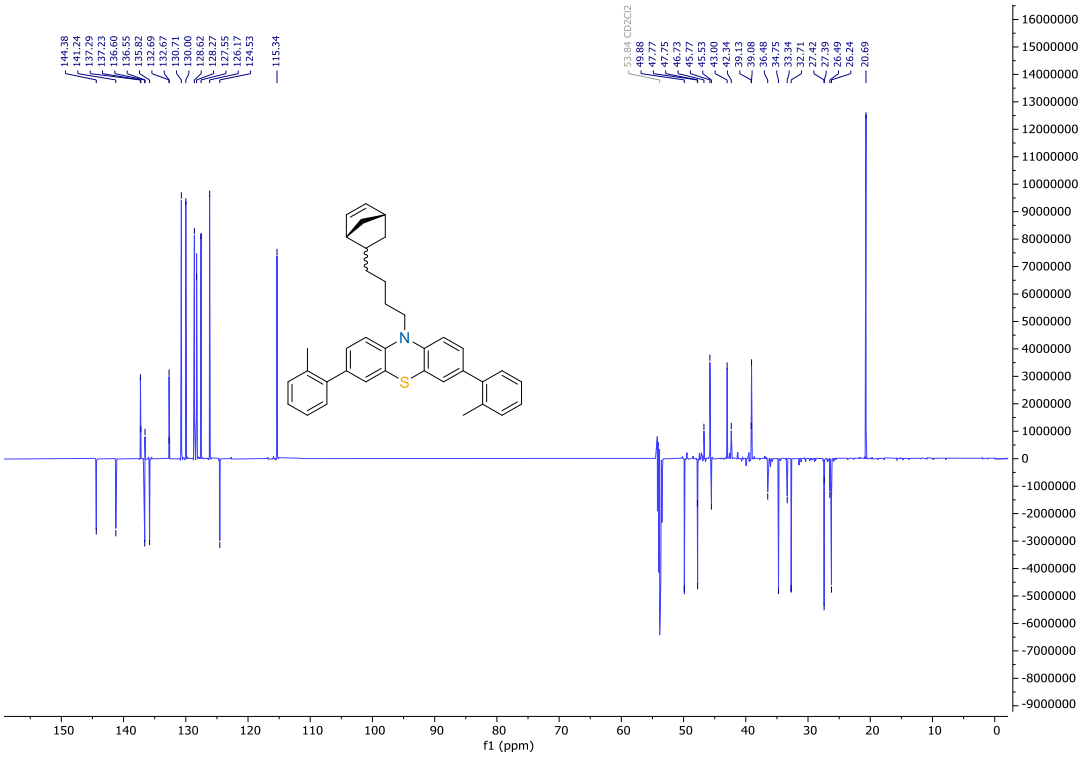


*Figure 46: $^{13}$C-NMR of **4** in $CD_2Cl_2$.*

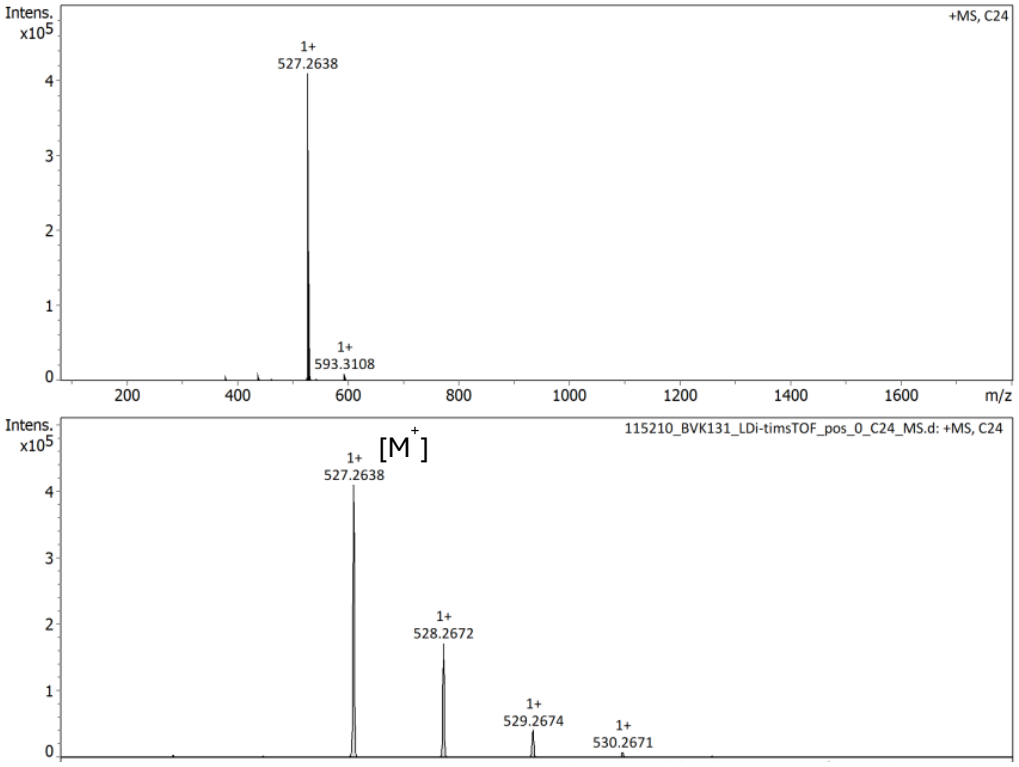


*Figure 47: HRMS (MALDI-timsTOF) mass spectrum of **4**.*

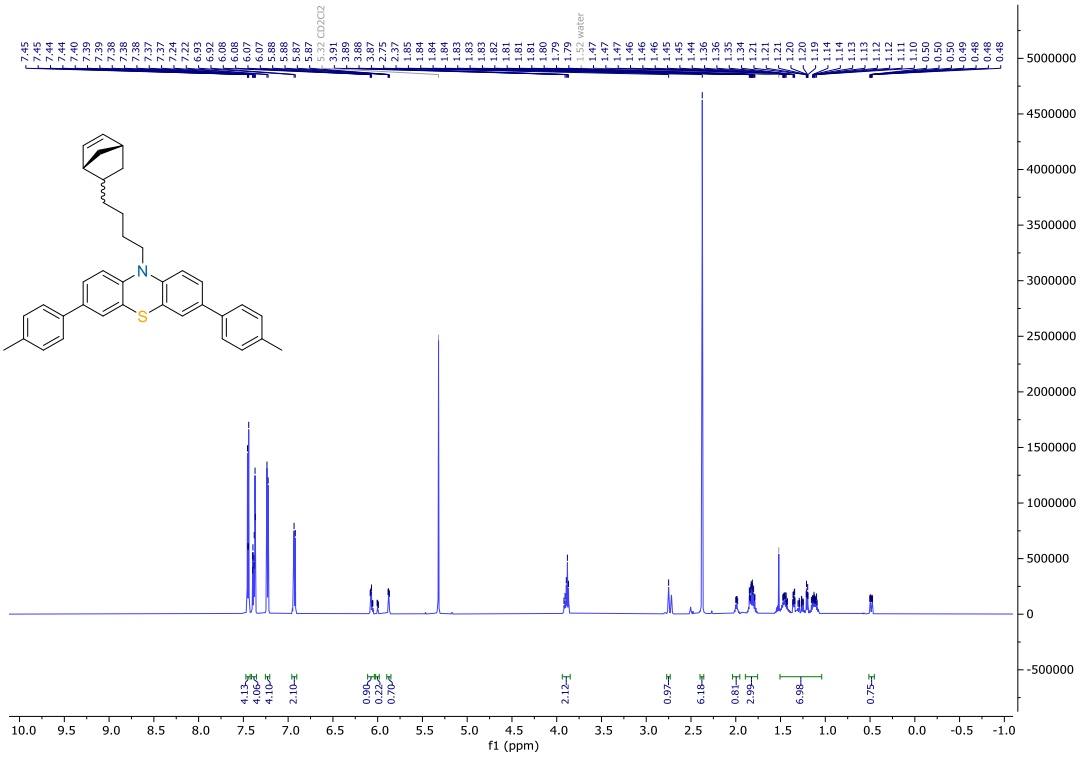


*Figure 48: $^{1}$H-NMR of **5** in $CD_2Cl_2$.*

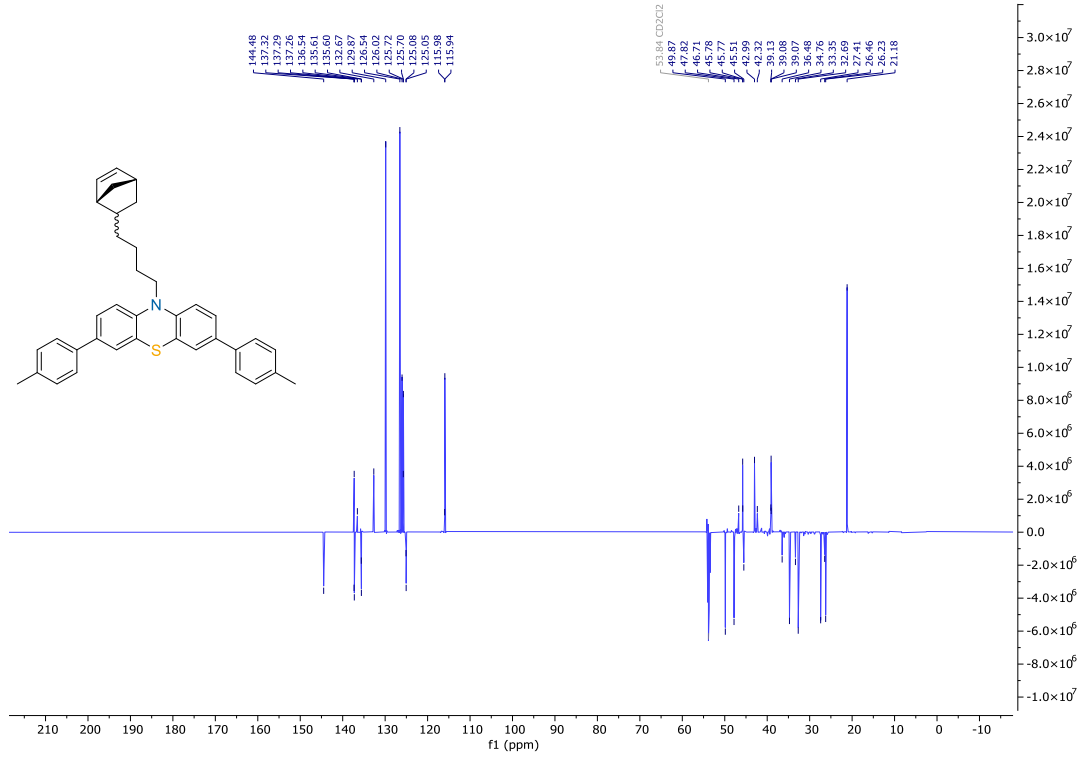


*Figure 49: $^{13}$C-NMR of **5** in $CD_2Cl_2$.*

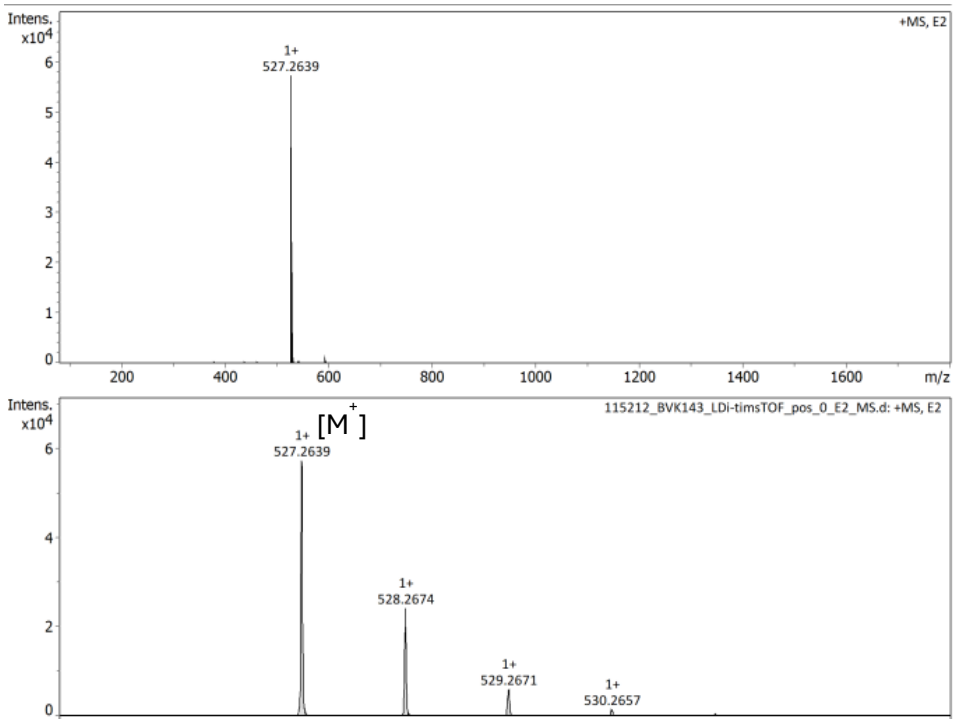


*Figure 50: HRMS (MALDI-timsTOF) mass spectrum of **5**.*

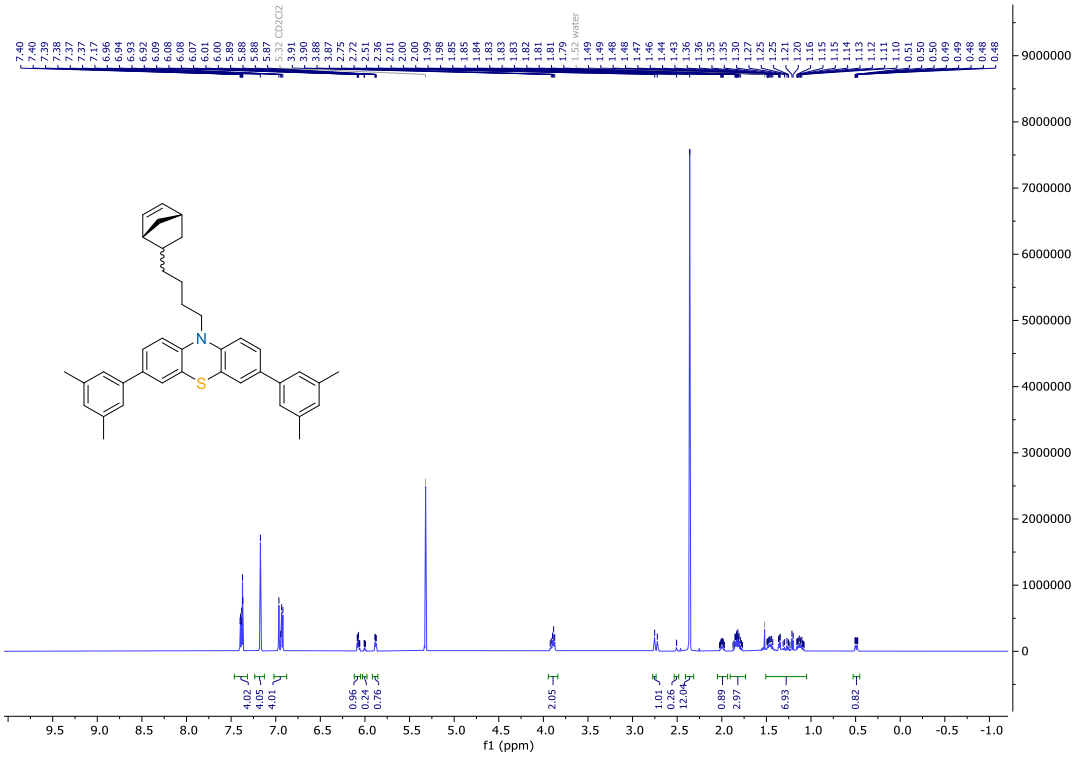


*Figure 51: $^{1}$H-NMR of **3** in $CD_2Cl_2$.*

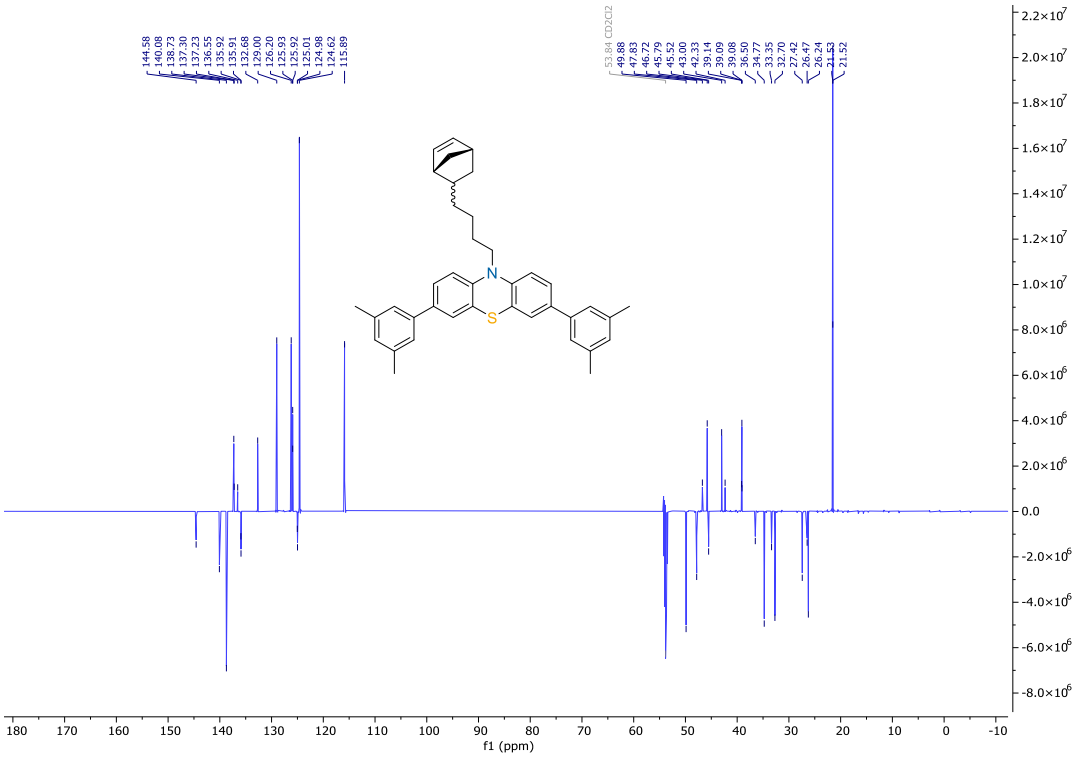


*Figure 52: $^{13}$C-NMR of **3** in $CD_2Cl_2$.*

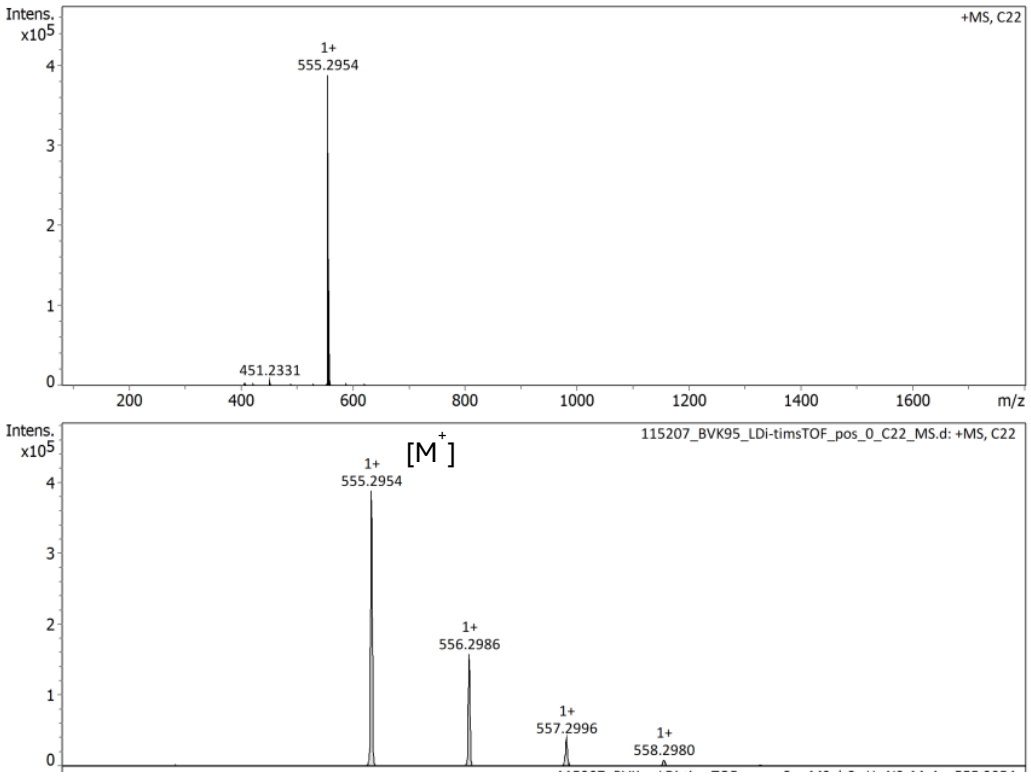


*Figure 53: HRMS (MALDI-timsTOF) mass spectrum of **3**.*

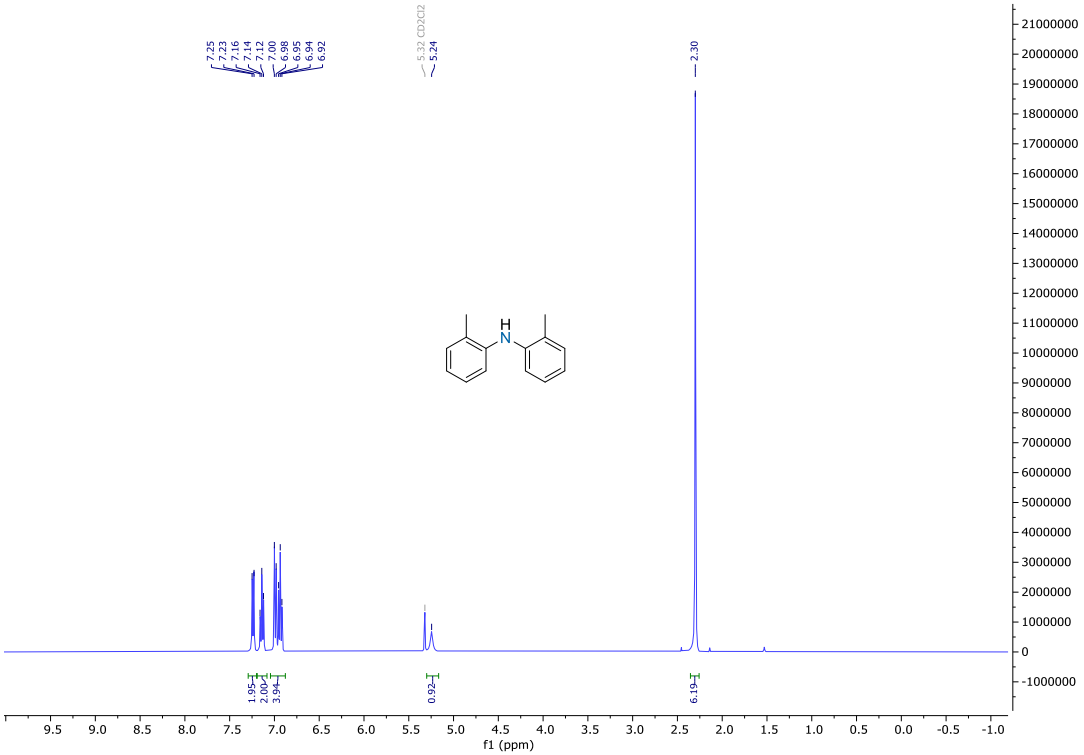


*Figure 54: $^{1}$H-NMR of **15** in $CD_2Cl_2$.*


*Figure 55: $^{13}$C-NMR of **15** in $CD_2Cl_2$.*

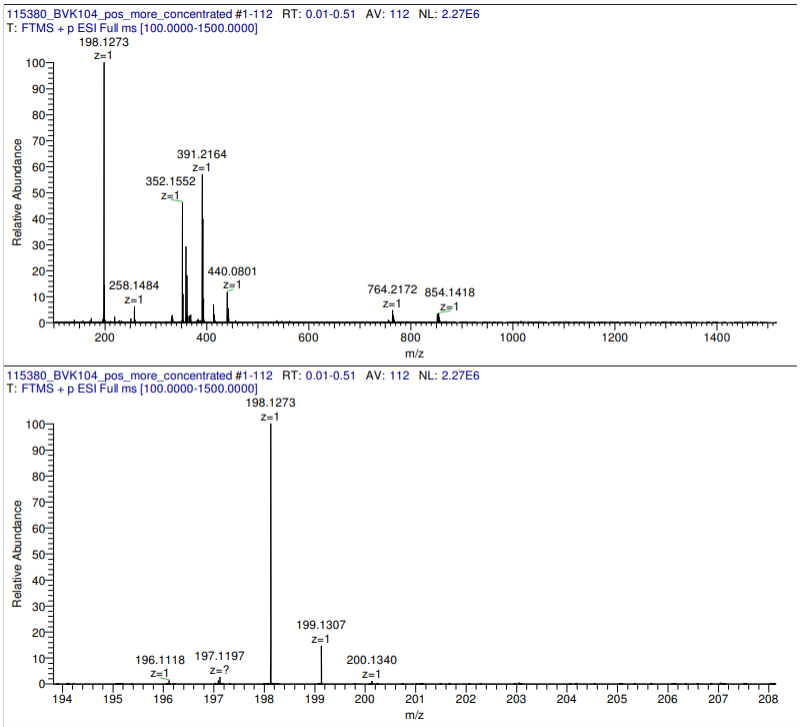


*Figure 56: HRMS (ESI) of **15**.*

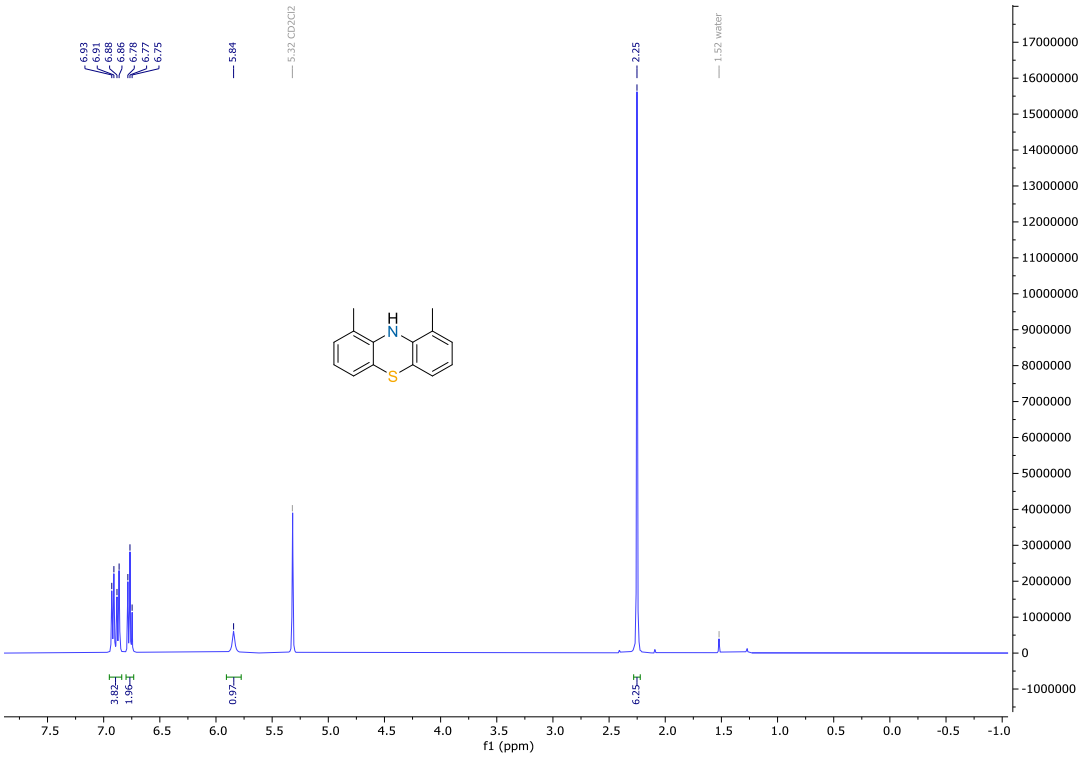


*Figure 57: $^{1}$H-NMR of **2** in $CD_2Cl_2$.*


*Figure 58: $^{13}$C-NMR of **2** in $CD_2Cl_2$.*

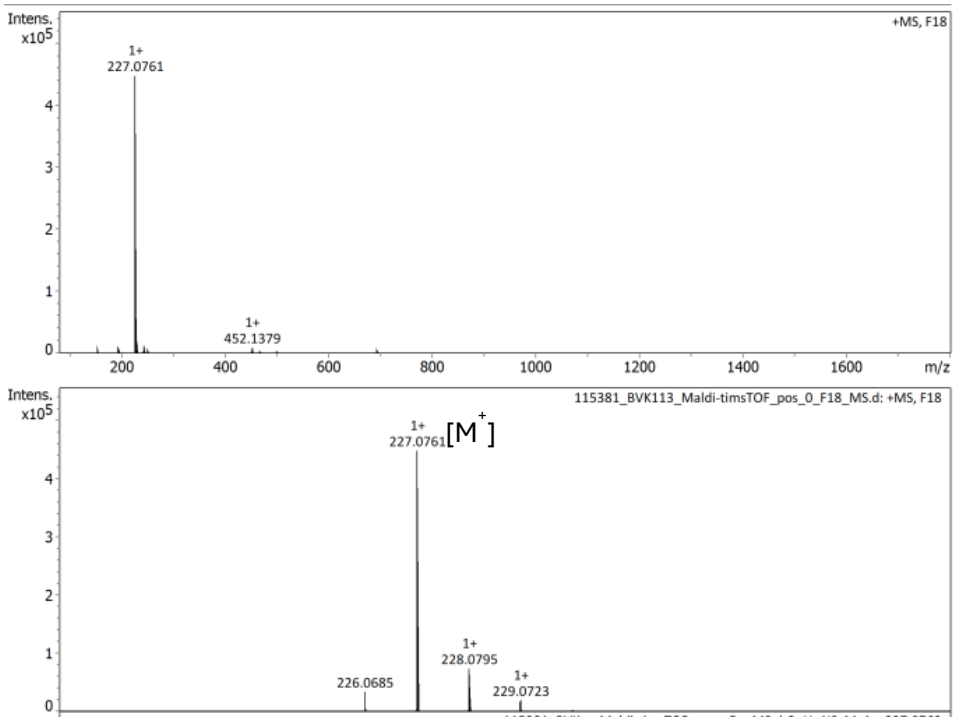


*Figure 59: HRMS (MALDI-timsTOF) mass spectrum of **2**.*

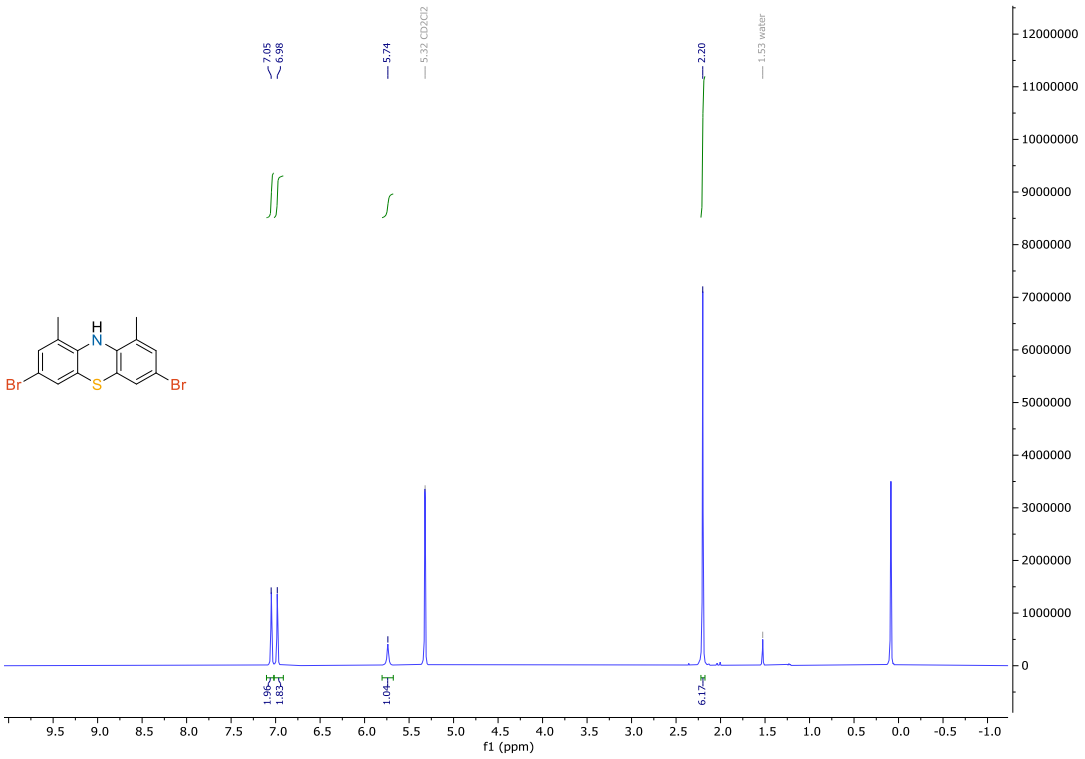


*Figure 60 $^{1}$H-NMR of **16** in $CD_2Cl_2$.*

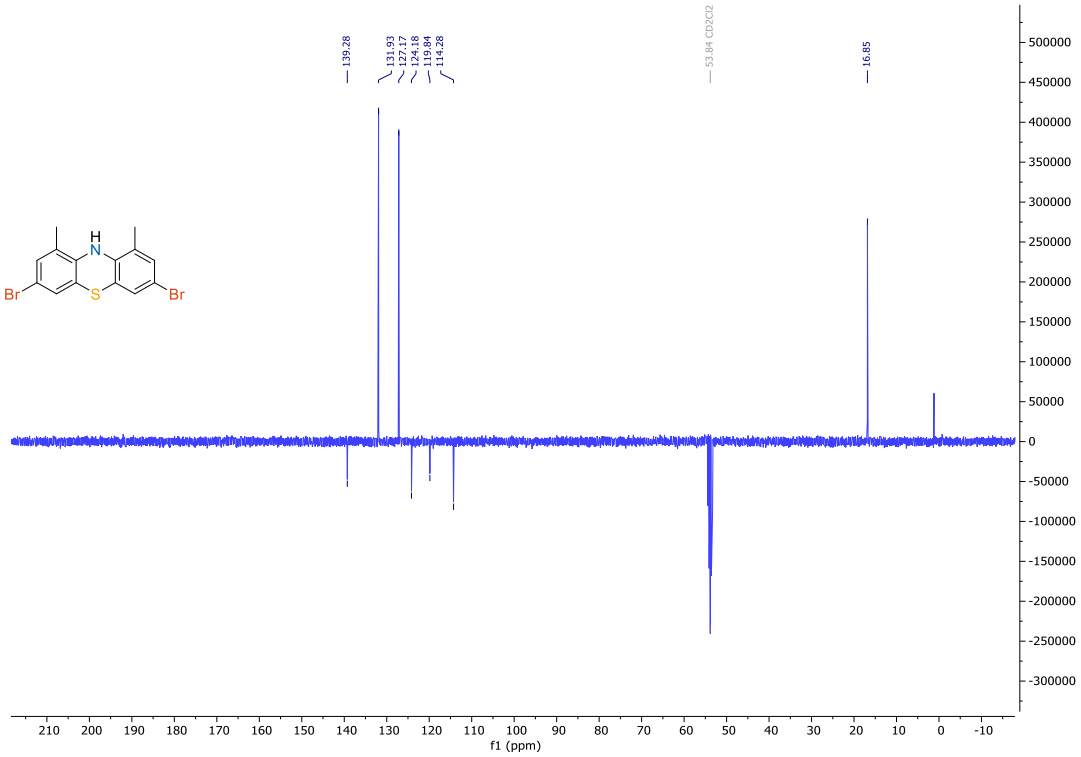


*Figure 61: $^{13}$C-NMR of **16** in $CD_2Cl_2$.*

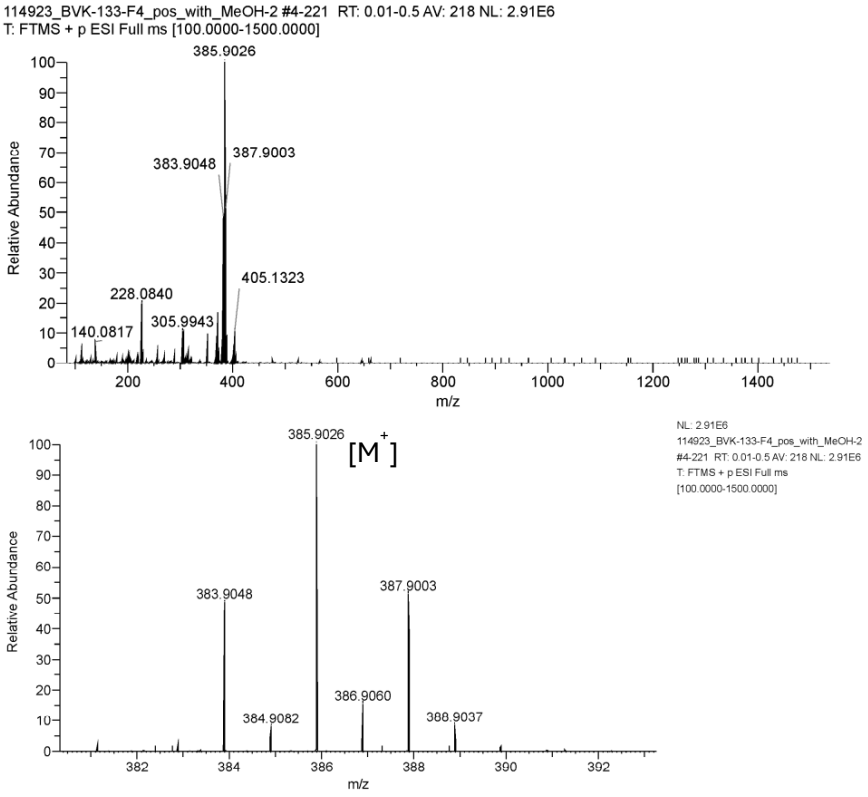


*Figure 62: HRMS (ESI-FTMS) mass spectrum of **16**.*

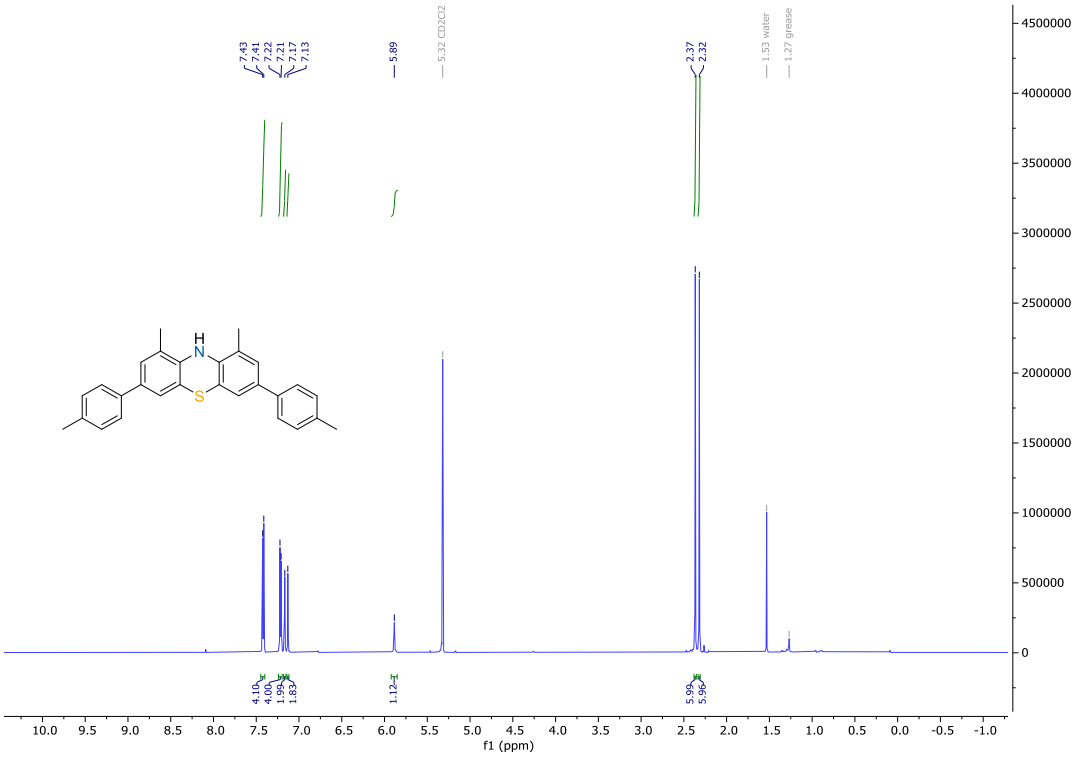


*Figure 63: $^{1}$H-NMR spectrum of **17** in $CD_2Cl_2$.*

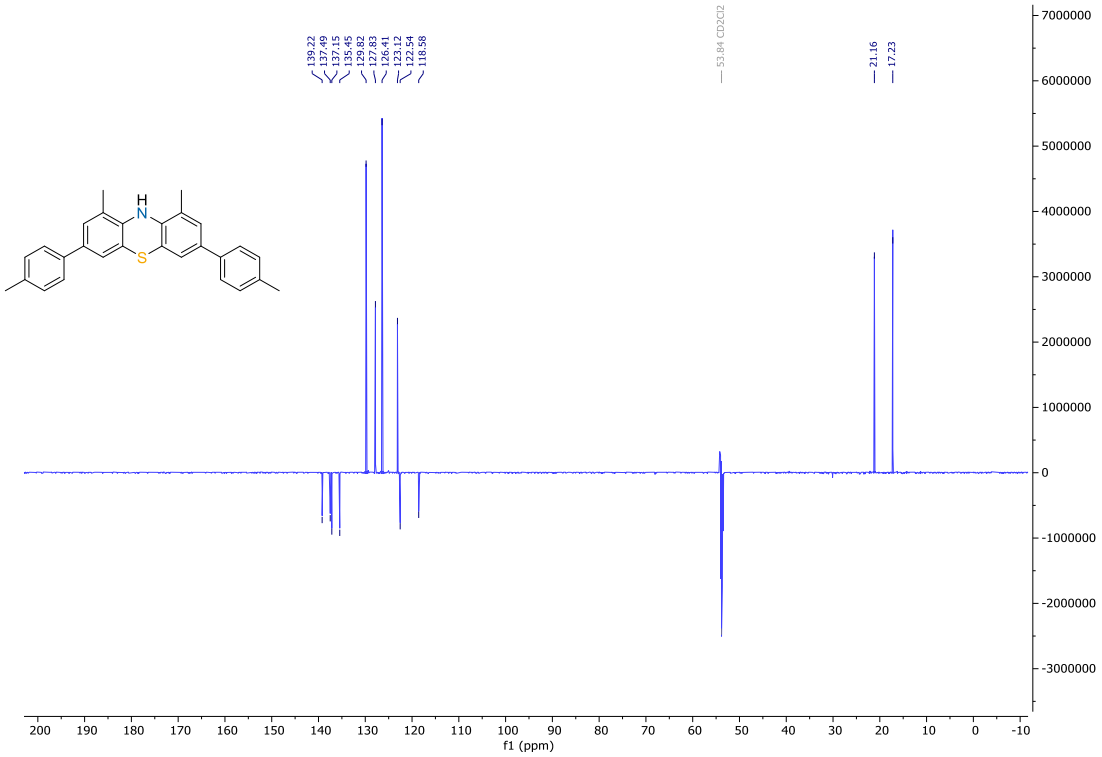


*Figure 64: $^{13}$C-NMR spectrum of **17** in $CD_2Cl_2$.*

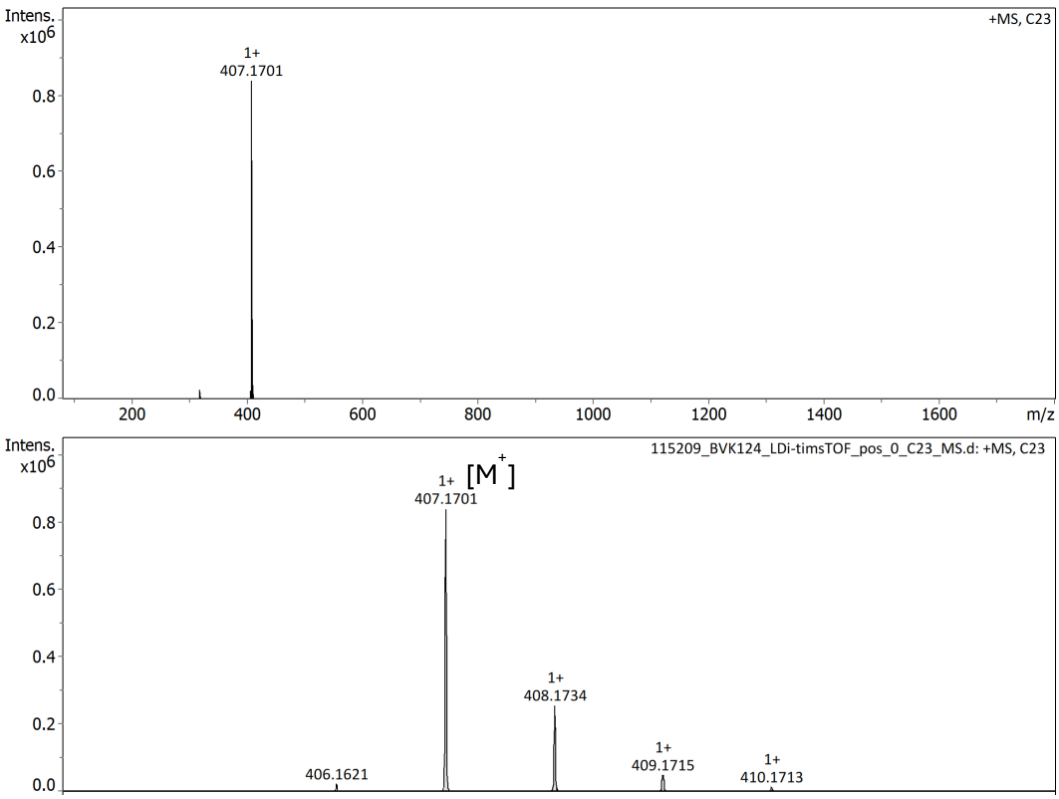


*Figure 65: HRMS (MALDI-timsTOF) mass spectrum of **17**.*

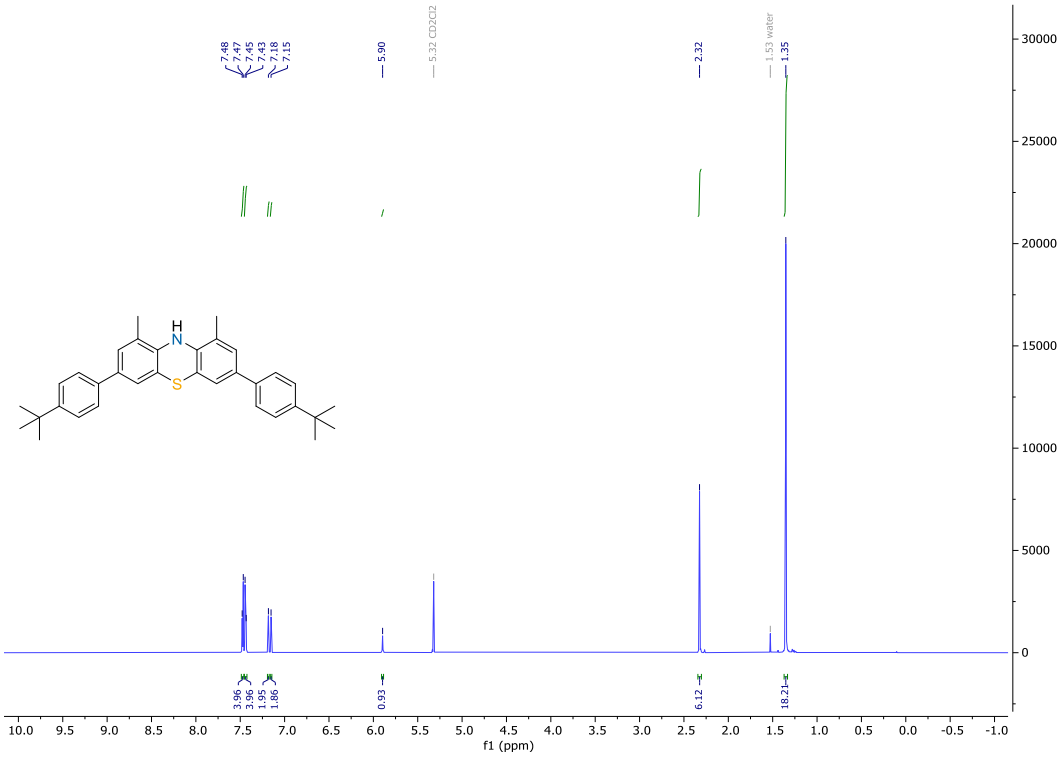


*Figure 66: $^{1}$H-NMR spectrum of **18** in $CD_2Cl_2$.*

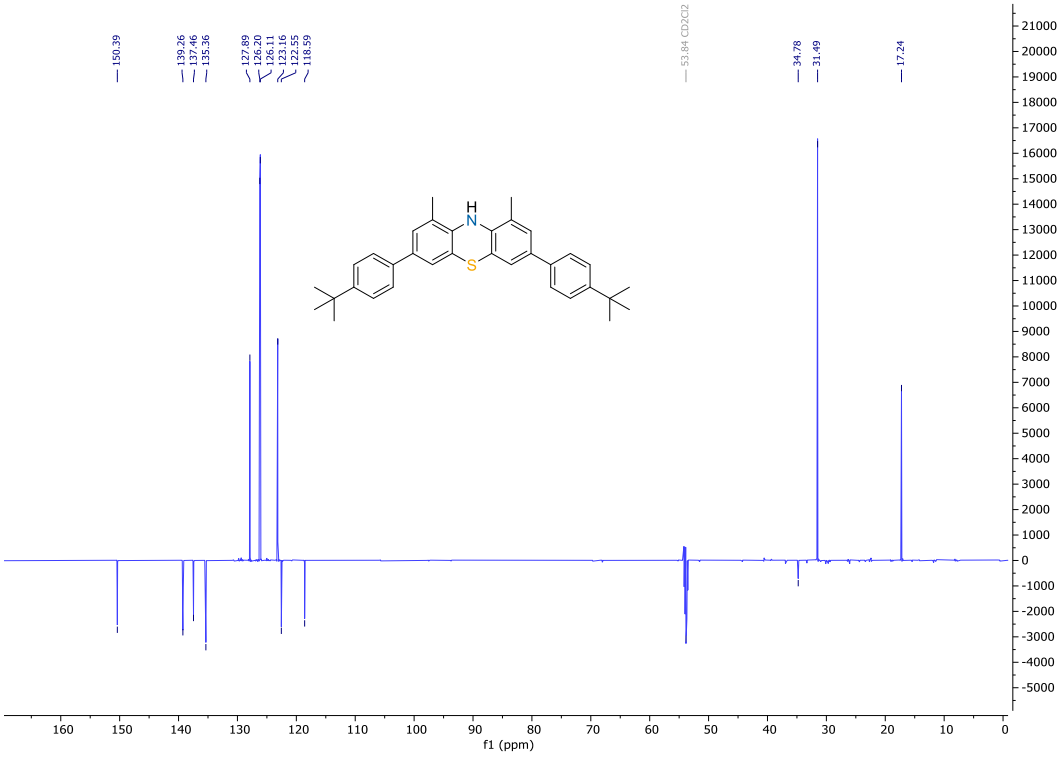


*Figure 67: $^{13}$C-NMR spectrum of **18** in $CD_2Cl_2$.*

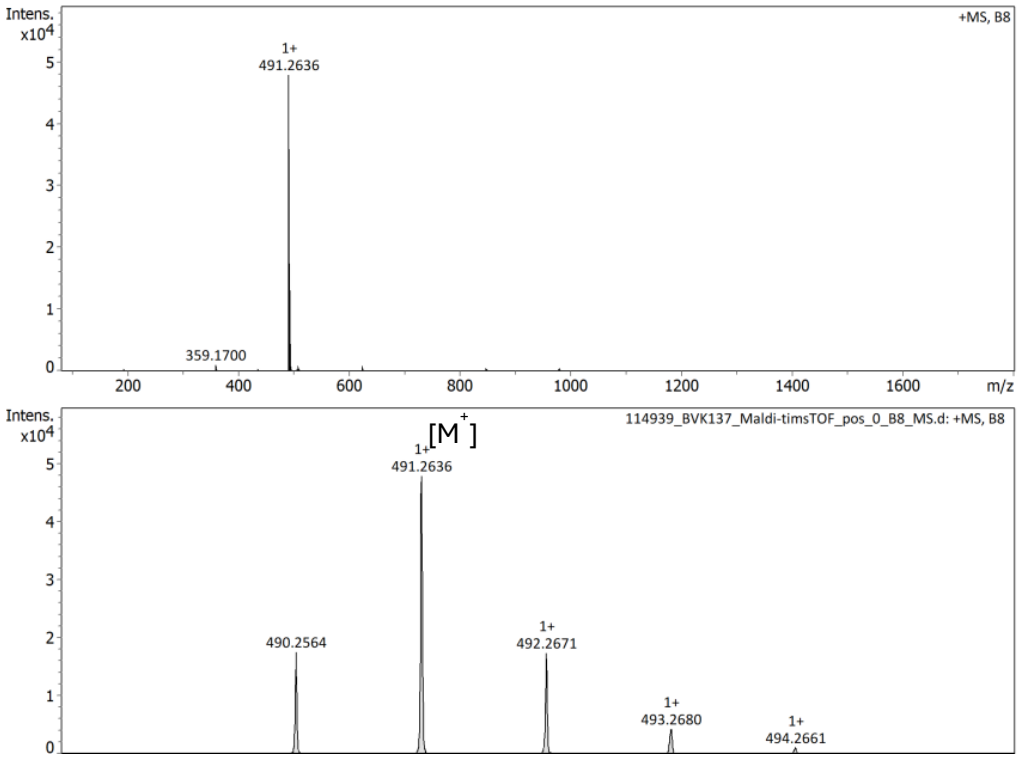


*Figure 68: HRMS (MALDI-timsTOF) mass spectrum of **18**.*

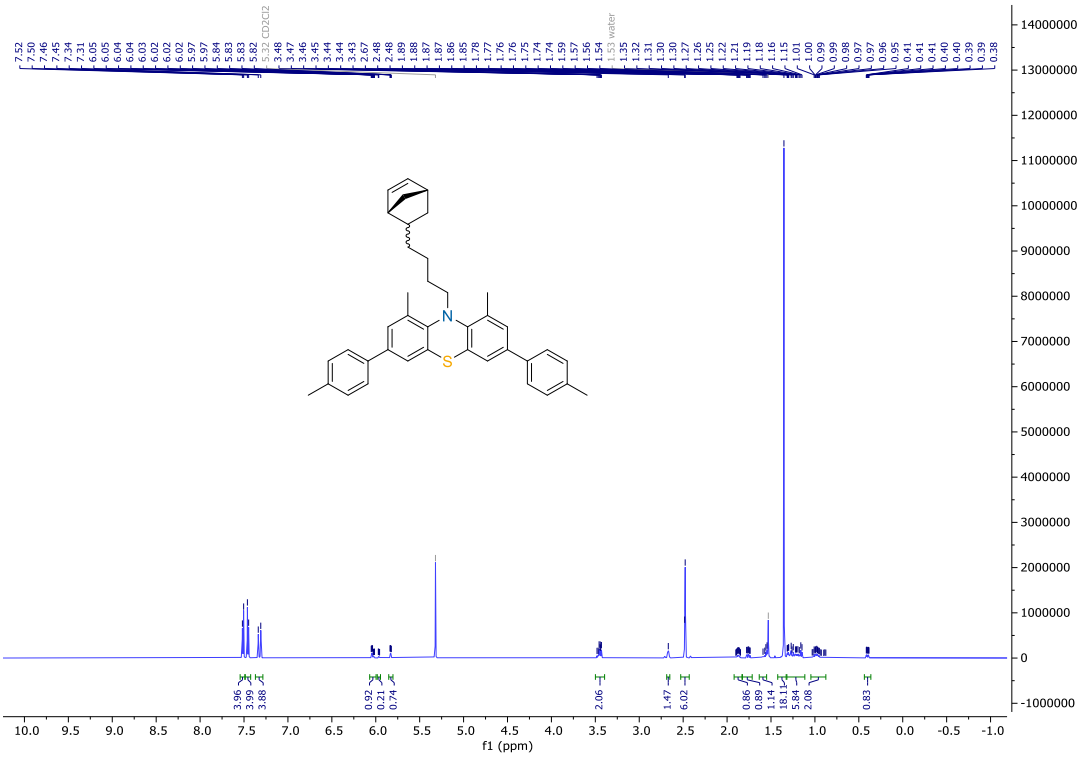


*Figure 69: $^{1}$H-NMR spectrum of **7** in $CD_2Cl_2$.*

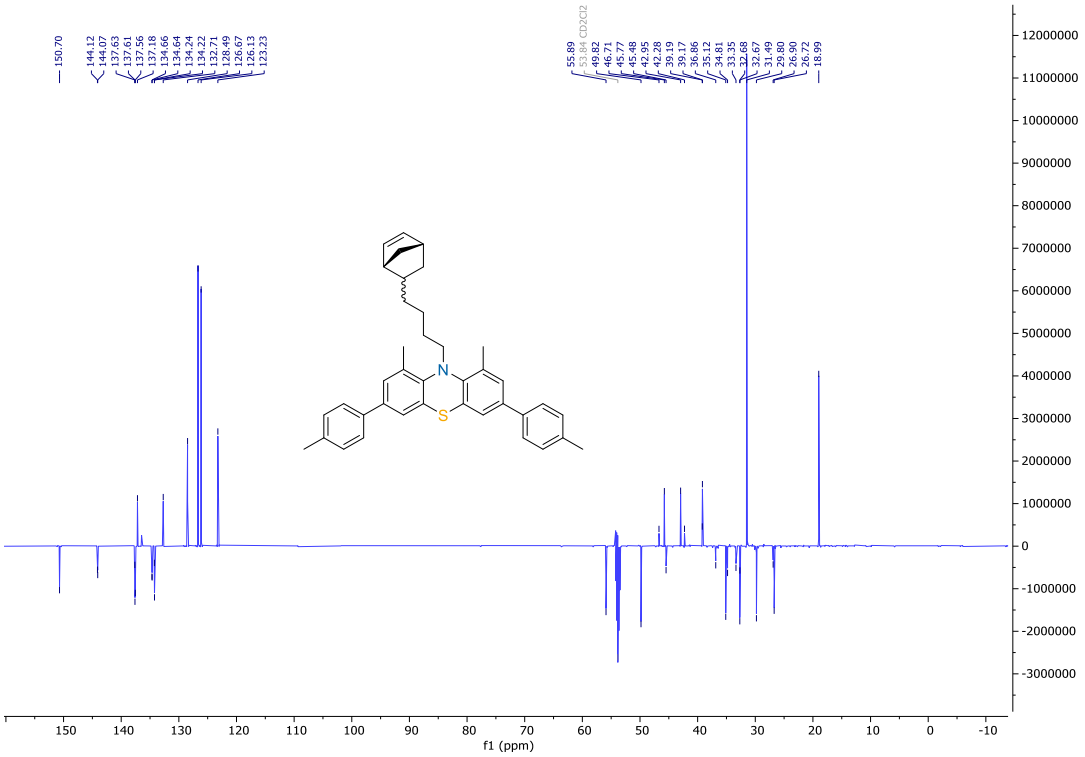


*Figure 70: $^{13}$C-NMR spectrum of **7** in $CD_2Cl_2$.*

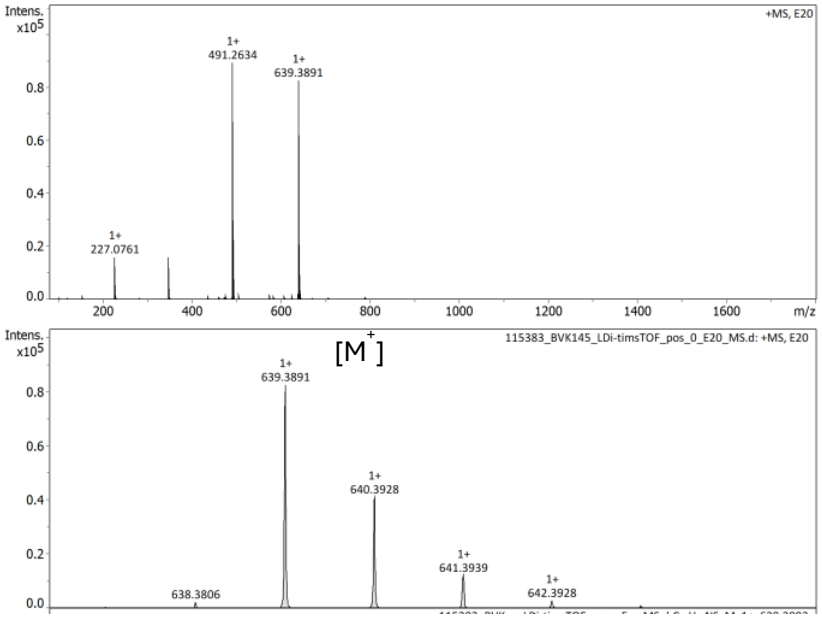


*Figure 71: HRMS (MALDI-timsTOF) mass spectrum of **7**.*

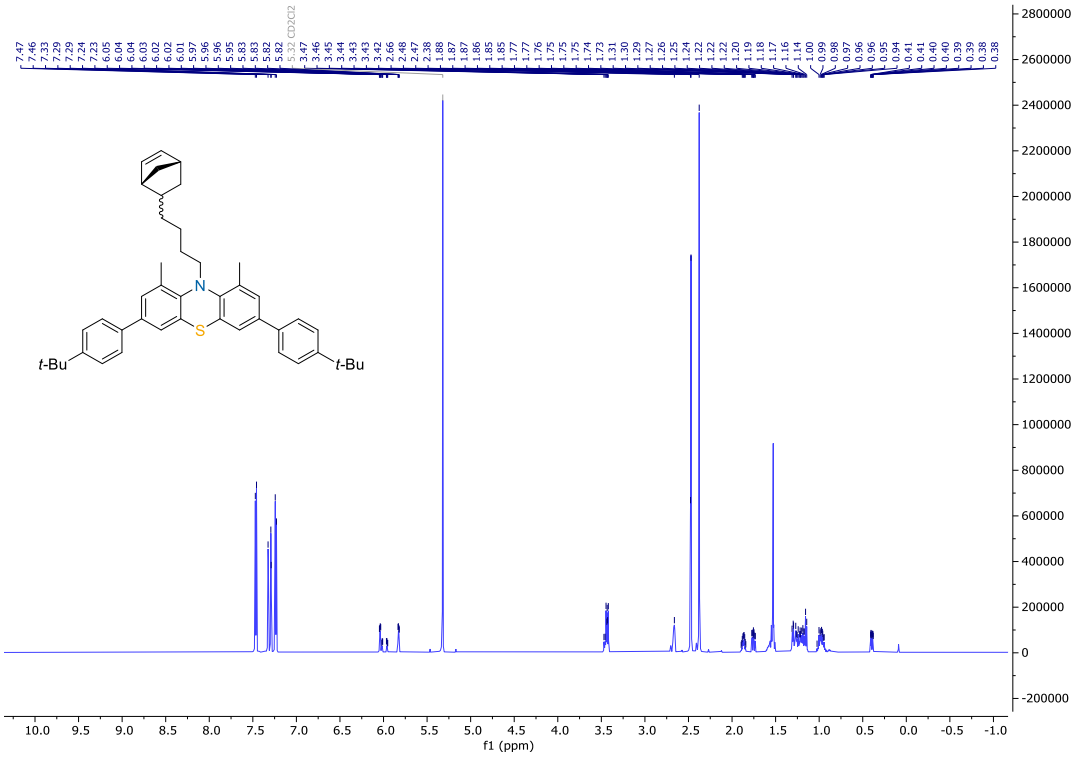


*Figure 72: $^{1}$H-NMR spectrum of **6** in $CD_2Cl_2$.*

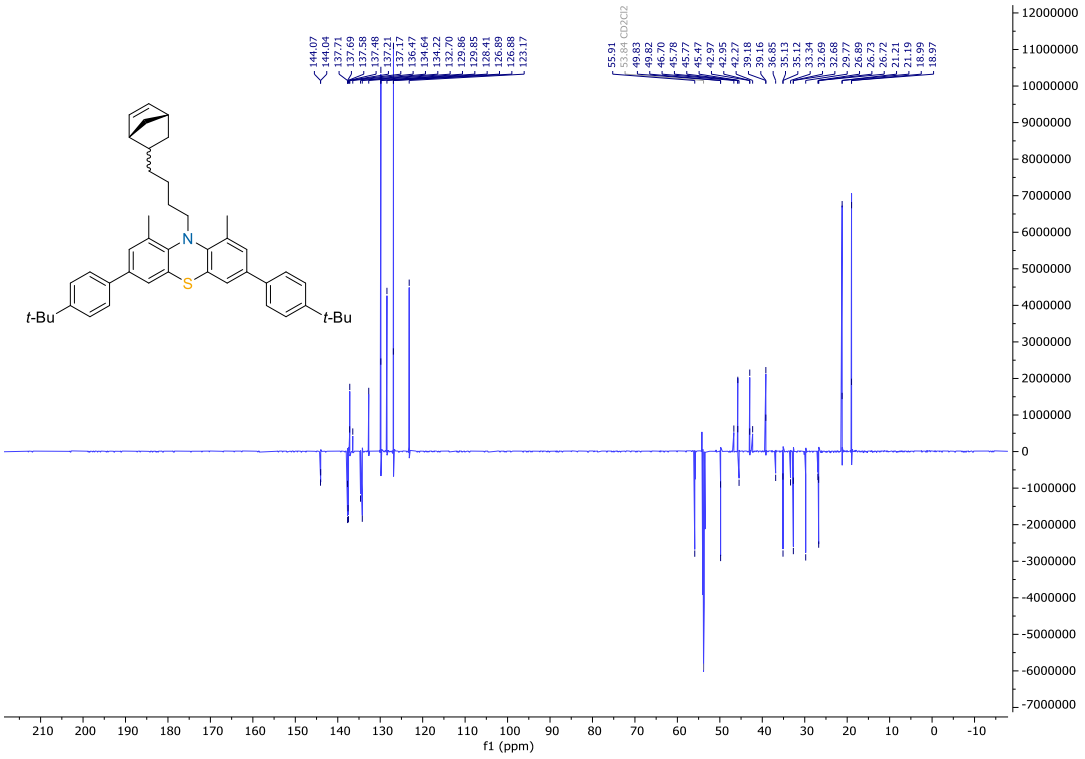


*Figure 73: $^{13}$C-NMR spectrum of **6** in $CD_2Cl_2$.*

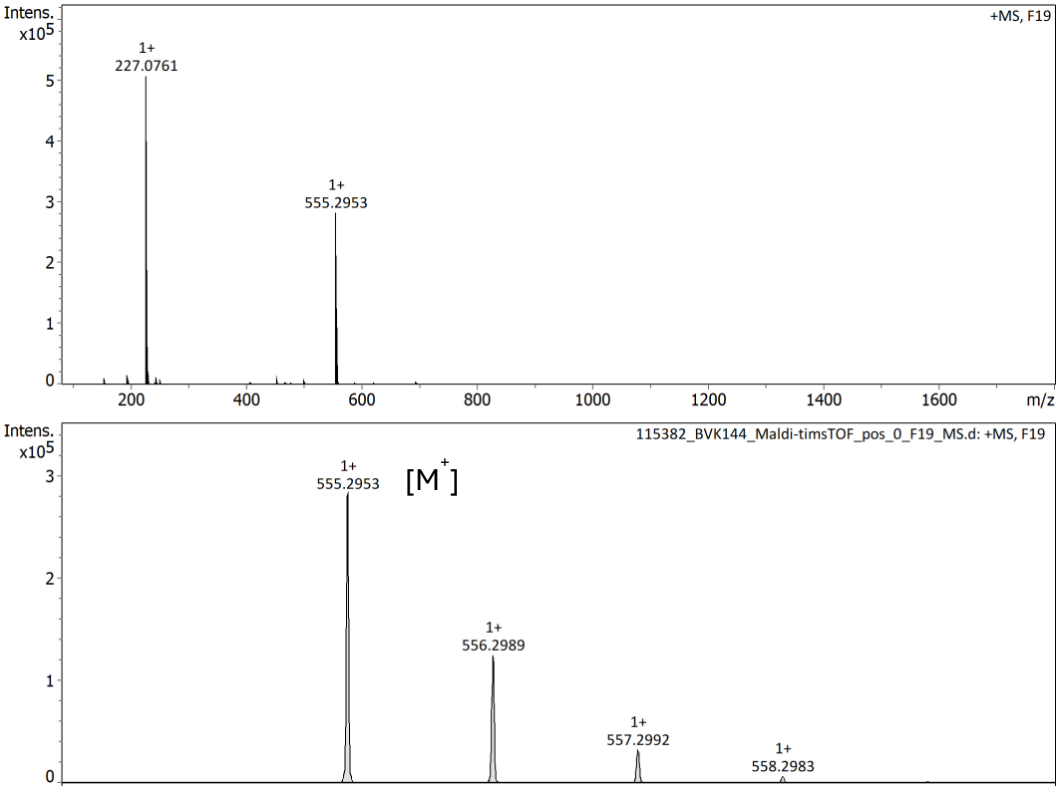


*Figure 74: HRMS (MALDI-timsTOF) mass spectrum of* ***6****.*